Irreversible Thermodynamic Studies on Electrochemical Systems

1998

Koji Amezawa

Irreversible Thermodynamic Studies on Electrochemical Systems

A Thesis Submitted to
Kyoto University
For the Requirements of
the Degree of Doctor of Engineering

1998

Koji Amezawa

Contents

General introduction 1

1. Single electrode Peltier heat 2
2. Electrolyte properties 3
3. Other engineering importance of thermoelectric power 4

References 6

Part I. Single Electrode Peltier Heats of Li-alloy Electrodes in LiCl-KCl Eutectic Melt 7

Chapter 1. Introduction 9

References 11

Chapter 2. Single electrode Peltier heats of Li-Al alloy electrodes in coexisting phase states 13

2.1 Introduction 13

2.2. Principles 13

2.2.1. Flux equations 14

2.2.2. Thermoelectric power 16

2.3. Experimental 20

2.4. Results and discussion 25

2.4.1. Electrochemical formation 25

2.4.2. Thermodynamic properties 29

2.4.3. Thermoelectric power 31
2.4.4. Single electrode Peltier heat 36
2.5. Conclusions 38
References 39

Chapter 3. Single electrode Peltier heats of Li-Al alloy electrodes in single phase states 41
3.1. Introduction 41
3.2. Principles 42
3.2.1. Thermodynamic properties on a coexisting-single phase boundary 42
3.2.2. Single electrode Peltier heat on a coexisting-single phase boundary 44
3.3. Experimental 45
3.4. Results and discussion 46
3.4.1. Thermodynamic properties of the single βLiAl phase 46
3.4.2. Single electrode Peltier heat as a function of lithium concentration 54
3.5. Conclusions 57
References 59

Chapter 4. Single electrode Peltier heats of Li-Si alloy electrodes 61
4.1. Introduction 61
4.2. Experimental 61
4.3. Results and discussion 63
4.3.1. Electrochemical formation 63
4.3.2. Thermodynamic properties 67
4.3.3. Thermoelectric power 70

4.3.4. Thermoelectric power of an alloy electrode in a solid-liquid coexisting phase 76
4.3.5. Single electrode Peltier heat 78
4.4. Conclusions 80
References 81

Chapter 5. Conclusions 83

Part II. Proton and Native Conduction in 5mol% Sr-substituted $LaPO_4$ Studied by Thermoelectric Power Measurements 85

1. Introduction 87
2. Principles 89
2.1. Thermoelectric power 89
2.1.1. Pure protonic conductor 90
2.1.2. Pure oxide ion conductor 93
2.1.3. Pure electronic conductor 93
2.1.4. Mixed conductor 94
2.2. Defect structures in Sr-substituted $LaPO_4$ 96
2.3. p_{H_2O} and p_{O_2} dependencies of thermoelectric power 98
3. Experimental 100
4. Results and discussion 102
4.1. Thermoelectric power 102
4.2. Identification of charge carrier species 103
4.3. Transported entropies 107
4.4. p_{H_2O} and p_{O_2} dependencies of the thermoelectric power under mixed conduction conditions 110

5. Conclusions 111

References 113

General conclusions 115

Appendix A. Transported entropy and thermodynamic entropy 119

Nomenclature 127

Acknowledgments 129

General introduction

An electrochemical system comprising an electrolyte and two reversible electrodes of the same kind produces an electromotive force (*emf*) if these electrodes are maintained at different temperatures. Such thermoelectric phenomena represent transport of heat, charge, and mass under the coexistence of temperature, electric potential, and chemical potential gradients. Thus, the proper understanding of the phenomena is expected to contribute to the understanding on heat transfer accompanied by charge and mass transfer, and on transport mechanism in the electrolyte. Thermoelectric power (or Seebeck coefficient), which is defined as the slope of the *emf* of a nonisothermal electrochemical system related to temperature difference, is one of the central experimental quantities for investigating thermoelectric phenomena.

In this work, measurements of thermoelectric power are applied to investigate the single electrode Peltier heats of an alloy electrode in part I of this thesis and the conduction properties in a mixed conductor in part II of this thesis. The background and the purpose of each work are outlined in detail in following section 1 and section 2. Other engineering importance of researches on thermoelectric power and the connection with this work are briefly described in section 3. Theory of irreversible thermodynamics is employed to describe thermoelectric power. Classical thermodynamics deals with equilibrium and the driving forces for reaction, but is not applicable where transport processes exist. Contrary to this, irreversible thermodynamics has been developed to deal such non-equilibrium situations, and is most suitable to describe interacting

transport processes [1].

1. Single electrode Peltier heat

For improving the energy conversion efficiency and ensuring the adequate temperature control of electrochemical systems, such as batteries, fuel cells, and electrolyzers, heat analysis in the system is important. Uncontrolled temperature changes in a cell or in a part of a cell may be disastrous. For instance, if sufficient heat is not supplied to an electrode where an endothermic process takes place, the temperature of the electrode falls down. This may lead to an increase in the ohmic resistance of the cell and that in the overpotential of the electrode reaction, and thus decrease the energy efficiency of the electrochemical system. For molten salt electrochemical systems, even freezing of the electrolyte may occur in an extreme case. On the other hand, if heat is not removed from an electrode where an exothermic process takes place, the temperature of the electrode rises. This may cause a breakdown of cell materials or boiling of the electrolyte.

The heat evolution in electrochemical systems is asymmetric [2]. In order to evaluate a detailed temperature distribution of an electrochemical system, it is thus not enough to know the heat of the total reaction. One should also know the single electrode heats of anodic and cathodic reactions respectively. The single electrode heat can be expressed as a sum of heats due to Peltier effect, overpotential of the electrode reaction and ohmic resistance of the cell [2];

$$Q^{\downarrow} = \pi^{\downarrow} I - \eta I - \rho \ell I^2 \qquad (1)$$

where $Q^{\downarrow}$ is the single electrode heat, $\pi^{\downarrow}$ is the single electrode Peltier heat, η is the overpotential, ρ is the electrical resistivity of the system, ℓ is the half distance between electrodes, and I is the current density. In contrast to the heats due to overpotential and

ohmic resistance, the single electrode Peltier heat is reversed on charge, and is independent of the cell design and size. The single electrode Peltier heat can be evaluated from the value of thermoelectric power [1, 3]. This experimental approach is more thermodynamically rigorous than a calorimetric measurement.

From an above engineering point of view, the single electrode Peltier heat of an alloy electrode is discussed theoretically and empirically in part I of this thesis. In spite of their importance, only few investigations on thermoelectric power of alloy electrodes have been reported [4]. Chapter 2 of part I describes the single electrode Peltier heats of a Li-Al alloy electrode in various coexisting phase states in LiCl-KCl eutectic melt. Based on the theory of irreversible thermodynamics, the relation between the thermoelectric power and thermodynamic properties of the alloy is established, and is validated by the experimental results. In chapter 3 of part I, the single electrode Peltier heats of a Li-Al alloy electrode in single phase states are presented. The effect of phase change on the single electrode Peltier heat is discussed thermodynamically. Chapter 4 of part I presents the single electrode Peltier heats of a Li-Si alloy electrode in LiCl-KCl eutectic melt. The results are used to confirm the theories derived in chapter 2 and chapter 3.

2. Electrolyte properties

Solid electrolytes are considered to be utilized as the electrolyte in fuel cells, sensors and so on, but they often show mixed ionic and electronic conduction depending on atmospheric conditions or states of compound. For instance, high temperature protonic conductors (HTPCs), which is investigated in this study, tend to exhibit mixed conduction by protons and native charge carriers, typically oxide ions and electrons or electron holes, depending on temperature, hydrogen partial pressure (or water vapor

partial pressure), oxygen partial pressure and dopant concentration [5, 6]. Such mixed conduction becomes a disadvantage for practical use. For optimization of the operation condition of electrochemical systems or proper material choice, it is therefore indispensable to clarify electrolyte properties under certain conditions. In order to reveal complicated conduction mechanisms in solid mixed conductors, different experimental techniques are necessary. Much attention has been paid to measurements in isothermal electrochemical systems, e.g. conductivity measurements and *emf* measurements on concentration cells, but, so far, little attention has been paid to measurements in nonisothermal electrochemical system, i.e. thermoelectric power measurements.

In part II of this thesis, thermoelectric power measurements are applied to investigate conduction properties in Sr-substituted $LaPO_4$. Sr-substituted $LaPO_4$ has been suggested as a candidate for a HTPC [6]. This work shows possibilities of thermoelectric power measurements for investigating electrolyte properties. The expressions of the thermoelectric power for materials conducting protons, oxide ions and electronic defects were derived, and the relation between thermoelectric power and conduction properties for a mixed protonic conductor is clarified. According to the derived expressions, the conditions where proton transport number can be regarded as unity are determined, and charge carrier species in Sr-substituted $LaPO_4$ under mixed conduction conditions are identified.

3. Other engineering importance of thermoelectric power

Thermoelectric effect can be applied to a direct energy conversion system from thermal into electrical energy. Such energy conversion system is one of attractive ways of energetic development when we consider the usage of industrial exhaust heat or geothermal water. As one of this type of energy conversion system, the thermogalvanic

cell has been proposed [7~12]. The thermogalvanic cell is expected to have advantages of longevity and simplicity of use, because there is no moving mechanical parts. To provide high cell voltages, it is preferable to use electrolyte materials in which large temperature difference can be put. Since the thermogalvanic cell has an efficiency which are Carnot limited [7, 8], cell operation at high temperature is also beneficial. From these aspects, molten salts and solid electrolytes are promising electrolyte materials for thermogalvanic cells. As an electrode active mass, gases, liquid metals, and redox ion couples have been investigated [9~12] since these can avoid electrode degradation by charge and discharge. Alloy electrodes are also suggested as interesting materials to provide high cell voltage [7]. Considering above backgrounds, the results on thermoelectric power obtained in this work could give fundamental information for developing thermogalvanic cells.

Thermoelectric effect is known as one of driving forces for the mass transfer phenomena [13~14]. In a circulating heat transfer loop of a molten salt breeder reactor (MSBR), this mass transfer phenomena can cause deterioration of the construction material: i.e. dissolution of elements in the construction material at higher temperature side and precipitation at lower temperature side [13]. In order to solve this problem, it is necessary to clarify the relation between thermoelectric power and thermodynamic properties of materials as well as to accumulate data on thermoelectric power in molten salt systems. At the present time, alloys, such as Hastelloy (Ni-Mo-Cr-Fe alloy) and Inconel (Ni-Cr-Fe alloy), are planned to be utilized as a construction material in MSBR [15]. Thus the knowledge on thermoelectric power of an alloy electrode obtained in part I of this work would be useful to estimate the thermoelectric effect of construction alloys and to develop better corrosion-resisting materials.

References

[1] K. S. Førland, T. Førland, and S. K. Ratkje, *Irreversible Thermodynamics; Theory and Application*, 2nd repr., Wiley, Chichester (1994).

[2] Y. Ito, F. R. Foulkes, and S. Yoshizawa, *J. Electrochem. Soc.*, **129**, 1936 (1982).

[3] Y. Ito, H. Kaiya, S. Yoshizawa, S. K. Ratkje, and T. Førland, *J. Electrochem. Soc.*, **131**, 2504 (1984).

[4] M. Kamata, Y. Ito, M. Inoue and J. Oishi, *J. Electrochem. Soc.*, **136**, 528 (1989).

[5] K. -D. Kreuer, *Chem. Mater.*, **8**, 610 (1996).

[6] T. Norby and N. Christiansen, *Solid State Ionics*, 77, 240 (1995).

[7] Y. Ito, *Denchi Gijyutsu*, **1**, 15 (1992).

[8] A. V. Sokirko, *Electrochim. Acta*, **39**, 597 (1994).

[9] J. L. Weininger, *J. Electrochem. Soc.*, **111**, 769 (1964).

[10] N. Weber, *Adv. Energy Conv.*, **14**, 1 (1974).

[11] B. Burrows, *J. Electrochem. Soc.*, **123**, 154 (1976).

[12] T. Hirai, K. Shindo, and T. Ogata, *Proceedings of the '95 Asian Conference on Electrochemistry*, 150 (1995).

[13] Y. Ito, M. Kamata, S. Horikawa, and J. Oishi, *Denki Kagaku*, **53**, 375 (1985).

[14] Y. Ito, S. Horikawa, and J. Oishi, *Electrochim. Acta*, **30**, 799 (1985).

[15] *Molten Salt Breeder Reactor*, edited by Atomic Energy Society of Japan (1981)

Part I

Single Electrode Peltier Heats of Li-Alloy Electrodes in LiCl-KCl Eutectic Melt

Chapter 1

Introduction

Heat analysis in electrochemical reactors is important for determining the adequate operation conditions and the cell design. In order to quantitatively understand the temperature distribution in electrochemical reactors, it is necessary to know the single electrode heat, which includes the single electrode Peltier heat [1]. The single electrode Peltier heat of an electrode can be evaluated from the value of its thermoelectric power [2, 3]. Though many concern the theoretical and/or experimental study of thermoelectric power for pure metal electrode systems [4~13], few concern that of alloy electrode systems [14]. However, from a practical point of view, it is very important to study thermoelectric power of alloy electrode systems, because alloy electrodes are used in many electrochemical reactors.

In part I of this thesis, thermoelectric power of Li-Al and Li-Si alloy electrodes in LiCl-KCl eutectic melt is investigated theoretically and experimentally. The purposes of the work are to establish methods for estimating the single electrode Peltier heat of an alloy electrode in a coexisting or a single phase state, and to investigate how this Peltier heat of an alloy electrode is affected by the phase change of the electrode itself.

Li-Al and Li-Si alloys are currently being utilized as an anode material in high temperature lithium-based batteries with molten salts, typically molten chloride salts, such as Li-alloy/metal sulfide, Li-alloy/lithiate oxide and Li-alloy/Cl_2 [15~21], since Li-Al and Li-Si alloys are relatively stable compared to pure liquid lithium. The use of a Li-

Al or a Li-Si alloy electrode provides higher energy and power density, and higher and more stable cell voltage than the use of other lithium alloy electrodes do, because of their low densities, high lithium diffusion coefficients (10^{-4}~10^{-6} $cm^2 \cdot s^{-1}$), high lithium activities (> 10^{-3}) and wide concentration ranges of coexisting phase regions at the cell operation conditions [16, 22~23]. High temperature lithium-based batteries have the capability to deliver electrical energy at extremely high specific power, and thus are being developed for uses as energy storage devices for load leveling and as power sources for electric vehicles [15]. The single electrode Peltier heats of Li-Al and Li-Si alloy electrodes obtained here can directly contribute to the heat analysis of such batteries.

References

[1] Y. Ito, F. R. Foulkes, and S. Yoshizawa, *J. Electrochem. Soc.*, **129**, 1936 (1982).

[2] K. S. Førland, T. Førland, and S. K. Ratkje, *Irreversible Thermodynamics; Theory and Application*, 2nd repr., Wiley, Chichester (1994).

[3] Y. Ito, H. Kaiya, S. Yoshizawa, S. K. Ratkje, and T. Førland, *J. Electrochem. Soc.*, **131**, 2504 (1984).

[4] Y. Ito, S. Horikawa, and J. Oishi, *Electrochimica Acta*, **30**,799 (1985).

[5] Y. Ito, M. Kamata, S. Horikawa, and J. Oishi, *Denki Kagaku*, **53**, 375 (1985).

[6] M. Kamata, Y. Ito, and J. Oishi, *Electrochimica Acta*, **31**, 521 (1986).

[7] Y. Ito, R. Takeda, S. Yoshizawa, and Y. Ogata, *J. Appl. Electrochem.*, **15**, 209 (1985).

[8] Y. Ito, H. Hayashi, N. Hayafuji, and S. Yoshizawa, *Electrochimica Acta*, **30**, 701 (1985).

[9] A. Grimstvedt, S. K. Ratkje, and T. Førland, *J. Electrochem. Soc.*, **141**, 1236 (1994).

[10] S. K. Ratkje, V. Sharivker, and B. Cleaver, *Electrochimica Acta*, **39**, 2659 (1994)

[11] R. Haase, U. Prüser, and J. Richter, *Ber. Bunsenges. Phys. Chem.*, **81**, 577 (1977).

[12] W. Fuchs and J. Richter, *Ber. Bunsenges. Phys. Chem.*, **86**, 46 (1982).

[13] K. E. Johnson and S. J. Sime, *Electrochimica Acta*, **22**, 1043 (1977).

[14] M. Kamata, Y. Ito, M. Inoue, and J. Oishi, *J. Electrochem. Soc.*, **136**, 528 (1989).

[15] G. L. Henriksen, *Handbook of Batteries, 2nd ed.*, Edited by D. Linden, McGraw-Hill, New York (1995).

[16] R. A. Huggins, *J. Power Sources*, **26**, 106 (1989).

[17] G. L. Henriksen and D. R. Vissers, *J. Power Sources*, **51**, 115 (1994).

[18] E. C. Gay, D. R. Vissers, F. J. Martino, and K. E. Anderson, *J. Electrochem. Soc.*, **123**, 1591 (1976).

[19] R. A. Sharma and R. N. Seefurth, *J. Electrochem. Soc.*, **123**, 1763 (1976).

[20] H. F. Gibbard, *J. Power Sources*, **26**, 81 (1989).

[21] D. L. Thomas and D. N. Bennion, *J. Electrochem. Soc.*,**136**, 3553 (1989).

[22] C. J. Wen, B. A. Boukamp, and R. A. Huggins, *J. Electrochem. Soc.*, **126**, 2258 (1979).

[23] C. J. Wen and R. A. Huggins, *J. Solid State Chem.*, **37**, 271 (1981).

Chapter 2

Single electrode Peltier heats of Li-Al alloy electrodes in coexisting phase states

2.1. Introduction

This chapter presents experimental results of the thermoelectric power and thermodynamic properties of Li-Al alloys in various coexisting phase states. The main purposes of this chapter are to understand relations between the thermoelectric power, thus the single electrode Peltier heat, of an alloy electrode and thermodynamic properties of the alloy, and to establish an estimation method of the thermoelectric power of an alloy electrode. The theoretical expression for the thermoelectric power of an alloy electrode is established based on a thermodynamic treatment of entropy production by heat, mass, and charge transfer developed by Førland et al. [1]. The applicability of the estimation method offered in this chapter is confirmed by the experimental results.

2.2. Principles

In this section, the thermoelectric power of the following nonisothermal cell (I-a) is derived;

$$(T_1)\ A_xM_{1-x} \mid AX\text{-}BX \mid A_xM_{1-x}\ (T_2) \qquad \text{(I-a)}$$

In the cell (I-a) electrolyte is a salt mixture melt of AX and BX. The electrodes are alloys, and the concentration of the component A in both electrodes are same. The electrodes are reversible to the cation A^+ in the electrolyte. The two electrodes are at different temperature T_1 and T_2 ($T_2 - T_1 = \Delta T$). In the following the theory of irreversible thermodynamics by Førland et al. [1] is applied for deriving the theoretical expression for the thermoelectric power of the nonisothermal cell (I-a). In this derivation, only operationally defined variables are used, while single ion chemical or electrochemical potentials which are not operationally defined are used in common methods.

2.2.1. Flux equations

The forces in the system are $-\nabla \ln T$, the gradients in chemical potential at constant temperature, $-\nabla \mu_{AX,T}$, $-\nabla \mu_{BX,T}$, and $-\nabla \mu_{A(A_xM_{1-x})T}$, and the electric potential gradient of the cell (I-a), $-\nabla \phi^{obs}$. The units used for forces are m^{-1} for $\nabla \ln T$, $J \cdot mol^{-1} \cdot m^{-1}$ for $\nabla \mu_{AX,T}$, $\nabla \mu_{BX,T}$, and $\nabla \mu_{A(A_xM_{1-x})T}$, and $J \cdot mol^{-1} \cdot m^{-1}$ for $\nabla \phi$. The electric force in $V \cdot m^{-1}$, ∇E, is related to $\nabla \phi^{obs}$ by $\nabla E = \nabla \phi^{obs} / F$, where F is the Faraday constant. The fluxes are the heat flux, J_q, the mass fluxes J_{AX}, J_{BX}, and $J_{A(A_xM_{1-x})}$ of the component AX, BX, and component A in the alloy electrode, and the electric current density j. The units used for fluxes are: $J \cdot m^{-2} \cdot s^{-1}$ for J_q, $mol \cdot m^{-2} \cdot s^{-1}$ for J_{AX}, J_{BX}, and $J_{A(A_xM_{1-x})}$, and $mol \cdot m^{-2} \cdot s^{-1}$ for j. The dissipation function of the system, $T\Theta$, can be expressed as the sum of the force-flux products [1];

$$T\Theta = -J_q \nabla \ln T - J_{AX} \nabla \mu_{AX,T} - J_{BX} \nabla \mu_{BX,T} - J_{A(A_xM_{1-x})} \nabla \mu_{A(A_xM_{1-x})T} - j \nabla \phi^{obs} \qquad \text{(I-1)}$$

where Θ is the entropy production per unit volume and unit time. The unit of the dissipation function is $J \cdot m^{-3} \cdot s^{-1}$.

The chemical potentials of the component AX and BX depend on each other through the Gibbs-Duhem relation;

$$\nabla \mu_{BX,T} = -\frac{x_{AX}}{x_{BX}} \nabla \mu_{AX,T} \tag{I-2}$$

where x_i is the molar fraction of the component i in the electrolyte. When the anion lattice is chosen as a frame of reference for transport in the electrolyte, the fluxes of the neutral components, AX and BX, are related as follows due to the electroneutrality principle;

$$J_{AX} + J_{BX} = 0 \tag{I-3}$$

The flux of the component A in the alloy electrode is related to the current density;

$$J_{A(A_xM_{1-x})} = j \tag{I-4}$$

By introducing eqs. (I-2)~(I-4) into eq. (I-1), we obtain;

$$T\Theta = -J_q \nabla \ln T - J_{AX} \frac{\nabla \mu_{AX,T}}{x_{BX}} - j \nabla \phi \tag{I-5}$$

where

$$\nabla \phi = \nabla \phi^{obs} + \nabla \mu_{A(A_xM_{1-x})T} \tag{I-6}$$

Equation (I-5) contains the three independent forces $\nabla \ln T$, $\nabla \mu_{AX,T}$, and $\nabla \phi$, and their conjugate fluxes J_q, J_{AX}, and j. The flux equations are then;

$$J_q = -L_{11} \nabla \ln T - L_{12} \frac{\nabla \mu_{AX,T}}{x_{BX}} - L_{13} \nabla \phi \tag{I-7}$$

$$J_{AX} = -L_{21} \nabla \ln T - L_{22} \frac{\nabla \mu_{AX,T}}{x_{BX}} - L_{23} \nabla \phi \tag{I-8}$$

$$j = -L_{31} \nabla \ln T - L_{32} \frac{\nabla \mu_{AX,T}}{x_{BX}} - L_{33} \nabla \phi \tag{I-9}$$

where the coefficient L_{ij} is the phenomenological coefficient. These coefficients are related by the Onsager reciprocal relations;

$$L_{ij} = L_{ji} \tag{I-10}$$

2.2.2. Thermoelectric power

When there exist no composition gradient and no pressure gradient in the system, the chemical potential gradients are zero, i.e. $\nabla\mu_{i,T}=0$. The condition of no composition gradient can be established when the system is far from the Soret equilibrium or when there exists convection in the system. Equation (I-6) is then reduced;

$$\nabla\phi=\nabla\phi^{obs} \tag{I-11}$$

Considering eq. (I-11) and $\nabla\mu_{i,T}=0$, equations (I-7)~(I-9) can be simplified as follows;

$$J_q=-L_{11}\nabla\ln T-L_{13}\nabla\phi^{obs} \tag{I-12}$$

$$J_{AX}=-L_{21}\nabla\ln T-L_{23}\nabla\phi^{obs} \tag{I-13}$$

$$j=-L_{31}\nabla\ln T-L_{33}\nabla\phi^{obs} \tag{I-14}$$

From eqs. (I-10), (I-12), and (I-14), the following expression for *emf* can be obtained;

$$\left(\nabla\phi^{obs}\right)_{j=0}=-\left(\frac{L_{31}}{L_{33}}\right)\nabla\ln T=-\left(\frac{L_{13}}{L_{33}}\right)\frac{\nabla T}{T}=-\left(\frac{J_q}{j}\right)_{\nabla T=0}\frac{\nabla T}{T} \tag{I-15}$$

In eq. (I-15), the term $(J_q/j)_{\nabla T=0}$ is the heat evolution or absorption per faraday in the individual electrode regions, and corresponds the Peltier heat, $\pi^{\downarrow}$ [a]. Equations (I-15) then provides;

$$\left(\frac{\nabla\phi^{obs}}{\nabla T}\right)_{j=0}=-\frac{\pi^{\downarrow}}{T} \tag{I-16}$$

The Peltier heat is obtained from the reversible heat balance at one electrode [1]. The reversible heat changes are given by entropy changes in the electrode region. When the anion lattice is chosen as the frame of reference, mass changes in the electrode regions of the nonisothermal cell (I-a) are summarized in Table I-1. In Table I-1, t_{A^-} and

---

[a] The electrode region defined in the anion quasi-lattice frame of reference is generally different from that defined in other frames of reference (for instance, the wall frame of reference). Thus, the value of the Peltier heat normally depends on frame choice as the values of the transference coefficient do. However, one should note that the Peltier heat is independent of frame choice when temperature is constant and we have stationary state.

Table I-1. Local mass changes at the electrode regions of the nonisothermal cell (I-a) when one farady of positive charges are transferred.

Species	Left-hand side electrode (T)	Right-hand side electrode (T)
A in A_XM_{1-X}	-1 mole	1 mole
AX	$(1-t_A+) = t_B+$ mole	$-(1-t_A+) = -t_B+$ mole
BX	$-t_B+$ mole	t_B+ mole

t_B. are the transport numbers of cations with reference to anions, i.e. internal transport numbers of cations. From Table I-1, the transference coefficients of the salts are related to the internal transport numbers of cations by the following equations;

$$t_{AX} = 1 - t_{A^-} = t_{B^-} \tag{I-17}$$

$$t_{BX} = -t_{B^-} \tag{I-18}$$

The reversible entropy changes in the nonisothermal cell (I-a) are then schematically illustrated as Fig. I-1, and they are summarized in Table I-2. From Table I-2, we have;

$$\frac{\pi^{\downarrow}}{T} + \bar{S}_A + t_{B^-}\bar{S}_{BX} = t_{B^-}\bar{S}_{AX} + t_{A^-}S^*_{A^-} + t_{B^-}S^*_{B^-} + S^*_{ele} \tag{I-19}$$

In eq. (I-19), $\bar{S}_A$ is the partial molar entropy of the component A in the alloy, $\bar{S}_{AX}$ and $\bar{S}_{BX}$ are the partial molar entropies of AX and BX, $S^*_{A^-}$ and $S^*_{B^-}$ are the transported entropies of A^+ and B^+ in the electrolyte [b], S^*_{ele} is the transported entropy of electrons

[b] In the theory of irreversible thermodynamics by Førland et al., only neutral chemical species are considered as thermodynamic components. This definition for thermodynamic components is based on the principle that it is impossible to vary the amount of only one kind of ion without violating the electroneutrality condition. According to this definition, thermodynamic properties of ions such as single ion chemical potentials, which are undefined and unmeasurable quantities, are avoided. Then, one may think that uses of the transported entropy of ions are contradictory with above definition for thermodynamic components. However, it should be noted that the transported entropy is a transport property and is not a thermodynamic property. We can define the transported entropy for the electrolyte as the entropy transferred when one faraday of positive charges are transferred in the electrolyte. The transfer of charges in the electrolyte can be assigned to charge carriers. Thus, when we know the charge carrier species and their respective contribution to the total conduction, i.e. transport numbers, it is possible to assign the transported entropy to charge carriers also. In this manner, the transported entropy of ions can be defined on the operational level. See appendix A for details.

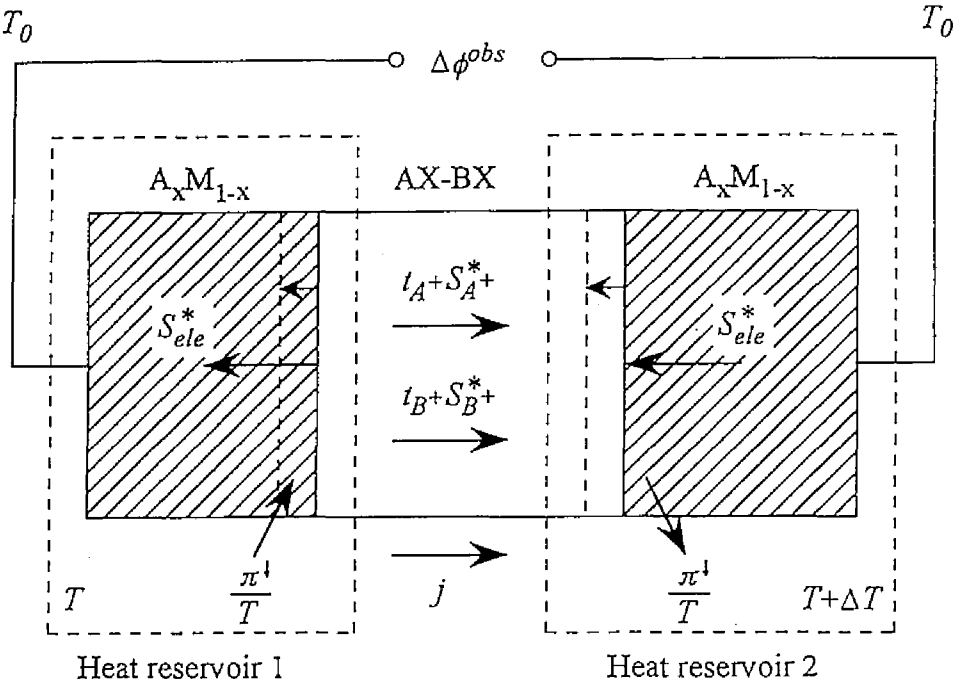

Fig.I-1. Schematic illustration of the nonisothermal cell (I-a) when one faraday of positive charges are trasferred.

Table I-2. Reversible entropy changes at the left hand electrode region of the nonthermal cell (I-a) when one farady of positive charges are transferred.

	Entropy received
$\pi^\downarrow/T$	the interface receives entropy from the heat reservoir.
$\overline{S}_A$	the dissolution of one mole A from the alloy liberates entropy.
$t_B{}^+\overline{S}_{BX}$	the disappearance of $t_B{}^+$ mole BX liberates entropy.
	Entropy consumed
$t_B{}^+\overline{S}_{AX}$	the formation of $t_B{}^+$ mole AX consumes entropy.
$t_A{}^+S_A^{*+}$	entropy transported by $t_A{}^+$ mole A^+ through the electrolyte away from the interface.
$t_B{}^+S_B^{*+}$	entropy transported by $t_B{}^+$ mole B^+ through the electrolyte away from the interface.
S_{ele}^*	entropy transported by electrons through the electrode away from the interface.

in the alloy electrode, and t_{A^+} and t_{B^+} are the internal transport numbers of A^+ and B^+ with reference to anion, X^-. By solving eq. (I-19) with respect to $\pi^{\downarrow}/T$, eq. (I-20) is obtained;

$$\frac{\pi^{\downarrow}}{T} = -\bar{S}_A + t_{B^+}\bar{S}_{AX} - t_{B^+}\bar{S}_{BX} + t_{A^+}S^*_{A^+} + t_{B^+}S^*_{B^+} + S^*_{ele} \qquad \text{(I-20)}$$

For practical measurements, different materials from the electrode alloy are often used as an electrical lead. In this case, the Peltier heat includes also the transported entropy of electrons in the electrical lead metal, S^*_{lead};

$$\frac{\pi^{\downarrow}}{T} = -\bar{S}_A + t_{B^+}\bar{S}_{AX} - t_{B^+}\bar{S}_{BX} + t_{A^+}S^*_{A^+} + t_{B^+}S^*_{B^+} + S^*_{ele} - S^*_{lead} \qquad \text{(I-21)}$$

However, since the transported entropy of electrons in a metal is generally very small, in the order of 10^{-1}~10^{0} $J\cdot mol^{-1}\cdot K^{-1}$ [2, 3], while the other entropies are generally in the order of 10^{1}~10^{3} $J\cdot mol^{-1}\cdot K^{-1}$. Thus, the contribution of S^*_{ele} and S^*_{lead} to the Peltier heat in eq. (I-20) or (I-21) can be regarded as negligibly small. From this consideration, the Peltier heats in eqs. (I-20) and (I-21) can be approximately expressed as eq. (I-22);

$$\frac{\pi^{\downarrow}}{T} = -\bar{S}_A + t_{B^+}\bar{S}_{AX} - t_{B^+}\bar{S}_{BX} + t_{A^+}S^*_{A^+} + t_{B^+}S^*_{B^+} \qquad \text{(I-22)}$$

From eqs. (I-16) and (I-22), the theoretical expression for the thermoelectric power of the nonisothermal cell (I-a), $\varepsilon_{A_xM_{1-x}}$, is obtained;

$$\varepsilon_{A_xM_{1-x}} = \lim_{\Delta T \to 0}\left(\frac{\Delta E}{\Delta T}\right) = \frac{1}{F}\left(\frac{\nabla\phi^{obs}}{\nabla T}\right)_{j=0}$$

$$= \frac{1}{F}\left\{\bar{S}_A - t_{B^+}\bar{S}_{AX} + t_{B^+}\bar{S}_{BX} - t_{A^+}S^*_{A^+} - t_{B^+}S^*_{B^+}\right\} \qquad \text{(I-23)}$$

Equations (I-23) can be rearranged in the following way;

$$\varepsilon_{A_xM_{1-x}} = \frac{1}{F}\left(S_A - t_{B^+}\bar{S}_{AX} + t_{B^+}\bar{S}_{BX} - t_{A^+}S^*_{A^+} - t_{B^+}S^*_{B^+}\right) + \frac{1}{F}\left(\bar{S}_A - S_A\right) \qquad \text{(I-24)}$$

where S_A is the molar entropy of pure A. In the right hand side of eq. (I-24), the terms in the first parentheses divided by the faraday constant are identical with the thermoelectric power of an A^+/A electrode in the AX-BX electrolyte, ε_A. On the other

hand, the terms in the second parentheses show the relative partial molar entropy of the component A in the alloy, $\Delta\bar{S}_A$. Then, eq. (I-24) gives;

$$\varepsilon_{A_xM_{1-x}} = \varepsilon_A + \frac{1}{F}\Delta\bar{S}_A \qquad \text{(I-25)}$$

Equation (I-25) tells us that the thermoelectric power of the nonisothermal cell (I-a) can be estimated from the values of the thermoelectric power of an A^+/A electrode in the AX-BX electrolyte and the relative partial molar entropy of the component A in the alloy.

2.3. Experimental

Before measuring the thermoelectric power and thermodynamic properties of Li-Al alloys, the electrochemical formation of Li-Al alloy was investigated in detail by using a chronopotentiometry and a potential-sweep method at 733 and 803 K. The experimental apparatus is shown in Fig. I-2. The atmosphere inside the cell was dry argon maintained by a gas flow. The experiments were conducted in LiCl-KCl eutectic melt (LiCl : KCl = 58.5 : 41.5 mole %). All chemicals were reagent grade (Wako Pure Chemical Industries, Ltd.). The eutectic mixture of the salts was contained in a high purity alumina crucible (99.5 % Al_2O_3; Nikkato Co., Ltd., SSA-S), and was dried under vacuum for more than 72 hours at 473 K to remove water. After the eutectic mixture was melted, a pre-electrolysis was carried out with the terminal voltage of 2.5 V, in order to remove residual water contamination further. A spiral of platinum wire and a glassy carbon rod were used as a cathode and an anode, respectively, for the pre-electrolysis. When the current density became less than 0.5 $mA \cdot cm^{-2}$, the pre-electrolysis was terminated.

A Ag^+/Ag electrode or a Li-Al alloy electrode in the two-phase (αAl+βLiAl) concentration region was used as a reference electrode. The Ag^+/Ag electrode comprised

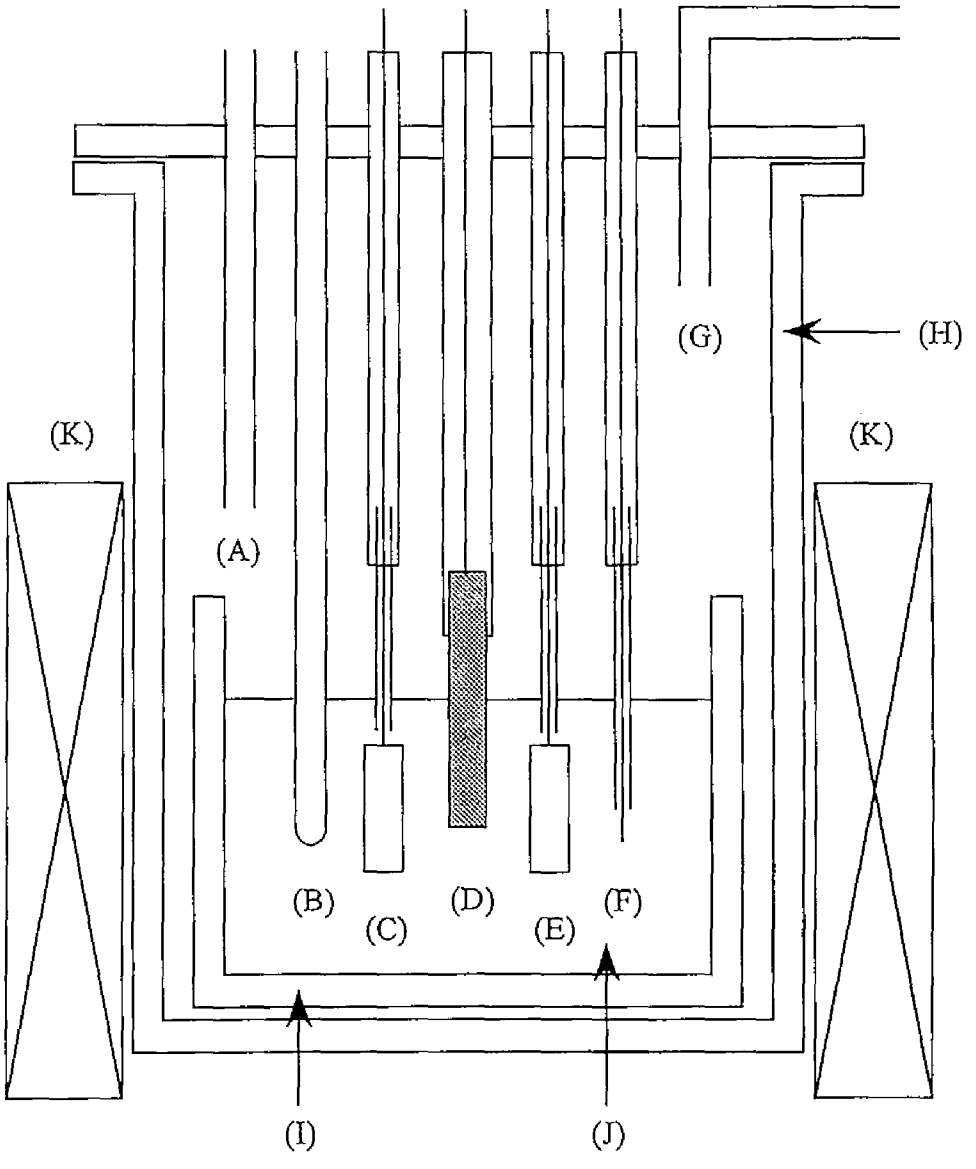

Fig.I-2. The experimental apparatus: (A) Ar gas inlet, (B) thermocouple, (C) working electrode, (D) counter electrode, (E) reference electrode, (F) Li^+/Li electrode, (G) Ar gas outlet, (H) pyrex holder, (I) crucible, (J) LiCl-KCl eutectic melt, and (K) furnace.

a silver wire and LiCl-KCl eutectic melt containing 1 mol% AgCl, which were both contained in a pyrex glass tube with a very thin bottom. The potential of the reference electrode was calibrated relative to the potential of a Li^+/Li electrode, which was prepared by electrodepositing lithium metal on a nickel wire [4]. A Li-Al alloy in the (αAl+βLiAl) phase or a glassy carbon (5 mm dia. x 25 mm) was used as a counter electrode. The Li-Al alloy used as the reference and the counter electrodes was prepared by electrodepositing lithium on an aluminum sheet (10 x 8 x 0.3 mm for the reference electrode and 30 x 10 x 0.8 mm for the counter electrode, Wako Pure Chemical Industries, Ltd.) in another cell. A working electrode was a pure aluminum sheet (99.99 %, 9 x 15 x 0.8 mm) or a pure aluminum wire (99.99 %, 1 mm dia. x 10 mm). The analysis of the electrochemically formed alloy electrodes were conducted by using the powder x-ray diffraction technique (XRD) in dry argon atmosphere.

Thermodynamic properties for the two-phase (αAl+βLiAl), (βLiAl+γLi_3Al_2), and (γLi_3Al_2+liq.) regions in Li-Al alloy were determined from *emf* measurements of the isothermal cell (I-b) at 670~760 K;

(T) Li | LiCl-KCl | Li-Al (T) (I-b)

The Li-Al alloy in each coexisting phase state was prepared by a constant current electrolysis from pure aluminum. The *emf* of the alloy was determined by a rest potential which was observed after a current interruption.

The thermoelectric power of a Li-Al alloy electrode is defined as the slope of the *emf* of the nonisothermal cell (I-c) related to temperature difference between the electrodes;

(T) Li -Al | LiCl-KCl | Li-Al ($T+\Delta T$) (I-c)

where both alloy electrodes have a same composition. The thermoelectric power of Li-Al alloy electrodes in the two-phase (αAl+βLiAl) region was measured in this type of

nonisothermal cell. The thermoelectric power of a Li-Al alloy electrode can be also determined from *emf* measurements of the nonisothermal cell (I-d);

$$(T)\ \text{Li}\ |\ \text{LiCl-KCl}\ |\ \text{Li-Al}\ (T+\Delta T) \qquad \text{(I-d)}$$

The *emf* value of the cell (I-d) is, of course, different from that of the cell (I-c). However, the slope of the *emf*, i.e. the thermoelectric power, should be identical with each other. Because of simple experimental procedures, the cell (I-d) was chosen for thermoelectric power measurements for Li-Al alloy electrodes in the two-phase (βLiAl+γLi_3Al_2), (γLi_3Al_2+liq.), and (βLiAl+liq.) regions in this study.

The experimental apparatus used for thermoelectric power measurements is shown in Fig. I-3. The purification procedure of the salt, each electrode used, and the atmosphere inside the cell were all the same as those described above. A temperature difference was established between the left part and the right part of the H-type cell by controlling two separate heaters independently. The temperatures were measured by Chromel-Alumel thermocouples placed close to the electrodes. Uncertainties in absolute temperature were ±2 K after careful calibration, while the uncertainty in the temperature difference was much lower, possibly ±0.5 K. The temperature of the left part which contains the reference electrode was kept constant at 735 K, while the temperature of the right part which contains the working electrode was varied from 673 to 823 K. After establishing a certain temperature difference, the potential of Li-Al alloy working electrode in each phase state was measured by two methods: (i) a potentiometric method and (ii) a potential-sweep method. In the former method, the Li-Al alloy in each phase state was formed by constant-current electrolysis, and the potential of Li-Al alloy electrode was determined by a rest potential after a current interruption. In the latter method, the potential of Li-Al alloy electrode was determined by the potential extrapolated to the point $I = 0$ when current increased sharply during the potential-sweep.

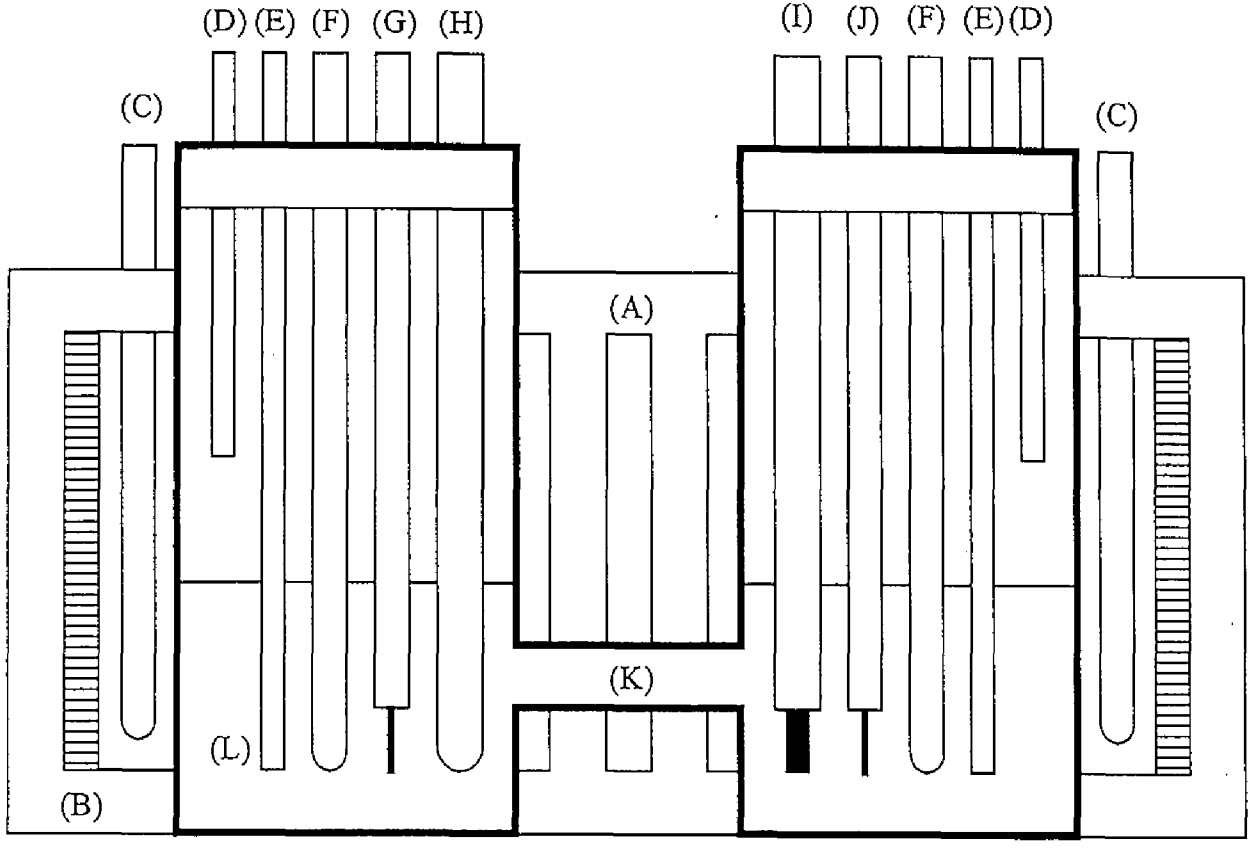

Fig.I-3. The experimental apparatus for thermoelectric power measurements: (A) fire brick, (B) electric furnance, (C) thermocouple (for control), (D) Ar gas outlet, (E) Ar gas inlet, (F) thermocouple (for measurement), (G) Li^+/Li electrode (nickel wire), (H) reference electrode, (I) counter electrode, (J) working electrode, (K) H-type cell, and (L) LiCl - KCl eutectic melt.

2.4. Results and discussion

2.4.1. Electrochemical formation

A constant current electrolysis was carried out with an aluminum electrode at 733 and 803 K. Figure I-4 shows a typical chronopotentiogram obtained during the constant current electrolysis (current density: -20 $mA \cdot cm^{-2}$). In the potential transient

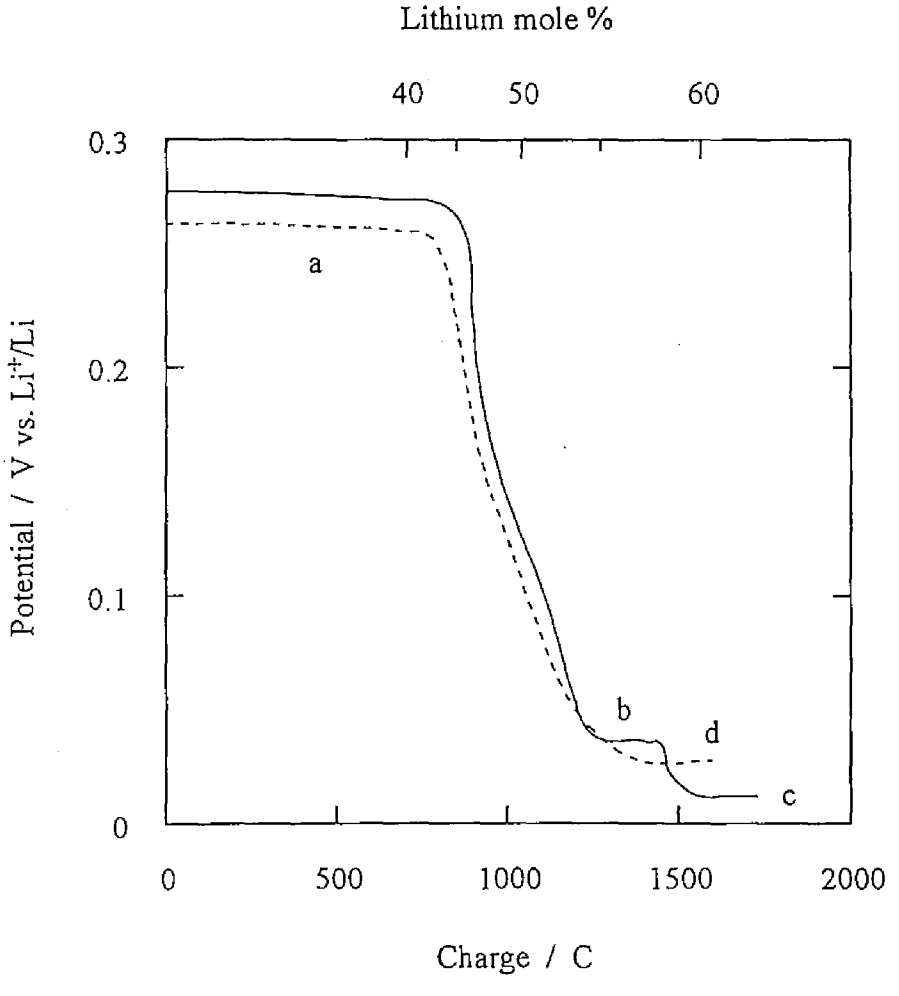

Fig.I-4. Potential transient curve of an aluminum electrode in LiCl-KCl eutectic melt at 733 K (——) and 803 K (- - -), current density: -20 $mA \cdot cm^{-2}$.

curve at 733 K represented by the solid line in Fig. I-4, three potential plateaus a, b, and c are observed. These three potential plateaus are attributed to the formation of various types of aluminum alloy with lithium, since they were not observed in a case of using a nickel electrode which does not form any alloys with lithium. XRD analysis of alloy electrodes at room temperature revealed that the alloy which showed the potential a contains the βLiAl, and the β'$LiAl_3$ phases, and the alloy which showed the potential b contains the γLi_3Al_2 phase. The β'$LiAl_3$ phase is a metastable phase, and is generally observed only at low temperature below around 620 K [5, 6]. From the results of XRD analysis and the phase diagram of the Li-Al alloy system shown in Fig. I-5 [6], the formation of the βLiAl, γLi_3Al_2, and liquid phases are considered to occur at the potential plateau a, b, and c, respectively, as represented by the following reaction

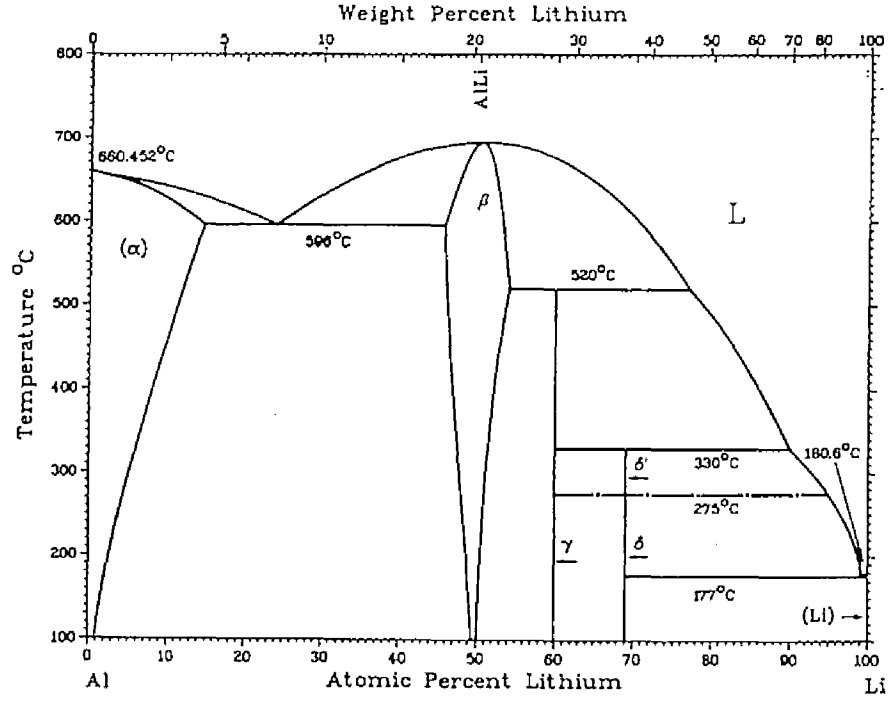

Fig.I-5. Phase diagram of Li-Al alloy system according to McAlister [6].

formulae [c] ;

a ; $\alpha Al + Li^+ + e^- \rightarrow \beta LiAl$ (I-i)

b ; $2\,\beta LiAl + Li^+ + e^- \rightarrow \gamma Li_3Al_2$ (I-ii)

c ; $\gamma Li_3Al_2 + Li^+ + e^- \rightarrow$ liq.-phase (I-iii)

In the reaction formula (I-i), αAl indicates the Li-saturated solid solution. In the reaction formula (I-iii), liq.-phase expresses the liquid Li-Al alloy at the solubility limit.

In the potential transient curve at 803 K shown by the dashed line in Fig. I-4, only two potential plateaus a and d are observed. At this temperature, the γLi_3Al_2 phase does not exist, as can be seen in the phase diagram. Thus, it is concluded that the liquid phase is formed from the βLiAl phase at the potential d, as represented by the following reaction formulae [c];

d ; $\beta LiAl + Li^+ + e^- \rightarrow$ liq.-phase (I-iv)

A potential sweeps with an aluminum electrode were carried out with a very slow scan rate (0.1 $mV \cdot s^{-1}$) at 735 and 803 K. Figure I-6 shows a typical voltammogram. Three cathodic current peaks are observed on the voltammogram at 733 K shown by the solid line in Fig. I-6. The current peaks a', b', and c' seem to correspond to the formation of the βLiAl, γLi_3Al_2, and liquid phase, respectively. On the anodic sweep, three anodic current peaks, corresponding to the cathodic current peaks, are observed. These three anodic current peaks come from the dissolution of lithium from each phase in Li-Al alloy. On the other hand, the current peak b' disappeared, and only two current peaks a' and d' are observed on the voltammogram at 803 K, represented by the dashed line in Fig. I-6. At the cathodic current peak d', liquid phase is formed from the βLiAl phase. Such tendencies and the potentials for the formation of each phase in Li-Al alloy

---

[c] The reaction formulae (I-i)~(I-iv) are simplified expressions and are not correct in a rigorous sense, because in Li-Al alloy system the chemical formula for each phase at the phase boundary is not simple as that used in these reaction formulae. For example, at 735 K, 'αAl' is $Li_{0.10}Al_{0.90}$, 'βLiAl' is $Li_{0.44}Al_{0.56}$ in (I-i) and $Li_{0.54}Al_{0.46}$ in (I-ii), and 'liq.-phase' is $Li_{0.93}Al_{0.07}$. It should be also noted that the lithium concentration in each phase at the phase boundary varies with temperature as shown in the phase diagram.

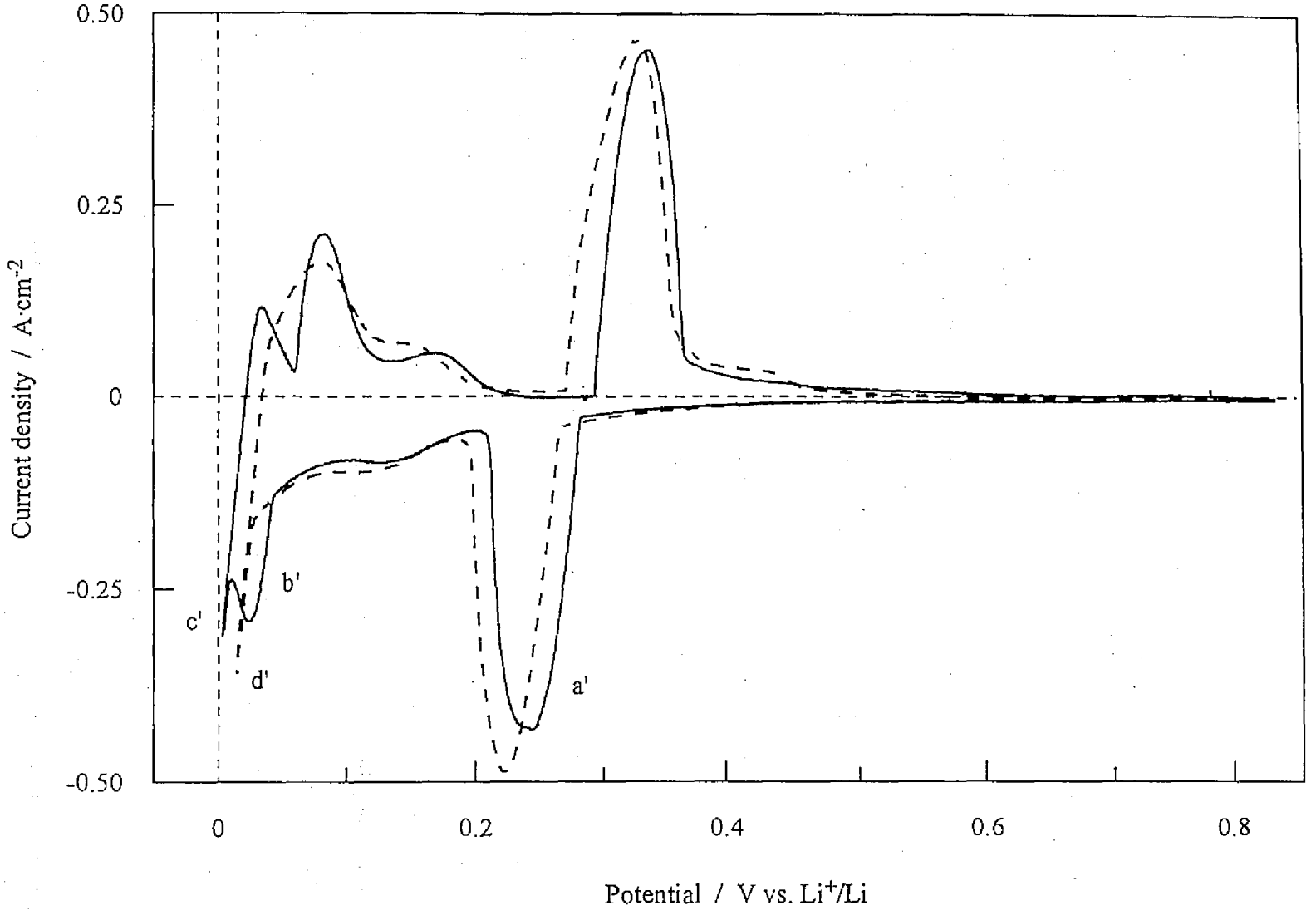

Fig.I-6. Cyclic voltammograms of an aluminum electrode in LiCl-KCl eutectic melt at 733 K (——) and 803 K (- - -),scan rate: 0.1 $mV \cdot s^{-1}$.

obtained by this method are in good agreement with those obtained by the potentiometric method.

2.4.2. Thermodynamic properties

The results for *emf* measurements of the isothermal cell (I-b) are presented in Figs. I-7(A)~(C). The relationship between *emf* and temperature is linear for the two-phase (αAl+βLiAl) and (βLiAl+γLi_3Al_2) regions, while the relation is not linear for the two-phase (γLi_3Al_2+liq.) region. In the temperature range of 670~760 K, they are also represented by the following relations;

αAl+βLiAl ; $E = 0.4627\ (\pm 0.0032) - 0.2457\ (\pm 0.004) \times 10^{-3} \times T$ (I-26)

βLiAl+γLi_3Al_2 ; $E = 0.2340\ (\pm 0.0016) - 0.2505\ (\pm 0.002) \times 10^{-3} \times T$ (I-27)

γLi_3Al_2+liq. ; $E = 0.3035\ (\pm 0.1952) - 9.728\ (\pm 5.425) \times 10^{-4} \times T + 7.915\ (\pm 3.766) \times 10^{-7} \times T^2$ (I-28)

where E is *emf* in V and T is temperature in K. In Fig. I-7(A), the values measured by Sharma et al. [7], Wen et al. [8] are also shown for comparison. The *emf* values for the two-phase (αAl+βLiAl) region obtained in this work agree fairly well with those obtained by Sharma et al..

These *emf* measurements under equilibrium conditions at various temperature made it possible to calculate the relative partial molar thermodynamic properties of lithium for each coexisting phase in Li-Al alloy: the lithium activity a_{Li}, the relative partial molar free energy $\Delta\overline{G}_{Li}$, the relative partial molar entropy $\Delta\overline{S}_{Li}$, and the relative partial molar enthalpy $\Delta\overline{H}_{Li}$, according to following well-known equations;

$$\Delta\overline{G}_{Li} = RT\ln a_{Li} = -nFE \tag{I-29}$$

$$\Delta\overline{S}_{Li} = -\frac{\partial\left(\Delta\overline{G}_{Li}\right)}{\partial T} \tag{I-30}$$

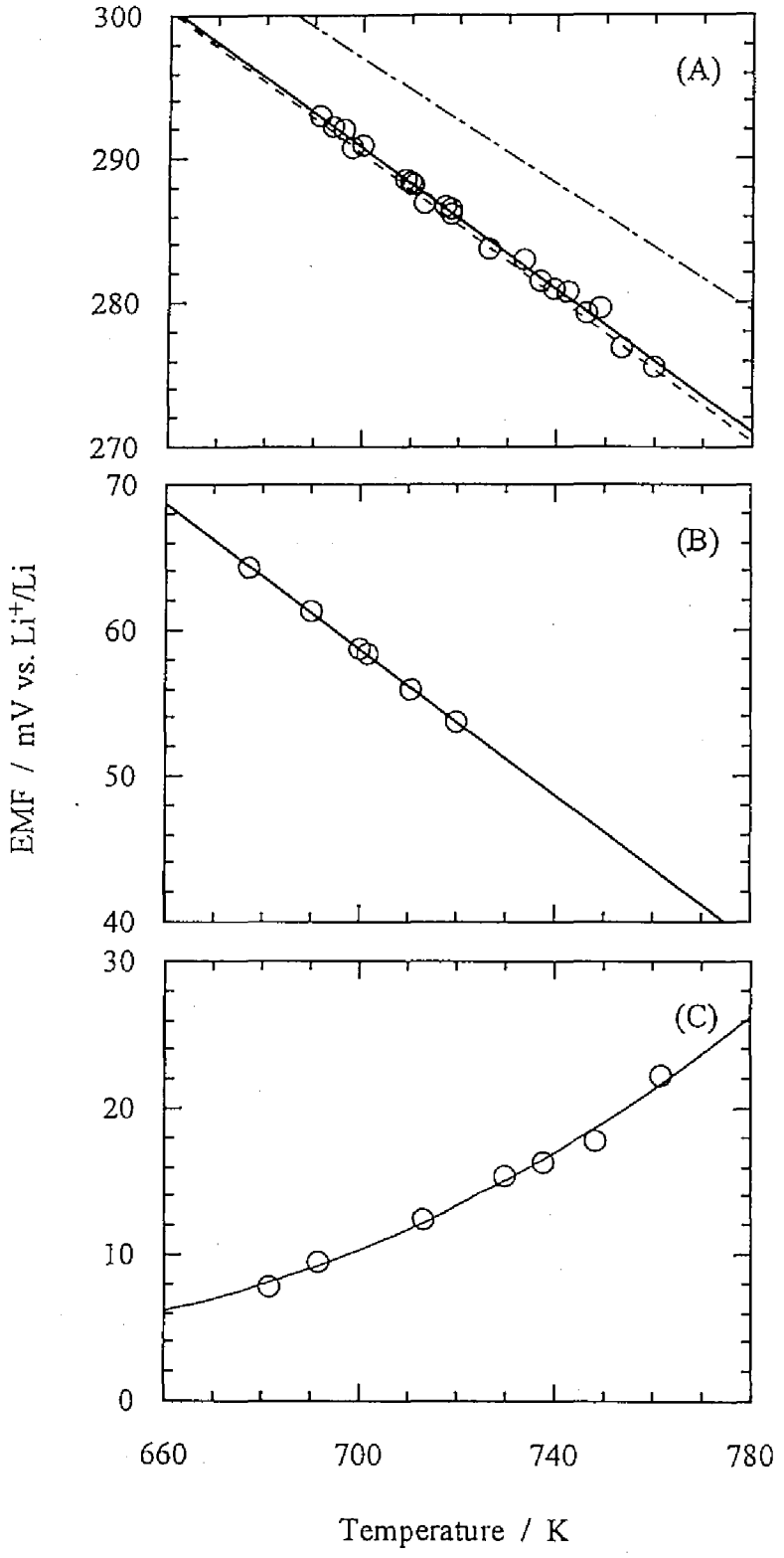

Fig.I-7. *Emf* as a function of temperature in the isothermal cell (I-b) with a Li-Al alloy electrode in the coexisting phase states: (A) αAl+βLiAl, (B) βLiAl+γLi_3Al_2, and (C) γLi_3Al_2+liq.. The dashed line (- - -) and the dash-dotted line (- · - · -) show the values obtained by Sharma et al. [7] and by Wen et al. [8], respectively.

$$\Delta\overline{H}_{Li} = \Delta\overline{G}_{Li} + T\frac{\partial\left(\Delta\overline{G}_{Li}\right)}{\partial T} \qquad \text{(I-31)}$$

The relative partial molar thermodynamic properties of lithium for the two-phase (αAl+βLiAl), (βLiAl+γLi_3Al_2), and (γLi_3Al_2+liq.) regions in Li-Al alloy at 735 K are given in Table I-3. The relative partial molar thermodynamic properties of lithium for the two-phase (αAl+βLiAl) region were determined from *emf* measurements by Sharma et al. [8] and by Wen et al. [9], and from hydrogen titration method by Veleckis [9]. The values obtained in this work for the two-phase (αAl+βLiAl) region are in good agreement with their values. For the two-phase (βLiAl+γLi_3Al_2) region, it was found that the relative partial molar entropy of lithium has a negative value, while the results by Wen et al. suggested a positive value [9].

2.4.3. Thermoelectric power

Figure I-8 shows the potential of a Li-Al alloy electrode in the coexisting (αAl+βLiAl) region as a function of temperature difference between electrodes. The vertical axis of this figure presents the potential of the alloy versus that of the alloy of

Table I-3. Relative partial molar thermodynamic properties of lithium in coexisting phase states of Li-Al alloy at 735 K.

Phase state	a_{Li}	$\Delta\overline{G}_{Li}$ kJ·mol^{-1}	$\Delta\overline{H}_{Li}$ kJ·mol^{-1}	$\Delta\overline{S}_{Li}$ J·mol^{-1}·K^{-1}
αAl + βLiAl	1.2 x 10^{-2}	-27.2	-44.6	-23.7
βLiAl + γLi_3Al_2	4.5 x 10^{-1}	-4.8	-22.6	-24.2
γLi_3Al_2 + liq.	7.8 x 10^{-1}	-1.5	+12.0	+18.4

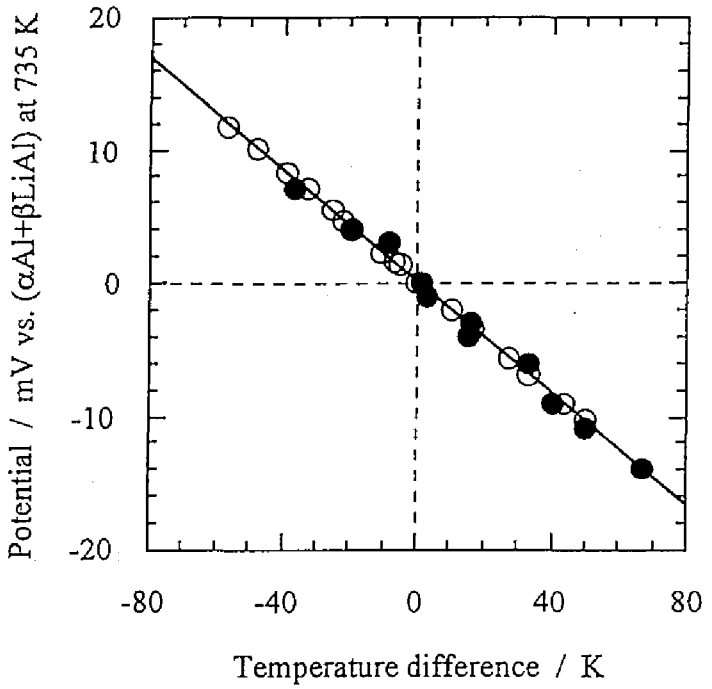

Fig.I-8. Potential for the two-phase (αAl+βLiAl) region as a function of temperature difference measured by the potentiometric (○) and the potential-sweep (●) methods.

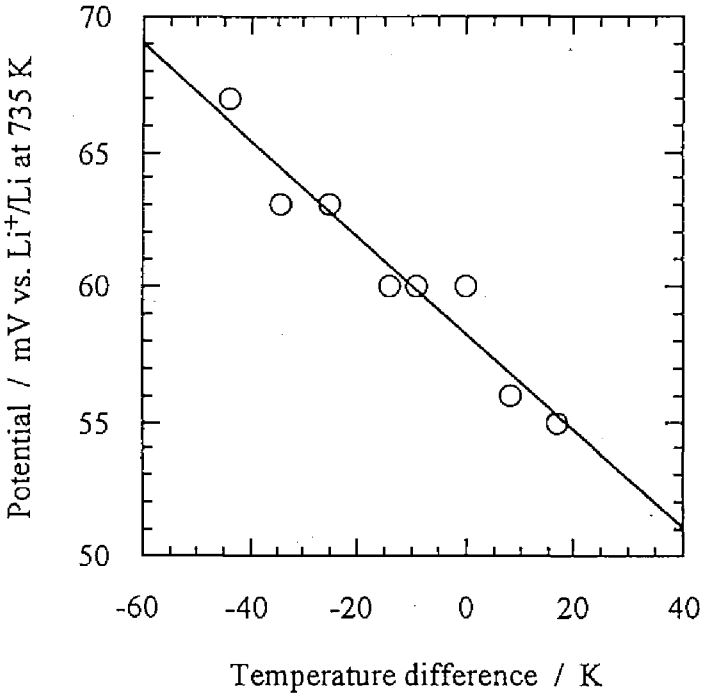

Fig.I-9. Potential for the two-phase (βLiAl+γLi_3Al_2) region as a function of temperature difference measured by the potential-sweep methods.

the same kind at 735 K, and horizontal axis shows the temperature difference from 735 K. The thermoelectric power is given as the derivative of the potential-temperature relation. A linear relationship between the potential of the alloy and temperature difference is observed in Fig. I-8. The thermoelectric power of Li-Al alloy in this phase region has a negative and constant value, -0.210 (±0.001) $mV \cdot K^{-1}$. The thermoelectric power obtained by two methods, the potentiometric method and the potential-sweep method, are in good agreement with each other. This shows that these two thermoelectric power measurement methods are both available.

The experimental results of thermoelectric power measurements obtained with a Li-Al alloy electrode in the two-phase ($\beta LiAl+\gamma Li_3Al_2$) region are presented in Fig. I-9. In this figure, the vertical axis shows the potential referred to Li^+/Li electrode at 735 K. The thermoelectric power for a Li-Al alloy electrode in this concentration region has the same tendencies with those in the two-phase ($\alpha Al+\beta LiAl$) region, and is obtained to be -0.180 (±0.019) $mV \cdot K^{-1}$.

The potential for a Li-Al alloy electrode in the two-phase (γLi_3Al_2+liq.) region as a function of temperature difference is shown in Fig. I-10. In this phase region, two quite different tendencies are observed from the results obtained with a Li-Al alloy in the two-phase ($\alpha Al+\beta LiAl$) and ($\beta LiAl+\gamma Li_3Al_2$) regions. First, the sign of thermoelectric power is positive, and second, its value significantly depends on temperature. The thermoelectric power of a Li-Al alloy electrode in this region can be approximately expressed as eq. (I-32) when ΔT is between -60 and +60 K;

$$\varepsilon = 0.237\ (\pm 0.06) + 1.63\ (\pm 0.39) \times 10^{-3} \times \Delta T \qquad mV \cdot K^{-1} \qquad \text{(I-32)}$$

where ΔT stands for the temperature difference from 735 K: $\Delta T = T - 735$.

The experimental result of the thermoelectric power measurements of a Li-Al alloy electrode in the coexisting ($\beta LiAl$+liq.) region is shown in Fig. I-11. In this concentration region, the thermoelectric power has the same tendencies as that of Li-Al alloy in the two-phase (γLi_3Al_2+liq.) region. The thermoelectric power in this region can

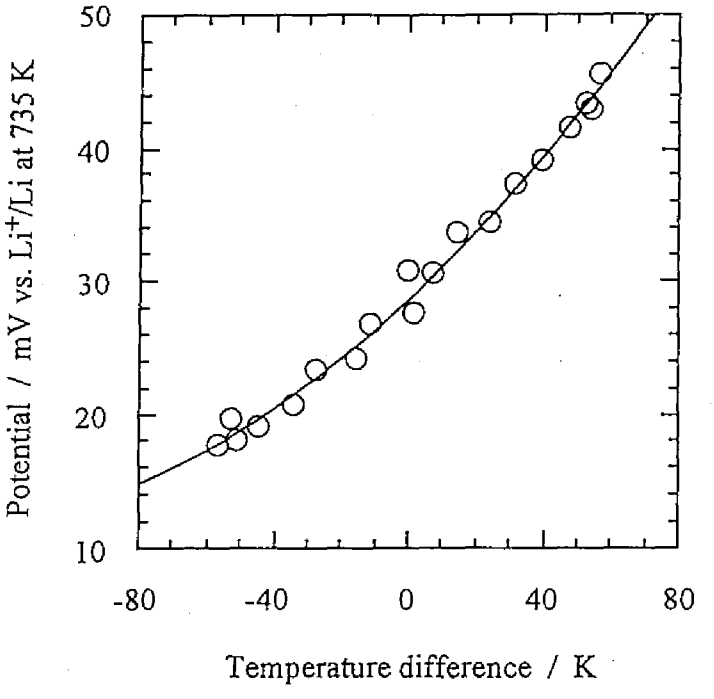

Fig.I-10. Potential for the two-phase (γLi_3Al_2+liq.) region as a function of temperature difference measured by the potential-sweep methods.

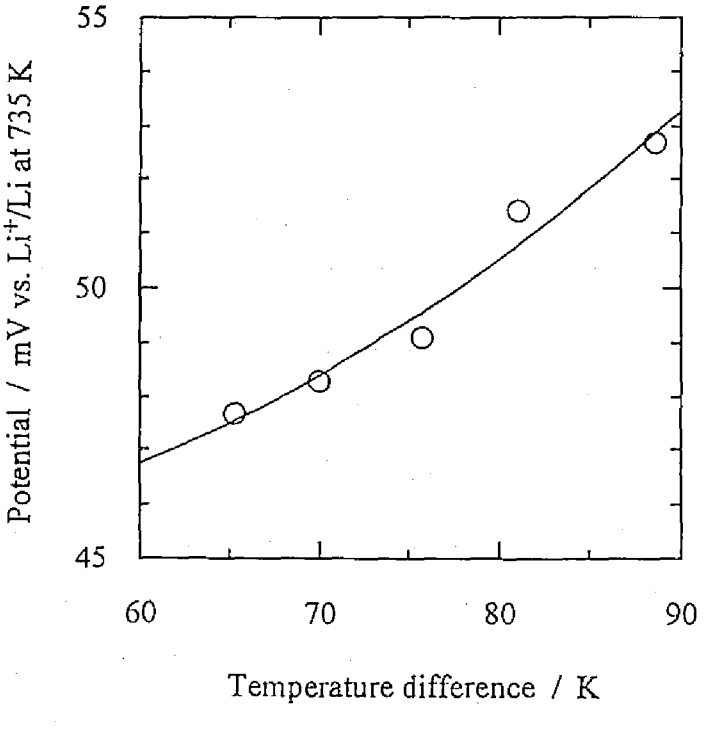

Fig.I-11. Potential for the two-phase (βLiAl+liq.) region as a function of temperature difference measured by the potential-sweep methods.

be approximately expressed as eq. (I-33) when ΔT is from +65 to +90K;

$$\varepsilon = 0.210\ (\pm 1.19) + 5.68\ (\pm 1.55) \times 10^{-3} \times \Delta T \qquad \text{mV·K}^{-1} \qquad \text{(I-33)}$$

According to eqs. (I-23) and (I-25), the thermoelectric power of the cell (I-c) or (I-d) can be expressed;

$$\varepsilon_{Li-Al} = \frac{1}{F}\left\{-\bar{S}_{Li} + t_{K^+}.\bar{S}_{LiCl} - t_{K^+}.\bar{S}_{KCl} + t_{Li^+}.S^{\bullet}_{Li^+} + t_{K^+}.S^{\bullet}_{K^+}\right\}$$

$$= \varepsilon_{Li} + \frac{1}{F}\Delta\bar{S}_{Li} \qquad \text{(I-34)}$$

The thermoelectric power of a Li^+/Li electrode in LiCl-KCl eutectic melt was measured to be +0.030 (±0.013) mV·K^{-1} by Kamata et al. [10]. The relative partial molar entropy of lithium in the alloy can be obtained from *emf* measurements of the alloy electrode at various temperature relative to the potential of a Li^+/Li electrode according to eq. (I-30). For the coexisting (αAl+βLiAl), (βLiAl+γLi_3Al_2), and (γLi_3Al_2+liq.) regions in Li-Al alloy, the values given in Table I-3 are available. The estimated values as well as the experimental values of the thermoelectric power for various coexisting phase states are presented in Table I-4. The estimated values agree with the observed values. These

Table I-4. Measured and estimated thermoelectric power of Li-Al alloy electrodes in coexisting phase states in LiCl-KCl eutectic melt.

Phase state	Thermoelectric power / mV·K^{-1}	
	Measured value	Estimated value
αAl+βLiAl	-0.210 (±0.001)	-0.216 (±0.017)
βLiAl+γLi_3Al_2	-0.180 (±0.019)	-0.221 (±0.015)
γLi_3Al_2+liq.	+0.237 *	+0.221 *
βLiAl+liq.	+0.176 **	——

The values labelled with * and ** are data at 735K and 803K, respectively.

results confirm that the thermoelectric power of a lithium alloy electrode can be estimated by using eq. (I-34). It was found from *emf* measurements that the relative partial molar entropy of lithium for the two-phase (γLi_3Al_2+liq.) region increases with increasing temperature while the relative partial molar entropies of lithium for the coexisting (αAl+βLiAl) and (βLiAl+γLi_3Al_2) regions are constant in the temperature range of 670~760 K. The temperature dependencies of the thermoelectric power of Li-Al alloy electrodes are also consistent with those of the relative partial molar entropies of lithium.

2.4.4. Single electrode Peltier heat

From eq. (I-16), the relation between the single electrode Peltier heat and the thermoelectric power can be obtained as follows;

$$\pi^{\downarrow} = \pm \varepsilon T \qquad \text{(I-35)}$$

where the signs + and - are for cathodic and anodic reactions, respectively. The unit of the single electrode Peltier heat in eq. (I-35) is $J \cdot C^{-1}$.

From the measured value of the thermoelectric power, the single electrode Peltier heat for the electrochemical formation of each phase in Li-Al alloy, i.e. for the cathodic reaction of a Li-alloy electrode, can be then evaluated as follows;

the formation of the βLiAl from the αAl;

$$\pi^{\downarrow} = -2.10 \times 10^{-4} \times T \qquad (673\text{K} \leq T \leq 823\text{K}) \qquad \text{(I-36)}$$

the formation of the γLi_3Al_2 from the βLiAl;

$$\pi^{\downarrow} = -1.80 \times 10^{-4} \times T \qquad (673\text{K} \leq T \leq 793\text{K}) \qquad \text{(I-37)}$$

the formation of the liquid phase from the γLi_3Al_2;

$$\pi^{\downarrow} = -9.61 \times 10^{-4} \times T + 1.63 \times 10^{-6} \times T^2 \qquad (673\text{K} \leq T \leq 793\text{K}) \qquad \text{(I-38)}$$

the formation of the liquid phase form the βLiAl;

$$\pi^{l} = -1.01 \times 10^{-1} \times T + 1.31 \times 10^{-4} \times T^{2} \quad (793\mathrm{K} \leq T \leq 843\mathrm{K}) \tag{I-39}$$

The values of the single electrode Peltier heats for electrochemical formation reactions of various phases in Li-Al alloy in LiCl-KCl eutectic melt are summarized in Table I-5. It is found that the electrochemical formation of the βLiAl from the αAl and that of the γLi_3Al_2 from the βLiAl, which are expressed by the reaction formulae (I-i) and (I-ii), respectively, are accompanied by heat evolution. On the other hand, heat is absorbed for the electrochemical formation of the liquid phase from the βLiAl and the γLi_3Al_2, which are represented by the reaction formulae (I-iii) and (I-iv), respectively.

Table I-5. Single electrode Peltier heats for the formation reactions of various phases in Li-Al alloy in LiCl-KCl eutectic melt.

Temperature / K	Single electrode Peltier heat / $J \cdot C^{-1}$			
	αAl → βLiAl	βLiAl → γLi_3Al_2	βLiAl → liq.	γLi_3Al_2 → liq.
650	-0.14	-0.12	——	+0.06
700	-0.15	-0.13	——	+0.13
750	-0.16	-0.14	——	+0.20
800	-0.17	——	+0.13	——

2.5. Conclusions

1. The single electrode Peltier heats of the formation reaction for various phases in Li-Al alloy could be estimated from the measured values of the thermoelectric power. It was found that the formation reaction of the βLiAl phase from the αAl phase and that of the γLi_3Al_2 phase from the βLiAl are exothermic, and the formation reactions of the liquid phase from the βLiAl and the γLi_3Al_2 phase are endothermic.

2. The general method of estimating the thermoelectric power of a Li-alloy electrode was derived thermodynamically: thermoelectric power of a Li-alloy electrode can be expressed as sum of the relative partial molar entropy of lithium in the alloy and the thermoelectric power of a Li^+/Li electrode. The experimental results for the two-phase (αAl+βLiAl), (βLiAl+γLi_3Al_2), and (γLi_3Al_2+liq.) regions validated this estimation method.

References

[1] K. S. Førland, T. Førland, and S. K. Ratkje, *Irreversible Thermodynamics, Theory and applications*, 2nd repr., Wiley, Chichester (1994).

[2] M. V. Vedernikov, *Advances in Phys.*, **18**, 337 (1969).

[3] P. W. Kendall, *Phys. and Chem. Liquids*, **1**, 33 (1968).

[4] T. Takenaka, Y. Ito, and J. Oishi, *Denki Kagaku*, **53**, 476 (1985).

[5] D. B. Williams and J. W. Edington, *Met. Sci.*, **9**, 529 (1975).

[6] A. J. McAlister, *Bull. Alloy Phase Diagrams*, **3**, 177 (1982).

[7] R. A. Sharma and R. N. Seefurth, *J. Electrochem. Soc.*, **123**, 1763 (1976).

[8] C. J. Wen, B. A. Boukamp, R. A. Huggins, and W. Weppner, *J. Electrochem. Soc.*, **126**, 2258 (1979).

[9] E. Veleckis, *J. Less-Common Met.*, **73**, 49 (1980).

[10] M. Kamata, M. Inoue, Y. Ito, and J. Oishi, *J. Electrochem. Soc.*, **136**, 528 (1989).

Chapter 3

Single electrode Peltier heats of Li-Al alloy electrodes in single phase states

3.1. Introduction

In the previous chapter, the single electrode Peltier heats of a Li-Al alloy electrodes in various coexisting phase states in LiCl-KCl eutectic melt were evaluated from measured thermoelectric power values. It was found that the thermoelectric power, thus the single electrode Peltier heat, of a Li-Al alloy electrode in each coexisting phase state has a constant value at a constant temperature. However, the value of the thermoelectric power of an alloy electrode changes drastically with change of its phase state. In order to understand the effect of the phase change on the single electrode Peltier heat, it is important to investigate how the thermoelectric power changes on a coexisting-single phase boundary, and to investigate how the thermoelectric power depends on the alloy composition in a single phase region.

In chapter 2, it was also shown that the thermoelectric power of a lithium alloy electrode can be expressed as the sum of the relative partial molar entropy of lithium in the alloy and the thermoelectric power of a Li^+/Li electrode. This relation should be valid for a lithium alloy electrode in a single phase state as well as for that in a coexisting phase state. The thermoelectric power of a Li^+/Li electrode is regarded as constant in LiCl-KCl eutectic melt [1]. Thus, the effect of the phase change on the thermoelectric

power is considered to arise from the change of the relative partial molar entropy of lithium in the alloy.

In this chapter thermodynamic properties of Li-Al alloy in the single βLiAl phase region are determined from *emf* measurements as a function of lithium concentration. The lithium concentration dependence of relative partial molar thermodynamic properties of the single βLiAl phase are discussed in terms of defect structure of the alloy. The single electrode Peltier heat of a Li-Al alloy electrode is evaluated as a function of lithium concentration. The effect of the phase change on the single electrode Peltier heat is discussed thermodynamically.

3.2. Principles

In this section we first derive the relation between thermodynamic properties of a binary alloy in a coexisting phase and those in its adjacent single phase. Thereafter, the change of the single electrode Peltier heat on a coexisting-single phase boundary is discussed.

3.2.1. Thermodynamic properties on a coexisting-single phase boundary

Here we discuss a binary alloy which consists of two components, A and M. We designate *i* and *j* for the two phases. In the coexisting phase state of *i* and *j* phases, the relative partial molar free energies of the component A in the two phases should be equal with each other;

$$\Delta\overline{G}_A^i = \Delta\overline{G}_A^j \qquad \text{(I-40)}$$

Differentiating eq. (I-40) with respect to temperature, eq. (I-41) is obtained;

$$\frac{d\left(\Delta\overline{G}_A^i\right)}{dT} = \frac{d\left(\Delta\overline{G}_A^j\right)}{dT} \tag{I-41}$$

Both of $\Delta\overline{G}_A^i$ and $\Delta\overline{G}_A^j$ are a function of not only temperature but also of the concentration of component A, x_A^i and x_A^j, on each coexisting-single phase boundary. Equation (I-41) then can be written as eq. (I-42);

$$\left\{\frac{\partial\left(\Delta\overline{G}_A^i\right)}{\partial T}\right\}_{x_A^i} + \left\{\frac{\partial\left(\Delta\overline{G}_A^i\right)}{\partial x_A^i}\right\}_T \left(\frac{dx_A^i}{dT}\right) = \left\{\frac{\partial\left(\Delta\overline{G}_A^j\right)}{\partial T}\right\}_{x_A^j} + \left\{\frac{\partial\left(\Delta\overline{G}_A^j\right)}{\partial x_A^j}\right\}_T \left(\frac{dx_A^j}{dT}\right) \tag{I-42}$$

The first terms in the right and left hand sides in eq. (I-42) correspond to the relative partial molar entropies of component A for the single *i* phase and for the single *j* phase on the phase boundaries, respectively. Then we obtain eq. (I-43);

$$\Delta\overline{S}_A^i - \left\{\frac{\partial\left(\Delta G_A^i\right)}{\partial x_A^i}\right\}_T \left(\frac{dx_A^i}{dT}\right) = \Delta\overline{S}_A^j - \left\{\frac{\partial\left(\Delta\overline{G}_{Ai}^j\right)}{\partial x_A^j}\right\}_T \left(\frac{dx_A^j}{dT}\right) \tag{I-43}$$

For component M, eq. (I-44) can be obtained in a similar way;

$$\Delta\overline{S}_M^i - \left\{\frac{\partial\left(\Delta\overline{G}_M^i\right)}{\partial x_M^i}\right\}_T \left(\frac{dx_M^i}{dT}\right) = \Delta\overline{S}_M^j - \left\{\frac{\partial\left(\Delta\overline{G}_M^j\right)}{\partial x_M^j}\right\}_T \left(\frac{dx_M^j}{dT}\right) \tag{I-44}$$

Since the concentration of component M is related to that of component A by $x_M = 1 - x_A$, eq. (I-44) is rewritten as follows;

$$\Delta\overline{S}_M^i - \left\{\frac{\partial\left(\Delta\overline{G}_M^i\right)}{\partial x_A^i}\right\}_T \left(\frac{dx_A^i}{dT}\right) = \Delta\overline{S}_M^j - \left\{\frac{\partial\left(\Delta\overline{G}_M^j\right)}{\partial x_A^j}\right\}_T \left(\frac{dx_A^j}{dT}\right) \tag{I-45}$$

In the two-phase (*i*+*j*) region, the following reaction takes place when 1 mol of component A is added to the alloy;

$$\frac{1-x_A^j}{x_A^j - x_A^i} A_{x_A^i} M_{1-x_A^i} + A \rightarrow \frac{1-x_A^i}{x_A^j - x_A^i} A_{x_A^j} M_{1-x_A^j} \tag{I-v}$$

The relative partial molar entropy of component A in the two-phase (*i*+*j*) region is equal to the entropy change of the reaction (I-v), and can be expressed by the following equation;

$$\Delta\bar{S}_A^{i+j} = \frac{1-x_A^i}{x_A^j - x_A^i}\left\{x_A^j \Delta\bar{S}_A^j + \left(1-x_A^j\right)\Delta\bar{S}_M^j\right\} - \frac{1-x_A^j}{x_A^j - x_A^i}\left\{x_A^i \Delta\bar{S}_A^i + \left(1-x_A^i\right)\Delta\bar{S}_M^i\right\} \tag{I-46}$$

From eqs. (I-43), (I-45), and (I-46), and the Gibbs-Duhem relation, we obtain;

$$\Delta\bar{S}_A^{i+j} = \Delta\bar{S}_A^i - \left\{\frac{\partial\left(\Delta\bar{G}_A^i\right)}{\partial x_A^i}\right\}_T \left(\frac{dx_A^i}{dT}\right) = \Delta\bar{S}_A^j - \left\{\frac{\partial\left(\Delta\bar{G}_A^j\right)}{\partial x_A^j}\right\}_T \left(\frac{dx_A^j}{dT}\right) \tag{I-47}$$

In a similar way, the relative partial molar free energy and enthalpy of component A in the coexisting phase state can be expressed as follows;

$$\Delta\bar{G}_A^{i+j} = \Delta\bar{G}_A^i = \Delta\bar{G}_A^j \tag{I-48}$$

$$\Delta\bar{H}_A^{i+j} = \Delta\bar{H}_A^i - T\left\{\frac{\partial\left(\Delta\bar{G}_A^i\right)}{\partial x_A^i}\right\}_T \left(\frac{dx_A^i}{dT}\right) = \Delta\bar{H}_A^j - T\left\{\frac{\partial\left(\Delta\bar{G}_A^j\right)}{\partial x_A^j}\right\}_T \left(\frac{dx_A^j}{dT}\right) \tag{I-49}$$

Equations (I-47)~(I-49) give the relations between the relative partial molar thermodynamic properties of the coexisting phase state and those of its adjacent single phase on the phase boundary. One should here note that the relative partial molar entropy, and enthalpy of the coexisting phase state is not identical with those of the adjacent single phase on the phase boundary, because the alloy composition on the phase boundary generally depends on temperature. On the other hand, the relative partial molar free energy of the coexisting phase is equal to that of the adjacent single phase on the phase boundary.

3.2.2. Single electrode Peltier heat on a coexisting-single phase boundary

As shown in eq. (I-25), the thermoelectric power of the nonisothermal cell (I-a) can be expressed by the sum of the relative partial molar entropy of the component A in the alloy and the thermoelectric power of an A^+/A electrode. This relation should be valid for an alloy electrode in a single phase state as well as for that in a coexisting phase state. Thus the change of the single electrode Peltier heat for the cathodic reaction on a coexisting-single phase boundary can be expressed by introducing eqs. (I-25) and (I-47)

into (I-35);

$$\pi^{i+j} - \pi^{i} = \frac{T}{F}\left(\Delta\bar{S}_A^{i+j} - \Delta\bar{S}_A^{i}\right)$$

$$= -\frac{T}{F}\left\{\frac{\partial\left(\Delta\bar{G}_A^{i}\right)}{\partial x_A^{i}}\right\}_T\left(\frac{dx_A^{i}}{dT}\right) \qquad \text{(I-50)}$$

Equation (I-50) predicts that the single electrode Peltier heat of an alloy electrode shows discontinuities at coexisting-single phase boundary compositions. The change of the single electrode Peltier heat on a coexisting-single phase boundary can be estimated from composition dependency of the relative partial molar free energy in the single phase and the temperature dependency of the phase boundary composition according to eq. (I-50).

3.3. Experimental

The experiments were conducted in LiCl-KCl eutectic melt. The experimental apparatus appeared in the previous chapter. The eutectic mixture of the salts was dried under vacuum at 473 K for more than 48 hours and then at 573 K for more than 48 hours. After the eutectic mixture was melted, a pre-electrolysis was carried out with the terminal voltage of 2.5 V until the current density became less than 0.2 $mA \cdot cm^{-2}$, in order to remove residual water contamination further.

Thermodynamic properties of the single βLiAl phase were determined from *emf* measurements of the isothermal cell (I-b). The reference and counter electrodes used were same as in experiments described in chapter 2. A working electrode was Li-Al alloy, which was electrochemically prepared by a constant current electrolysis with the current density of 5.0 $mA \cdot cm^{-2}$ from a pure aluminum plate (7 x 5 x 0.3 mm, Wako Pure Chemical Industries, Ltd., 99.99 %). The weight of the aluminum plate was measured to an accuracy of 0.1 mg before the electrolysis. The lithium concentration was calculated from the charge passed during the constant current electrolysis and the current

efficiency. The current efficiency was estimated from the values of the applied current and the residual current observed at the pre-electrolysis. The *emf* of the alloy was determined by a rest potential observed immediately after a current interruption.

3.4. Results and discussion

3.4.1. Thermodynamic properties of the single βLiAl phase

Figure I-12 shows the lithium concentration dependence of the *emf* for the single βLiAl phase at four different temperatures. At all temperatures, a similar concentration dependency of the *emf* is observed. The *emf* curve exhibits two inflections near 47 mol% of lithium and the stoichiometric composition. The temperature dependency of the *emf* is negative for the whole composition range of the single βLiAl phase region.

The experimental data obtained by Wen et al. [2] are also plotted for comparison in Fig. I-12. Though each *emf* curve shows a similar lithium concentration dependency, results obtained in this work disagree with those by Wen et al. in two points. First, *emf* values in this work are lower than those by Wen et al.. Secondly, the *emf* shows a negative temperature dependency at 47-52 mol% of lithium and a positive temperature dependency at 52-56 mol% of lithium in the data of Wen et al., while the *emf* shows a negative temperature dependency in the whole concentration range of the single βLiAl phase region in this work. The former disagreement may come from experimental error for the lithium concentration in the data of Wen et al., as pointed out by Chen et al. [3]. Considering the consistencies with the phase diagram data and with the thermodynamic data of liquid and αAl phases, Chen et al. concluded that the lithium concentrations presented by Wen et al. are higher than real lithium concentrations. In

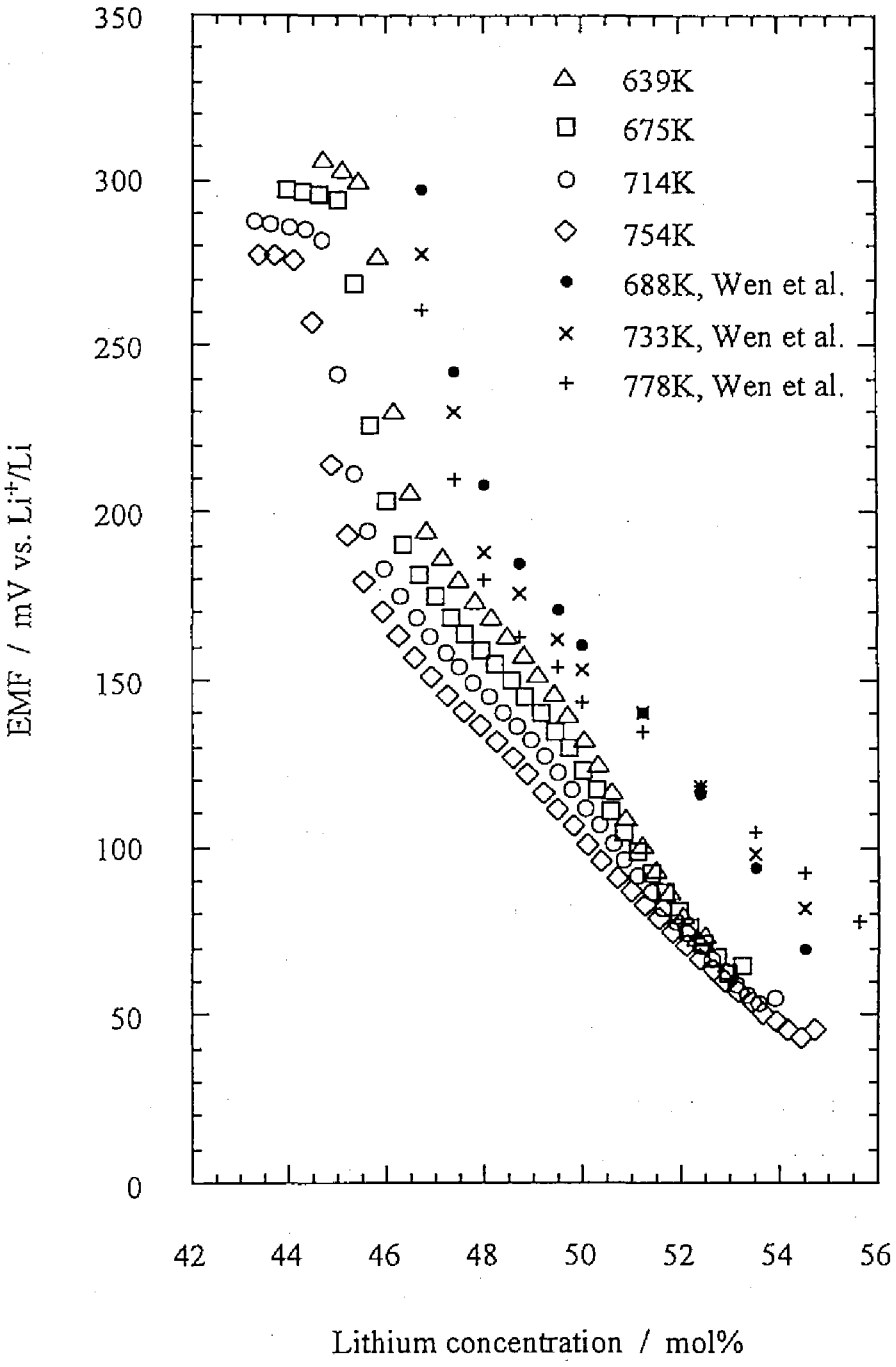

Fig.I-12. *Emf* for the single βLiAl phase plotted versus lithium concentration at different temperatures.

fact, if the data by Wen et al. are shifted to lower lithium concentration by ~2 mol%, as suggested by Chen et al., there would be reasonable agreements between the data in this work and those in Wen et al.. Concerning the latter disagreement, the data of Wen et al. implies that the *emf* for the two-phase (βLiAl+γLi_3Al_2) region shows a positive temperature dependency. However, this conflicts with the results of *emf* measurements for the coexisting (βLiAl+γLi_3Al_2) phase state presented in the previous chapter. Thus we concluded that the data of Wen et al. are in error also in this point.

Constant *emf* values observed at the lithium deficient and the lithium rich sides in Fig. I-12 correspond to the *emf* values for the two-phase (αAl+βLiAl) and (βLiAl+γLi_3Al_2) regions, respectively. The lithium concentration range for the single βLiAl phase is then evaluated as shown in Fig. I-13. Experimental data by Wen et al. [2], by Levine et al. [4], by Veleckis [5], and by Schürmann et al. [6] are also presented in Fig. I-13. The difference of ~2 mol% is again observed for both lithium deficient and rich phase boundaries between the results in this work and those by Wen et al.. The lithium concentrations for the lithium deficient limit obtained in this work are in agreement with those obtained by Schürmann et al. [6].

Relative partial molar thermodynamic properties of lithium in the single βLiAl phase can be determined according to eqs. (I-27)~(I-29). Figures I-14(A)~(C) show the relative partial molar free energy, entropy, and enthalpy of lithium at 714 K, in order, as a function of lithium concentration. Experimental curves of all these thermodynamic properties show inflections near the stoichiometric composition and in the vicinities of phase boundary compositions for the single phase region. Such composition dependencies of the thermodynamic properties may be correlated with structural properties' change of the alloy.

The stoichiometric βLiAl compound crystallizes in the f.c.c B32 (Zintl) structure (space group: $Fd\bar{3}m$; prototype: NaTl), which consists of two distinct diamond sublattices interpenetrating each other [7, 8]. The unit cell of the βLiAl

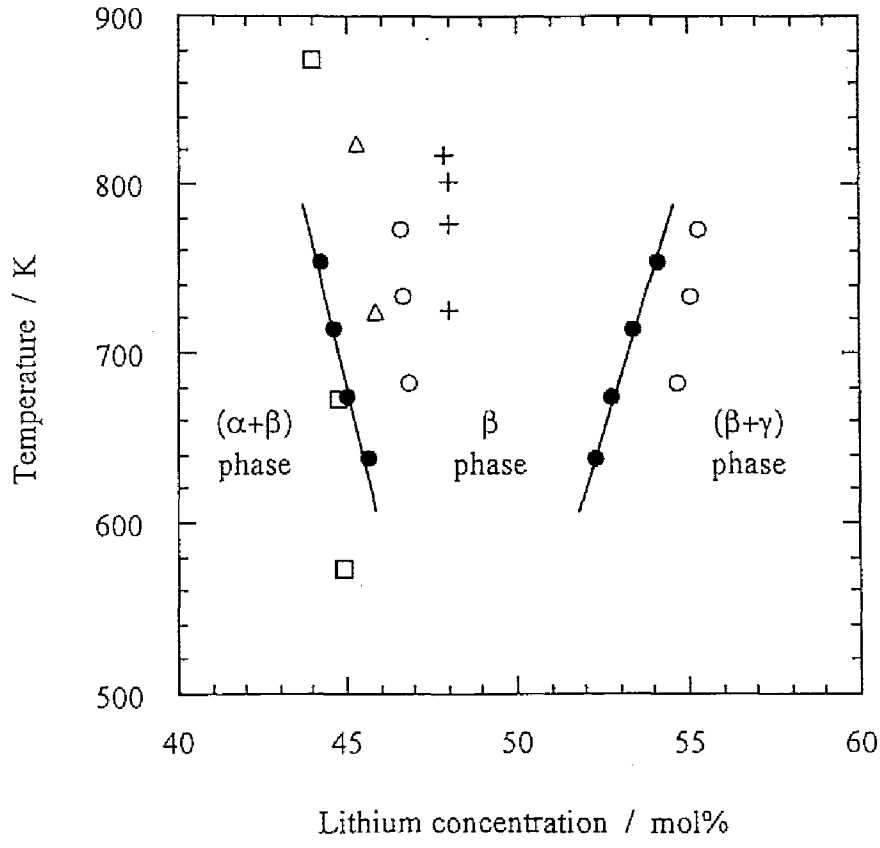

Fig.I-13. Lithium concentration range of the single βLiAl phase; this work (●), Wen et al. (○) [2], Levine et al. (△) [4], Veleckis (+) [5] and Schür mann et al. (□) [6].

compound is shown in Fig. I-15. The defect structures in stoichiometric and nonstoichiometric βLiAl phase have been studied by using various techniques such as lattice parameter and density measurements, nuclear magnetic resonance, and neutron diffraction [9~11]. It was concluded that vacancies on Li sites and Li antistructure atoms on Al sites are the dominant defects for lithium deficient and lithium rich compositions, respectively. For single phase alloys with such crystal and defect structures, Chang and co-workers have statistically derived expressions of thermodynamic properties under

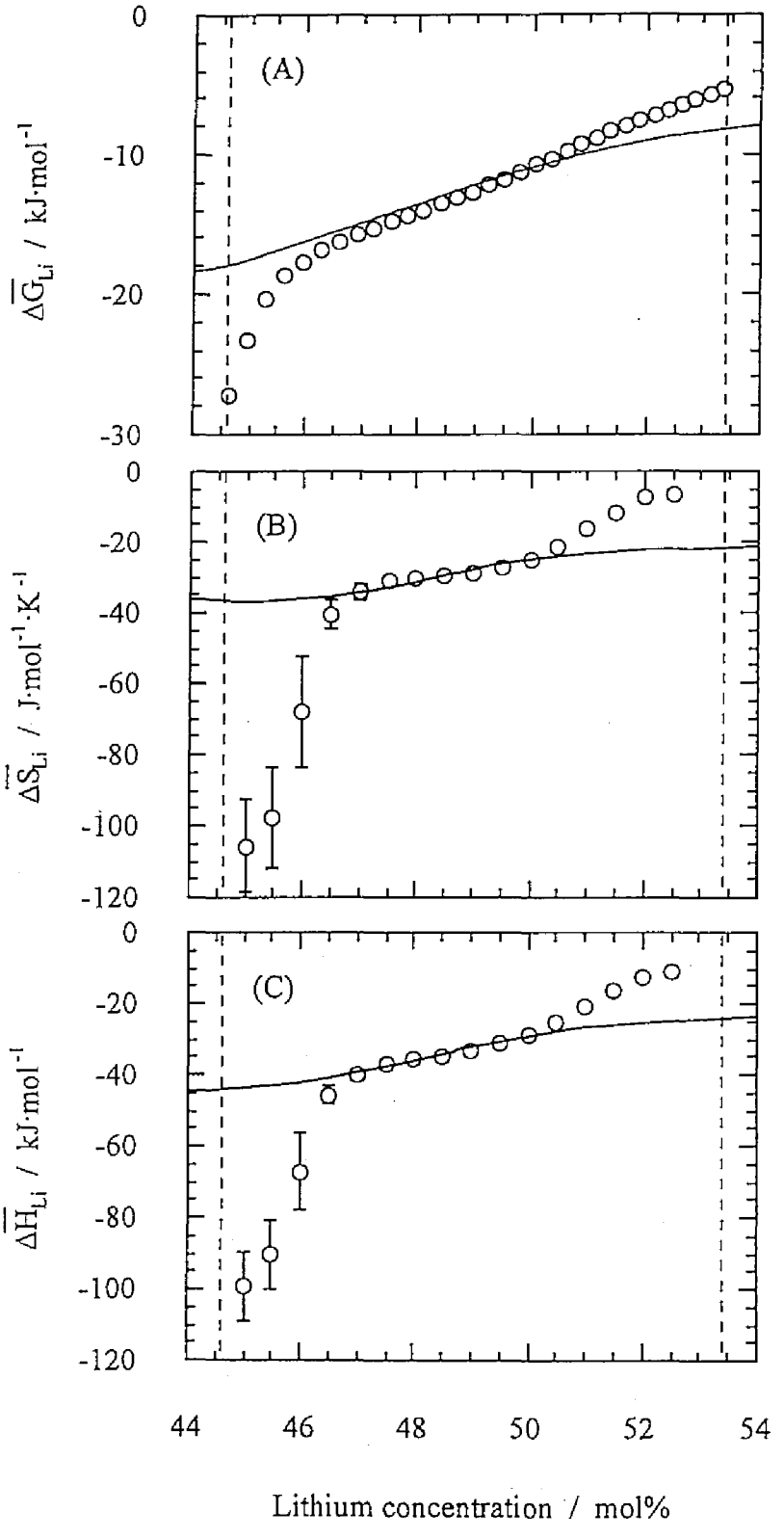

Fig.I-14. Relative partial molar thermodynamic properties of lithium in the single βLiAl phase. The solid lines show calculated values by using eqs. (I-51), (I-52) and (I-53). The dashed lines present the phase boundaries for the single βLiAl phase concentration region.

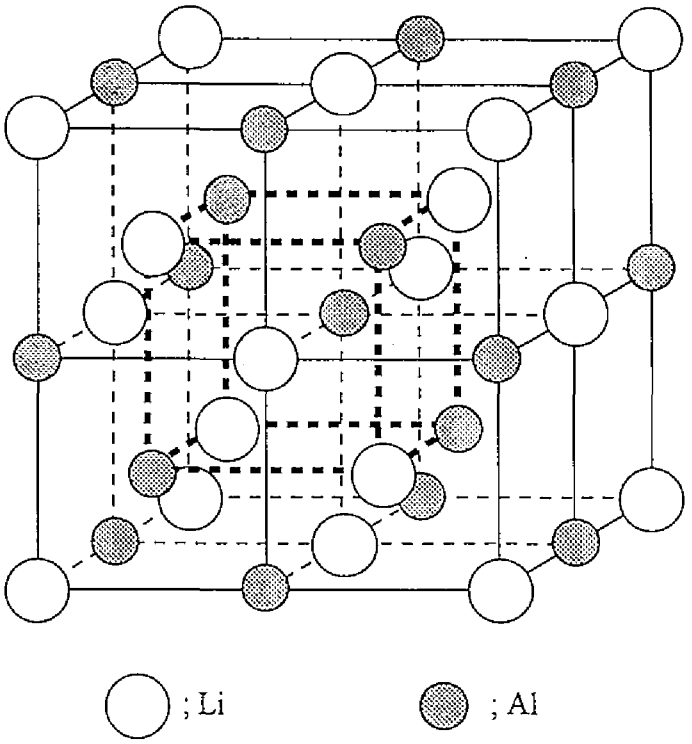

Fig.I-15. Unit cell of βLiAl.

the following assumptions: (1) interactions, i.e. bond energies, only between first-nearest neighbor atoms are taken into account and are independent of the composition, (2) the concentration of the defects are small and thus the distribution of the defects is statistically random, and (3) all entropy contributions other than the configurational entropy are independent of the composition [3, 12, 13]. Relative partial molar thermodynamic properties of lithium with reference to those at the stoichiometric composition are then expressed as follows;

$$\frac{\left(\Delta\overline{G}_{Li}-\Delta\overline{G}_{Li,0}\right)}{RT}=\ln\left(\frac{a_{Li}}{a_{Li,0}}\right)=-\frac{1}{2}\ln\frac{\alpha(1+z)^2(1-\alpha)}{(1-z)(z+2\chi)(1+\alpha)^2} \tag{I-51}$$

$$\frac{\left(\Delta\overline{H}_{Li}-\Delta\overline{H}_{Li,0}\right)}{RT}=\frac{1}{2}\ln\frac{(1+\alpha)^2(1-\alpha)}{4\alpha^3}\left[(z-\alpha)-\chi\left(\frac{dz}{d\chi}\right)+\frac{1}{2}\left\{\left(\frac{dz}{d\chi}\right)-\left(\frac{dz}{d\chi}\right)_0\right\}\right] \tag{I-52}$$

$$\frac{\left(\Delta\bar{S}_{Li} - \Delta\bar{S}_{Li,0}\right)}{R} = \frac{\left(\Delta\bar{H}_{Li} - \Delta\bar{H}_{Li,0}\right)}{RT} - \ln\left(\frac{a_{Li}}{a_{Li,0}}\right) \tag{I-53}$$

where the subscript 0 indicates the state at the stoichiometric composition. In eqs. (I-51)~(I-53), z is the vacancy concentration, χ is the deviation of the lithium concentration from the stoichiometry, and α is the vacancy concentration at the stoichiometric composition, i.e. the intrinsic disorder parameter;

$$\chi = x_{Li} - \frac{1}{2} \tag{I-54}$$

$$\alpha = z_0 \tag{I-55}$$

The intrinsic disorder parameter α is related to z and χ by the following equation [3, 12, 13];

$$\alpha^3 = z^2(z + 2\chi) \tag{I-56}$$

From eqs. (I-51)~(I-56), the relative partial molar thermodynamic properties of lithium can be calculated as a function of the lithium concentration under the assumptions given, if the intrinsic disorder parameter is known.

Kishio et al. evaluated the vacancy concentration of the single βLiAl phase at room temperature [9], and found that it is 1.8 mol% at the stoichiometric composition, i.e. $\alpha = 0.018$. Vacancies at the stoichiometric composition are considered to be formed mainly as a consequence of the thermal agitation. The value of the intrinsic disorder parameter for the stoichiometric βLiAl compound at high temperature is therefore expected to be higher than above value. Since there exists no available data of the intrinsic disorder parameter for the βLiAl phase at high temperature, we here assume $\alpha = 0.04$, as Brun et al. have done [14]. The solid lines in Figs. I-14(A)~(C) show the relative partial molar thermodynamic properties of lithium for the single βLiAl phase calculated by using eqs. (I-49)~(I-54) when $\alpha = 0.04$ is assumed and our experimental values of $\Delta\bar{G}_{Li,0} = -10.9\ \mathrm{kJ\cdot mol^{-1}}$, $\Delta\bar{S}_{Li,0} = -25.1\ \mathrm{J\cdot mol^{-1}\cdot K^{-1}}$, and $\Delta\bar{H}_{Li,0} = -28.8\ \mathrm{kJ\cdot mol^{-1}}$ are used. The calculated curves are seen to reproduce the shape of the experimental

results near the stoichiometric composition, 47~51 mol%. The calculated curves also show inflections near the stoichiometric composition, though the inflections observed in experimental results are much larger than those in the calculated curves. These results imply that the inflections observed in the experimental curves near the stoichiometric composition are related by the change of the defect structure of this alloy phase, i.e. the change of the dominant defects from vacancies on Li sites in lithium deficient composition to Li antistructure atoms on Al sites in lithium rich composition.

In the vicinities of the phase boundaries for the single βLiAl phase region, i.e. in the lithium concentration ranges below 47 mol% and above 51 mol%, the experimental results considerably deviate from the calculated curves. In these composition ranges, defect concentration is considered to be relatively high: approximately, 10 % of Li sites are expected being vacant at the lithium deficient limit and 5 % of Al sites are expected being substituted by lithium at the lithium rich limit. Such high defect concentration may cause ordering or clustering of the defects, or lattice relaxations, as suggested from the results of neutron diffraction, heat capacity and electronic resistivity measurements [14~18]. In such situations, the assumptions used to derive eqs. (I-51)~(I.53), thus eqs. (I-51)~(I-53), may not be valid. Krachelar and Ipser have derived statistical expressions for activity by taking the effect of vacancy ordering into account, and have applied the expressions to interpret experimental data in transition metal-chalcogen systems [19~21]. According to their expressions, activity-composition curve shows inflections at the ordering composition as well as the stoichiometric composition, and the shape of the curve seems similar as that obtained in this work. This may imply that defect ordering takes place in the single βLiAl phase near the phase boundaries. However, at the present time, it is difficult to conclude whether defect ordering accompanies the anomalies on thermodynamic properties of the single βLiAl phase near the phase boundaries because of lack of detailed crystal analysis data at high temperature.

3.4.2. Single electrode Peltier heat as a function of lithium concentration

According to eqs. (I-34) and (I-35), one can obtain the single electrode Peltier heat of a Li-Al alloy electrode in LiCl-KCl eutectic melt from the value of the relative partial molar entropy of lithium in the alloy and the thermoelectric power of a Li^+/Li electrode in LiCl-KCl eutectic melt. The thermoelectric power of a Li^+/Li electrode was determined to be +0.030 (±0.030) $mV \cdot K^{-1}$ by Kamata et al. [1]. For the relative partial molar entropy of lithium in each coexisting phase state of Li-Al alloy and that the single βLiAl phase, values shown in Table I-3 and Fig. I-14(B) are available. In order to estimate the relative partial molar entropy of lithium in the single αAl and the single liquid phases, the subregular solution model is employed here. In this model, the relative partial molar free energy of component A is approximated as eq. (I-57);

$$\Delta\overline{G}_A^i = F_A^i + RT\ln x_A + A_A^i(1-x_A)^2 + B_A^i x_A(1-x_A)^2 \qquad \text{(I-57)}$$

where F_A^i is the lattice stability parameter of component A in *i* phase, A_A^i and B_A^i are the interaction parameters of component A in *i* phase. These three parameters are all independent of x_A. As special cases, eq. (I-57) gives the relative partial molar free energy of lithium in the ideal solution when $A_A^i = B_A^i = 0$, and that in the regular solution when $B_A^i = 0$. Differentiating eq. (I-57) with respect to temperature at constant x_A, the relative partial molar entropy of component A are obtained as follows;

$$\Delta\overline{S}_A^i = -\left(\frac{dF_A^i}{dT}\right) - R\ln x_A - \left(\frac{dA_A^i}{dT}\right)(1-x_A)^2 - \left(\frac{dB_A^i}{dT}\right)x_A(1-x_A)^2 \qquad \text{(I-58)}$$

The lattice stability parameters and the interaction parameters for the single αAl phase and the single liquid phase were given by McAlister [22], and are summarized in Table I-6. The lithium concentration of the single αAl phase at the Li-saturated limit was obtained as a function of temperature by Wen et al. [2], by Schürmann et al. [6], by Jones et al. [23], and by Costa et al. [24].The lithium concentration of the single liquid phase at the solubility limit was measured by Schürmann et al. [6], Grube et al. [25],

Table I-6. The lattice stability and the interaction parameters for solution phases in LiAl alloy system [21].

Phase state	F_{Li}^{i}	A_{Li}^{i}	B_{Li}^{i}
αAl	-1787+7.16T	-14873	-13200
liquid	0	-11000	-36000

and Sharmray et al. [26].

Figure I-16 shows the single electrode Peltier heat for the cathodic reaction of a Li-Al alloy electrode at 714 K, which is evaluated from the relative partial molar entropy of lithium and the thermoelectric power of a Li^+/Li electrode. For the two-phase (αAl+βLiAl), (βLiAl+γLi_3Al_2), and (γLi_3Al_2+liq.) regions, the single electrode Peltier heats evaluated from thermoelectric power values are also shown by the short-dashed lines in Fig. I-16. From Fig. I-16, it turns out that the single electrode Peltier heat of a Li-Al alloy electrode exhibits discontinuities at the phase boundary compositions.

As shown in eq. (I-50), the change of the single electrode Peltier heat for the cathodic reaction of a lithium alloy electrode on a coexisting-single phase boundary can be estimated from composition dependency of the relative partial molar free energy of lithium in the single phase and the temperature dependency of the lithium concentration on the phase boundary. From the results shown in Fig. I-14(A) and Fig. I-13, the values for $\left\{\partial\left(\Delta G_{Li}^{\beta}\right)/\partial x_{Li}^{\beta}\right\}$ and $\left(dx_{Li}^{\beta}/dT\right)$ are estimated to be 8.6 x 10^2 kJ·mol^{-1} and -1.0 x 10^{-4} K^{-1} on the (αAl+βLiAl)-βLiAl phase boundary, and to be 1.3 x 10^2 kJ·mol^{-1} and 1.6 x 10^{-4} K^{-1} on the βLiAl-(βLiAl+γLi_3Al_2) phase boundary at 714 K. The change of the single electrode Peltier heat is then expected to be -0.64 J·C^{-1} on the (αAl+βLiAl)-βLiAl phase boundary, and to be -0.15 J·C^{-1} on the βLiAl-(βLiAl+γLi_3Al_2) phase boundary at

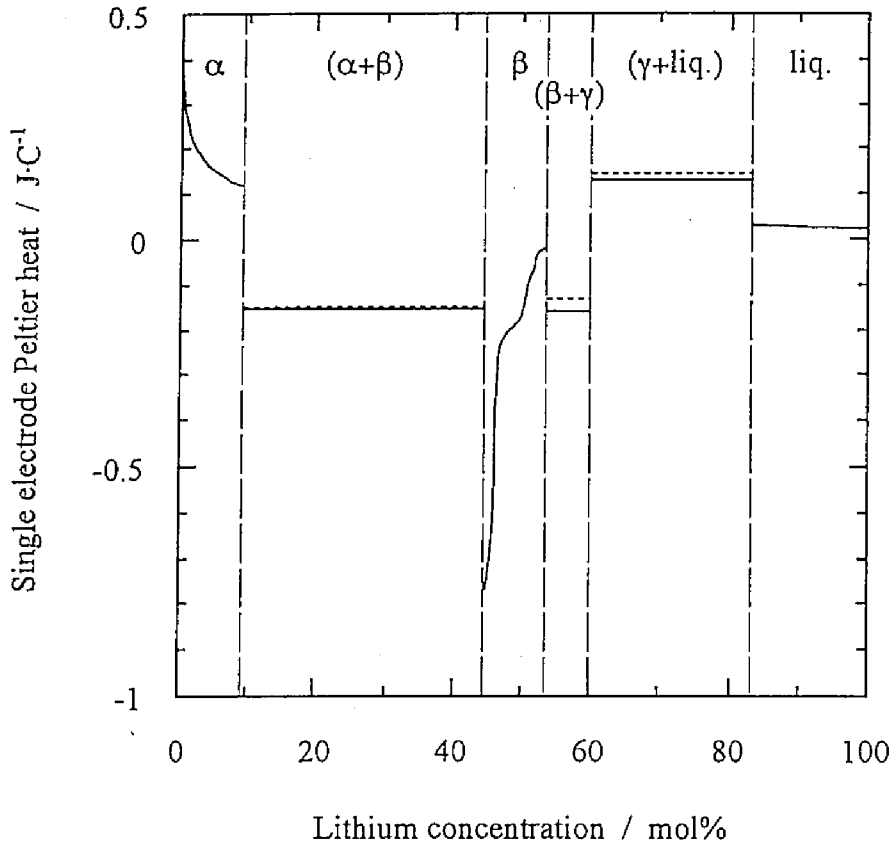

Fig.I-16. Single electrode Peltier heat for the cathodic reaction of a Li-Al alloy electrode in LiCl-KCl eutectic melt at 714 K. The solid line presents values evaluated from the relative partial molar entropy of lithium. The short-dashed lines show values determined from thermoelectric power values.

714 K. These values are in good agreement with the results shown in Fig. I-16, which are -0.64 $J \cdot C^{-1}$ on the (αAl+βLiAl)-βLiAl phase boundary -0.14 $J \cdot C^{-1}$ on the βLiAl-(βLiAl+γLi_3Al_2) phase boundary, respectively. In a similar way, the change of the single electrode Peltier heat can be estimated to be -0.19 $J \cdot C^{-1}$ on the αAl-(αAl+βLiAl) phase boundary, and to be -0.10 $J \cdot C^{-1}$ on the (γLi_3Al_2+liq.)-liq. phase boundary by applying the subregular solution models by McAlister [21] and the phase diagram data in literature [2, 6, 23~26]. The value for the (γLi_3Al_2+liq.)-liq. phase boundary agrees well

with the result in Fig. I-16, -0.09 $J \cdot C^{-1}$, while that for the αAl-(αAl+βLiAl) phase boundary is slightly different from the results in Fig. I-16, -0.26 $J \cdot C^{-1}$. McAlister has determined the parameters in the subregular solution model for the single αAl phase to fit experimental data on the lithium solubility limit of this phase. However, experimental data of the lithium solubility data are inconsistent with thermodynamic data obtained by Wen et al. at 969 K [2]. Such experimental uncertainties on the phase diagram data and thermodynamic data for the single αAl phase may cause the discrepancy between the result shown in Fig. I-16 and the estimated result.

In Fig. I-16 we treat the γLi_3Al_2 phase as a line compound. However, the γLi_3Al_2 phase is considered to have a certain concentration range like the single βLiAl phase, though the concentration range of the single γLi_3Al_2 phase may be very narrow. From the phase diagram data and the activity data for the two-phase (βLiAl+γLi_3Al_2) region and (γLi_3Al_2+liq.) regions, the values of $\left(dx_{Li}^{\gamma}/dT\right)$ and $\left\{\partial\left(\Delta G_{Li}^{\gamma}\right)/\partial x_{Li}^{\gamma}\right\}$ are expected to be very small. Thus, the changes of the single electrode Peltier heat on the (βLiAl+γLi_3Al_2)-γLi_3Al_2 and γLi_3Al_2-(γLi_3Al_2+liq.) phase boundaries may be negligibly small, and the single electrode Peltier heat for the single γLi_3Al_2 phase may vary from the value for the coexisting (βLiAl+γLi_3Al_2) phase to that for the coexisting (γLi_3Al_2+liq.) phase as the lithium concentration increases.

3.5. Conclusions

1. The single electrode Peltier heat of a Li-Al alloy electrode was evaluated as a function of lithium concentration in the alloy. It was found that the single electrode Peltier heat shows discontinuities at the compositions of coexisting-single phase boundaries. The changes of the single electrode Peltier heat at the phase boundary compositions can be

estimated from thermodynamic data in the single phase and phase diagram data.

2. In the single βLiAl phase, the relative partial molar thermodynamic properties, thus the single electrode Peltier heat, considerably depends on lithium concentration. The lithium concentration dependence of the relative partial molar thermodynamic properties near the stoichiometric composition can be statistically interpreted in terms of its defect structure. In the vicinities of the phase boundaries, relative partial molar thermodynamic properties exhibit anomalies, which is considered to be caused by ordering or clustering of the defects, or lattice relaxations.

References

[1] M. Kamata, Y. Ito, M. Inoue, and J. Oishi, *J. Electrochem. Soc.*, **136**, 528 (1989).

[2] C. J. Wen, B. A. Boukamp, R. A. Huggins, and W. Weppner, *J. Electrochem. Soc.*, **126**, 2258 (1979).

[3] S. W. Chen, C. H. Jan, J. C. Lin and Y. A. Chang, *Metal. Trans. A*, **20A**, 2247 (1989).

[4] E. D. Levine and E. J. Rapperport, *Trans. AIME*, **227**, 1204 (1963).

[5] E. Veleckis, *J. Less-Common Met.*, **73**, 49 (1980).

[6] E. Schürmann and H. J. Voss, *Giessereiforshung*, **33**, 33 (1981).

[7] E. Zintl and G. Woltersdorf, *Z. Elektrochem.*, **41**, 876 (1935).

[8] K. Kuriyama and N. Masaki, *Acta Cryst.*, **B31**, 1793 (1975).

[9] K. Kishio and J. O. Brittain, *J. Phys. Chem. Solids*, **40**, 933 (1979).

[10] K. Kishio and J. O. Brittain, *Mater. Sci. Eng.*, **49**, 1 (1981).

[11] K. Kishio, J. R. Owers-Bradley, W. P. Halperin, and J. O. Brittain, *J. Phys. Chem. Solids*, **42**, 1031 (1981).

[12] Y. A. Chang and J. P. Neumann, *Prog. Solid State Chem.*, **14**, 221 (1982).

[13] J. P. Neumann, Y. A. Chang, and C. M. Lee, *Acta Metall.*, **24**, 593 (1976).

[14] T. O. Brun, J. D. Jorgensen, M. Misawa, F. J. Rotella, and S. Susman, *J. Electrochem. Soc.*, **129**, 2509 (1982).

[15] J. -E.Jørgensen, S. Susman, T. O. Brun, K. J. Volin, and J. Faber, Jr., *Solid State Ionics*, **18/19**, 852 (1986).

[16] K. Kuriyama, T. Kamijoh, and T. Nozaki, *Phys. Rev. B*, **22**, 470 (1980).

[17] K. Kuriyama, S. Yanada, T. Nozaki, and T. Kamijoh, *Phys. Rev. B*, **24**, 6158 (1980).

[18] H. Sugai, M. Tanase, M. Yahagi, T. Ashida, H. Hamanaka, K. Kuriyama, and K. Iwamura, *Rhys. Rev. B*, **52**, 4050 (1995).

[19] R. Krachler, H. Ipser, and K. L. Komarek, *J. Phys. Chem. Solids*, **50**, 1127 (1989).

[20] R. Krachler, *J. Alloys. Comp.*, **200**, 1 (1993).

[21] H. Ipser and R. Krachler, *Z. Metllkd.*, **84**, 9 (1993).

[22] A. J. McAlister, *Bull. Alloy Phase Diagrams*, **3**, 177 (1982).

[23] W. R. D. Jones and P. P. Das, *J. Inst. Met.*, **87**, 338 (1959).

[24] L. P. Costa and R. P. Marshall, *Trans. AIME*, **224**, 970 (1962).

[25] G. Grube, L. Mohr, and W. Breuning, *Z. Elektrochem.*, **41**, 880 (1935).

[26] F. I. Shamray and P. Y. Saldau, *Izv. Akad. Nauk SSSR, Otdel. Khim.*, 631 (1937).

Chapter 4

Single electrode Peltier heats of Li-Si alloy electrodes

4.1. Introduction

In chapter 2 and chapter 3, relations between thermoelectric power of an alloy electrode and its thermodynamic properties were theoretically derived, and were validated by experimental results of a Li-Al alloy electrode system in LiCl-KCl eutectic melt. In this chapter, the thermoelectric power and thermodynamic properties of various coexisting phase states of Li-Si alloy in LiCl-KCl eutectic melt were experimentally determined, and the thermodynamic relations derived in chapter 2 and chapter 3 are confirmed by experimental results of this alloy system.

4.2. Experimental

The experimental apparatus used is schematically illustrated in Fig. I-17. The experiments were conducted in LiCl-KCl eutectic melt. The pretreatment of the electrolyte salts and the atmosphere inside the cell were the same as those described in chapter 2. A working electrode was a single crystal silicon plate (13 x 7 x 0.5 mm, P doped silicon, Nilaco Co., Ltd., 99.999 %) held in a nickel mesh cage (mesh size: 1 mm). The reference and the counter electrodes were the same kinds as described in chapter 2.

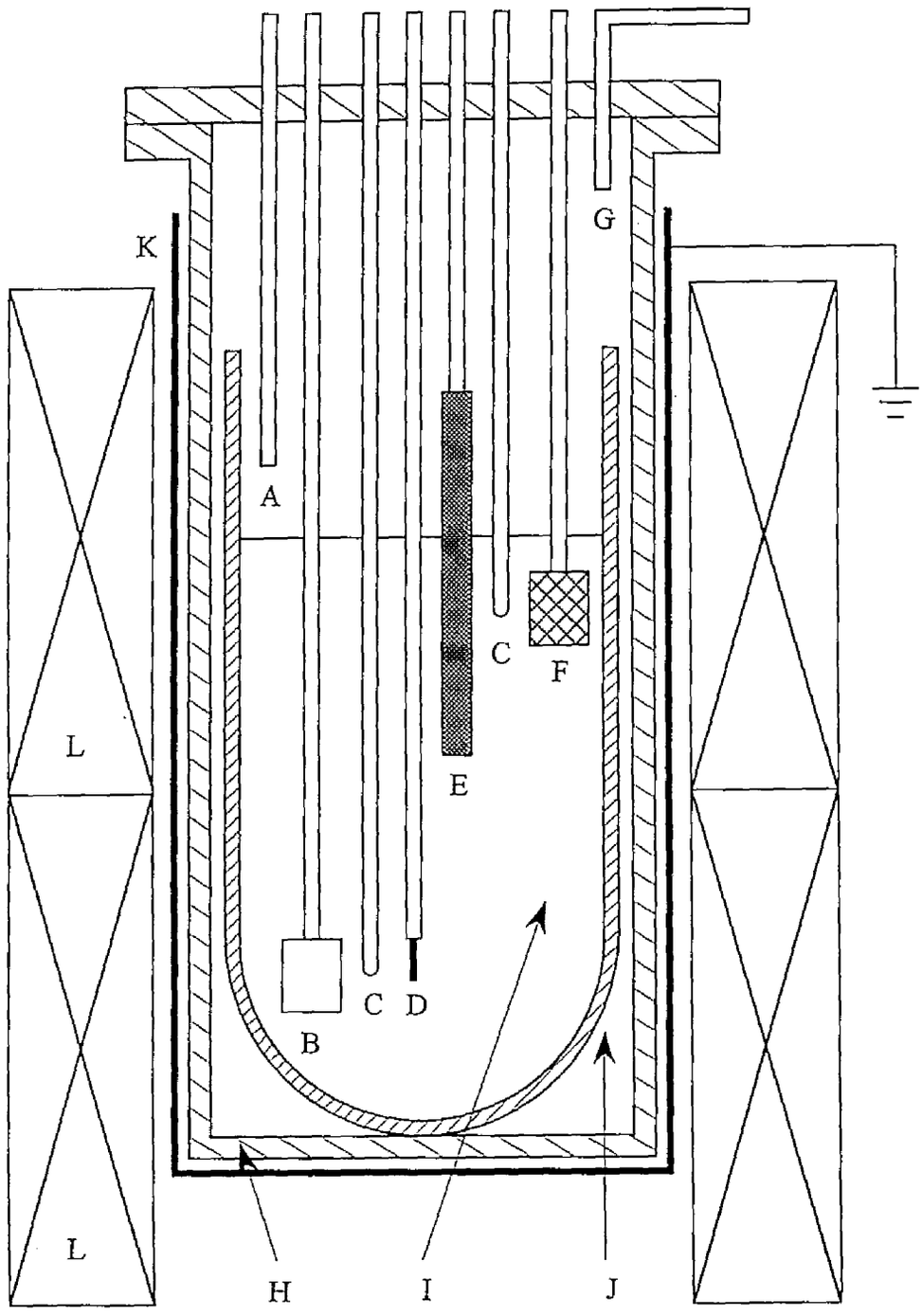

Fig.I-17. Schematic illustration of the experimental appratus: (A) Ar gas inlet, (B) working electrode, (C) thermocouple, (D) Li^+/Li electrode (nickel wire), (E) counter electrode, (F) reference electrode, (G) Ar gas outlet, (H) pyrex holder, (I) LiCl-KCl eutectic melt, (J) crucible, (K) nicke foil holder, and (L) furnace.

A nickel wire was employed as an electrical lead for each electrode.

The electrochemical formation reaction of Li-Si alloy was investigated by using a constant current electrolysis and a potential sweep method at 713 K. The electrochemically formed alloy electrodes were analyzed by using the powder x-ray diffraction technique (XRD) in dry argon atmosphere. Thermodynamic properties of Li-Si alloy in each coexisting phase state were determined from *emf* measurements of the isothermal cell (I-e) at 670~770 K;

$$(T)\ \text{Li} \mid \text{LiCl-KCl} \mid \text{Li-Si}\ (T) \qquad \text{(I-e)}$$

The lithium silicon alloy in each coexisting phase state was electrochemically prepared by a constant current electrolysis from pure silicon. The *emf* of the alloy was determined by a rest potential which was observed after a current interruption.

The thermoelectric power of a Li-Si alloy electrode in each coexisting phase state was determined from *emf* measurements of the nonisothermal cell (I-f);

$$(T)\ \text{Li} \mid \text{LiCl-KCl} \mid \text{Li-Si}\ (T+\Delta T) \qquad \text{(I-f)}$$

A temperature difference between the electrodes was established vertically by controlling two electric heaters individually. The temperature of the Li-Al alloy and the Li^+/Li reference electrodes was kept constant at 713 K, while the temperature of the Li-Si alloy working electrode was varied from 703~743 K. After setting a certain temperature difference, the potential of the Li-Si alloy was measured in the same manner as the *emf* measurements of the isothermal cell (I-e).

4.3. Results and discussion

4.3.1. Electrochemical formation

A constant current electrolysis was carried out with a silicon electrode at 713 K. Figure I-18 shows a typical potential transient curve during the electrolysis (current

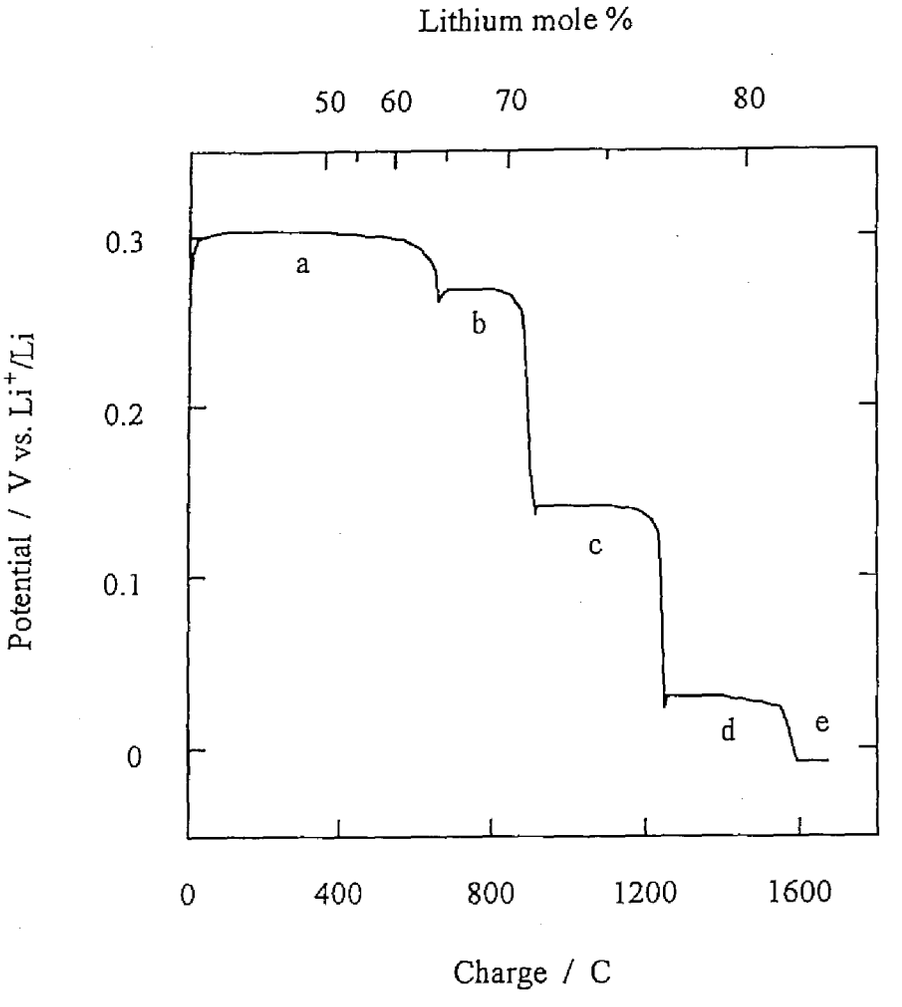

Fig.I-18. Potential transient curve of a silicon electrode in LiCl-KCl eutectic melt at 713 K. Current density; 20 $mA \cdot cm^{-2}$.

density: -20 $mA \cdot cm^{-2}$). Five clear potential plateaus a~e are observed. These potential plateaus are attributed to the formation of various types of silicon alloy with lithium, since they were not observed in a case of using nickel electrode which does not form any alloys with lithium. For Li-Si alloy system, it is known that four intermetallic compound phases, $Li_{12}Si_7$, Li_7Si_3, $Li_{13}Si_4$, $Li_{22}Si_5$, and a liquid phase exist at this temperature, as shown in Fig. I-19 [1, 2]. From the results of XRD analysis, it was found that each electrode, which showed the potentials a~d, contained the $Li_{12}Si_7$, Li_7Si_3,

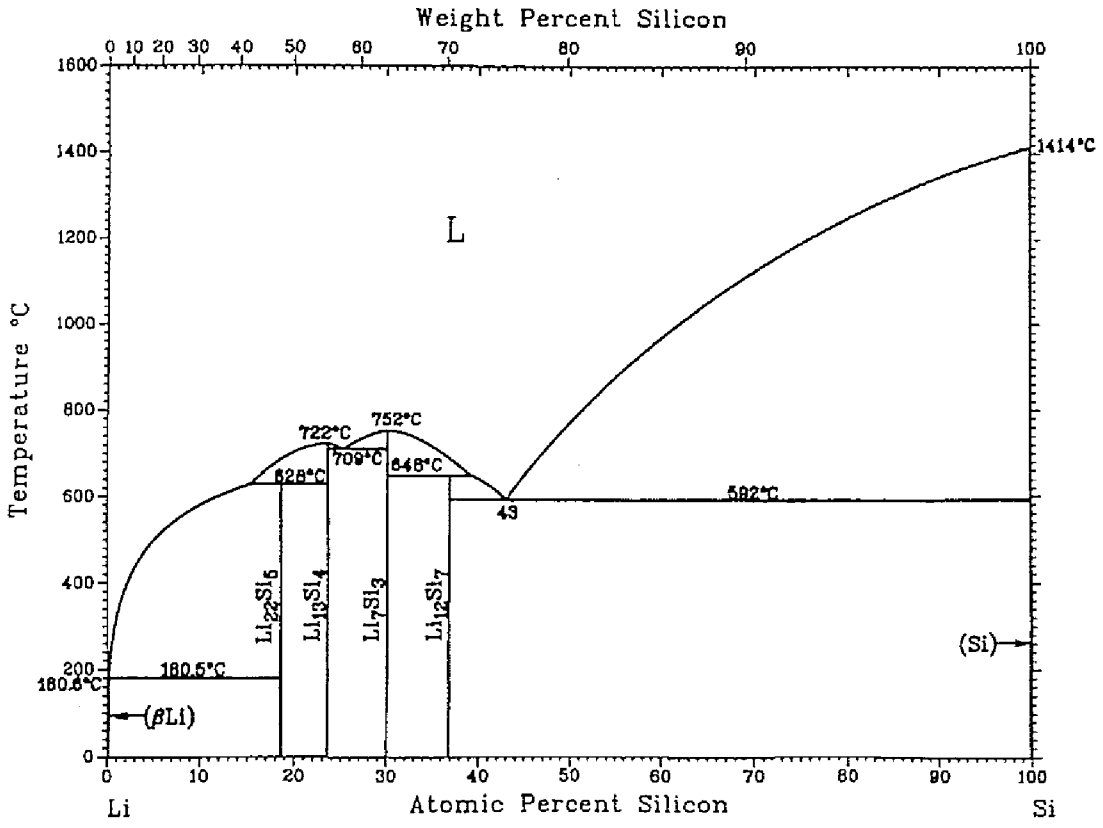

Fig.I-19. Phase diagram of Li-Si alloy system according to Okamoto [2].

$Li_{13}Si_4$ and $Li_{22}Si_5$ phases, respectively. This suggests that the formation of the $Li_{12}Si_7$, Li_7Si_3, $Li_{13}Si_4$, $Li_{22}Si_5$ and liquid phases occur at the potentials a~e, as represented by the following reaction formulae (I-vi)~(I-x);

$$\text{a} \;;\; \frac{7}{12}Si + Li^+ + e^- \rightarrow \frac{1}{12}Li_{12}Si_7 \qquad \text{(I-vi)}$$

$$\text{b} \;;\; \frac{3}{13}Li_{12}Si_7 + Li^+ + e^- \rightarrow \frac{7}{13}Li_7Si_3 \qquad \text{(I-vii)}$$

$$\text{c} \;;\; \frac{4}{11}Li_7Si_3 + Li^+ + e^- \rightarrow \frac{3}{11}Li_{13}Si_4 \qquad \text{(I-viii)}$$

$$\text{d} \;;\; \frac{5}{23}Li_{13}Si_4 + Li^+ + e^- \rightarrow \frac{4}{23}Li_{22}Si_5 \qquad \text{(I-ix)}$$

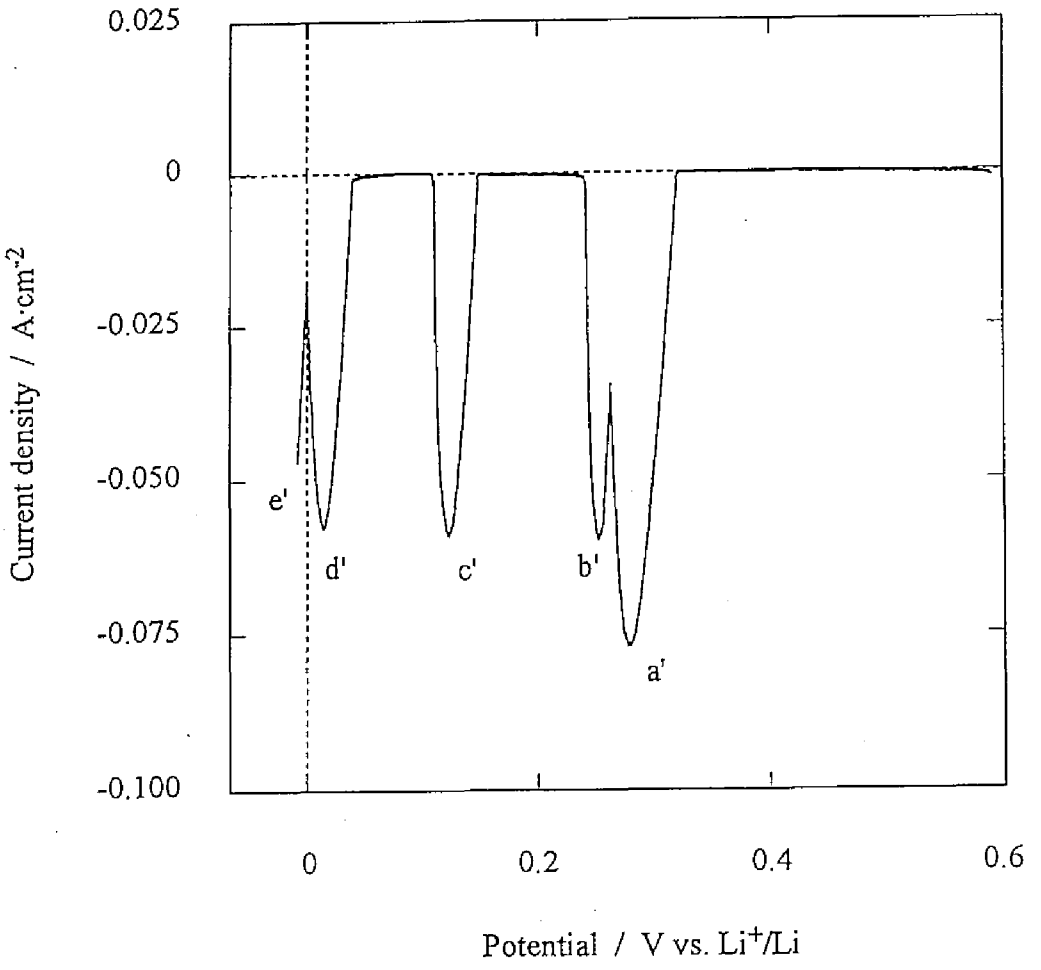

Fig.I-20. Voltammogram of a silicon electrode in LiCl-KCl eutectic melt at 713 K. Scan rate; 0.01 $mV \cdot s^{-1}$.

$$e \quad ; \quad y\,Li_{22}Si_5 + Li^+ + e^- \quad \rightarrow \quad \text{liq.-phase} \qquad \text{(I-x)}^{a}$$

In the reaction formula (I-x), the liq.-phase expresses the liquid Li-Si alloy at the solubility limit. Though a single crystal silicon with (100) or (111) surface was used as a starting material, no significant difference was observed on the potential behavior during

[a] Since the lithium concentration of the liquid phase in Li-Si alloy at the solubility limit depends on temperature, the quantity of the $Li_{22}Si_5$ phase needed to produce one mole of the liq.-phase by 1F of charge varies with temperature. Therefore, the symbol 'y' is introduced to designate the quantity of the $Li_{22}Si_5$ phase in the reaction formula (I-x). The value of y is 7.2×10^{-3} mole at 713 K.

the electrolysis.

A cathodic potential sweep with a silicon electrode was performed with a very slow scan rate (0.01 $mV \cdot s^{-1}$) at 713 K. The result is presented in Fig. I-20. Five clear cathodic current peaks a'~e' are observed. The current peaks a'~e' correspond to the formation of the $Li_{12}Si_7$, Li_7Si_3, $Li_{13}Si_4$, $Li_{22}Si_5$ and liquid phases, respectively. The potentials for the formation of each phase in Li-Si alloy obtained by this method are in good agreement with that observed during the constant current electrolysis.

4.3.2. Thermodynamic properties

The results for *emf* measurements of the isothermal cell (I-e) are presented in Figs. I-21(A)~(E). In the temperature range of 670~760 K, they are also represented by the following relations;

$Si+Li_{12}Si_7$; $E = 0.4383\ (\pm 0.0013) - 0.146\ (\pm 0.007) \times 10^{-3} \times T$ (I-59)

$Li_{12}Si_7+Li_7Si_3$; $E = 0.3855\ (\pm 0.0040) - 0.146\ (\pm 0.013) \times 10^{-3} \times T$ (I-60)

$Li_7Si_3+Li_{13}Si_4$; $E = 0.2783\ (\pm 0.0022) - 0.174\ (\pm 0.009) \times 10^{-3} \times T$ (I-61)

$Li_{13}Si_4+Li_{22}Si_5$; $E = 0.1624\ (\pm 0.0044) - 0.165\ (\pm 0.014) \times 10^{-3} \times T$ (I-62)

$Li_{22}Si_5$+liq. ; $E = -0.0113\ (\pm 0.0016) + 0.018\ (\pm 0.008) \times 10^{-3} \times T$ (I-63)

where E is *emf* in V and T is temperature in K. In Figs. I-21(A)~(E), the values measured by Sharma et al. [3], Lai [4] and Nikolaiev et al. [5] are also shown for comparison. The *emf* values for the two-phase ($Si+Li_{12}Si_7$), ($Li_{12}Si_7+Li_7Si_3$), ($Li_7Si_3+Li_{13}Si_4$) and ($Li_{22}Si_5$+liq.) regions obtained in this work agree with those in the literature. For the two-phase ($Li_{13}Si_4+Li_{22}Si_5$) region, *emf* values in the literature are inconsistent with each other. Our *emf* values for this coexisting phase state are close to those by Lai, though their results showed different temperature dependence from ours. With regard to temperature dependence of the *emf*, the results obtained in this work are in agreement with those by Sharma et al. for all coexisting phase states.

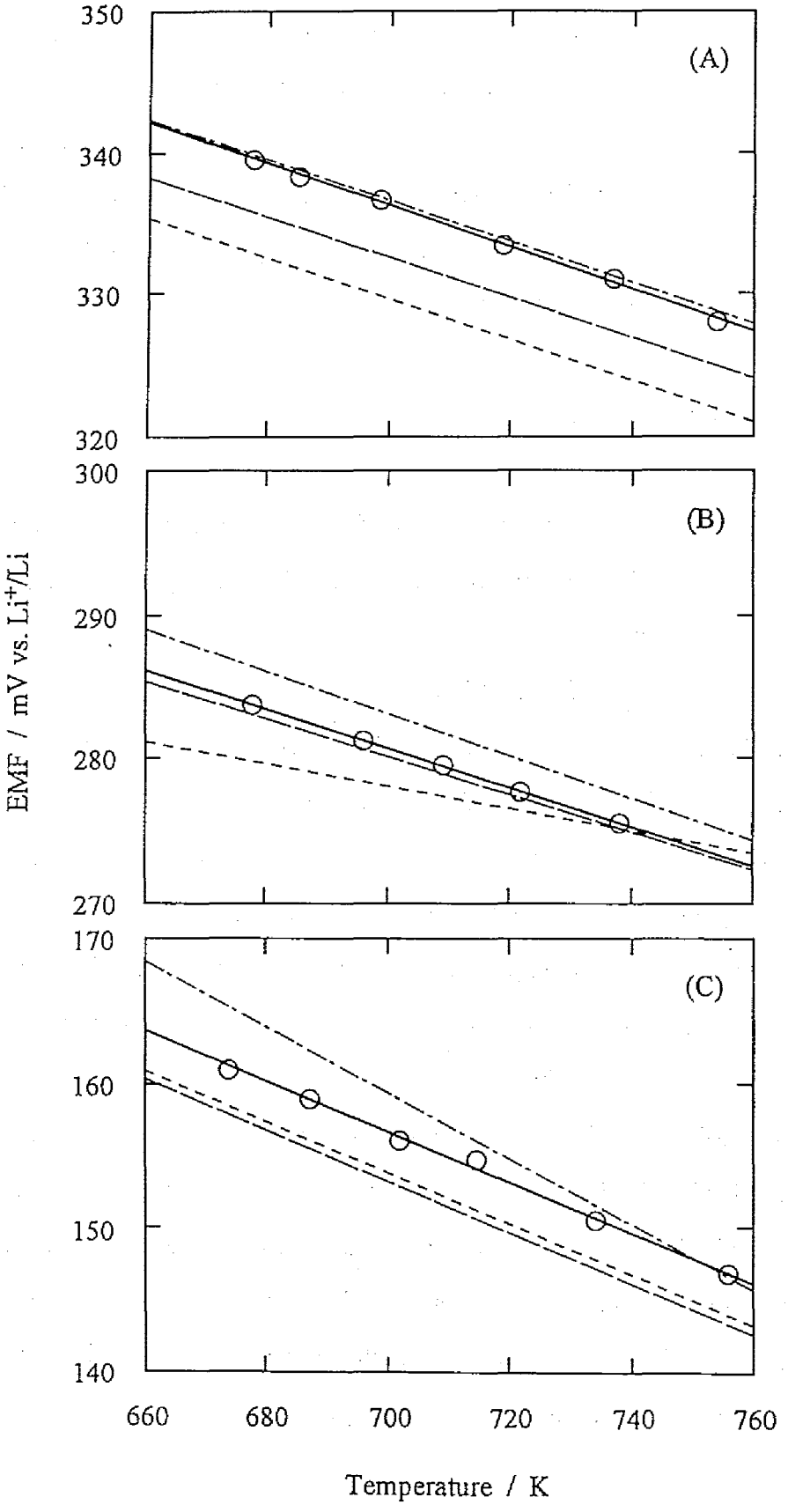
350
340
330
320
(A)
300
290
280
270
(B)
170
160
150
140
(C)
660
680
700
720
740
760
EMF / mV vs. Li+/Li
Temperature / K

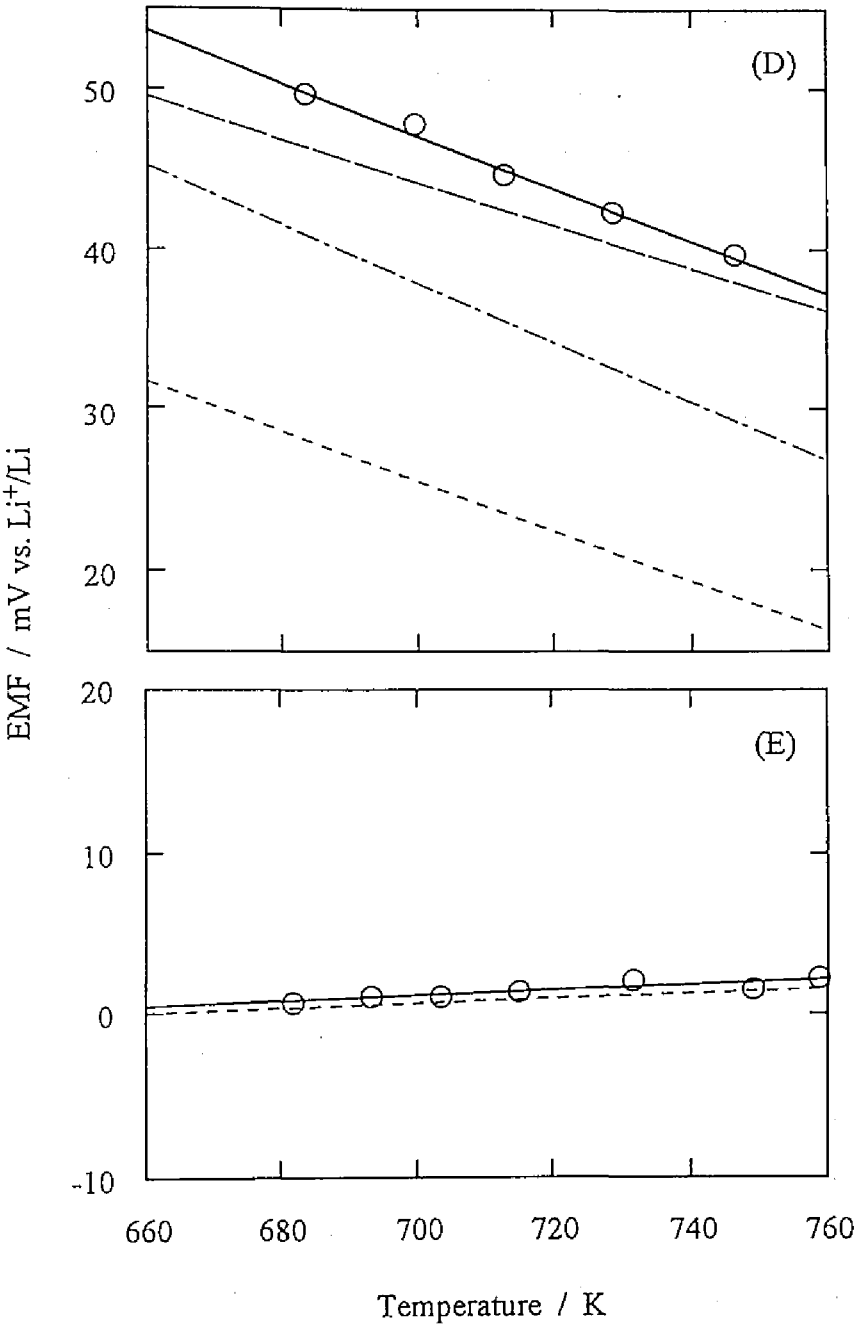

Fig.I-21. *Emf* as a function of temperature in the isothermal cell (I-e) with a Li-Si alloy electrode in the coexisting phase state: (A) $Si+Li_{12}Si_7$, (B) $Li_{12}Si_7+Li_7Si_3$, (C) $Li_7Si_3+Li_{13}Si_4$, (D) $Li_{13}Si_4+Li_{22}Si_4$, and (E) $Li_{22}Si_5$+liq.. The short-dashed line, the long-dashed line, and the dash-dotted line show the values obtained by Sharma et al. [3], Lai et al. [4] and Nikolaiev et al. [5], respectively.

These *emf* measurements under equilibrium conditions at various temperature permitted us to calculate the thermodynamic properties of each coexisting phase in Li-Si alloy: the activity a_i, the relative partial molar free energy $\Delta\overline{G}_i$, the relative partial molar entropy $\Delta\overline{S}_i$, and the relative partial molar enthalpy $\Delta\overline{H}_i$ of component i;

$$\Delta\overline{G}_{Li} = RT\ln a_{Li} = -nFE \tag{I-64}$$

$$\Delta\overline{G}_{Si} = RT\ln a_{Si} = -RT\int_{a_{Li}=0}^{a_{Li}} \frac{x_{Li}}{1-x_{Li}} d\left(\ln a_{Li}\right) \tag{I-65}$$

$$\Delta\overline{S}_i = -\frac{\partial\left(\Delta\overline{G}_i\right)}{\partial T} \tag{I-66}$$

$$\Delta\overline{H}_i = \Delta\overline{G}_i + T\frac{\partial\left(\Delta\overline{G}_i\right)}{\partial T} \tag{I-67}$$

where F and R have their usual meanings, and x_{Li} is lithium mole fraction in the alloy. Thermodynamic properties of various coexisting phase states in Li-Si alloy at 713 K are given in Table I-7.

4.3.3. Thermoelectric power

Typical experimental observations for the *emf* of the nonisothermal cell (I-f) are shown in Figs. I-22(A)~(E). A linear relationship between the *emf* and the temperature difference was observed in each measurement. The gradient of the line corresponds to the thermoelectric power. Measured thermoelectric power values of Li-Si alloy electrodes in various two-phase regions are summarized in Table I-8.

Equation (I-34) is valid to express the thermoelectric power of a Li-Si alloy electrode as well as that of a Li-Al alloy electrode. That is, the thermoelectric power of a Li-Si alloy electrode can be estimated from the values of the relative partial molar entropy and the thermoelectric power of a Li^+/Li electrode. The thermoelectric power of a Li^+/Li electrode in LiCl-KCl eutectic melt was measured to be +0.030(±0.013) $mV\cdot K^{-1}$ by Kamata et al. [6]. The values of relative partial molar entropy of lithium in the alloy

Table I-7. Relative partial molar thermodynamic properties of coexisting phase states in Li-Si alloy at 713 K.

Phase state	a_{Li}	$\Delta\overline{G}_{Li}$ kJ·mol^{-1}	$\Delta\overline{H}_{Li}$ kJ·mol^{-1}	$\Delta\overline{S}_{Li}$ J·mol^{-1}·K^{-1}	a_{Si}	$\Delta\overline{G}_{Si}$ kJ·mol^{-1}	$\Delta\overline{H}_{Si}$ kJ·mol^{-1}	$\Delta\overline{S}_{Si}$ J·mol^{-1}·K^{-1}
, Si + $Li_{12}Si_7$	4.3×10^{-3}	-32.2	-42.3	-14.1	1.0	0.0	0.0	
$Li_{12}Si_7$ + Li_7Si_3	1.0×10^{-2}	-27.2	-37.2	-14.1	2.3×10^{-1}	-8.7	-8.7	0.0
Li_7Si_3 + $Li_{13}Si_4$	8.1×10^{-2}	-14.9	-26.9	-16.8	1.8×10^{-3}	-37.3	-32.9	+6.3
$Li_{13}Si_4$ + $Li_{22}Si_5$	4.8×10^{-1}	-4.3	-15.7	-15.9	5.6×10^{-6}	-71.7	-69.2	+3.5
$Li_{22}Si_5$ + liq.	9.8×10^{-1}	-0.1	+1.1	+1.7	2.5×10^{-7}	-90.0	-142.9	-74.2

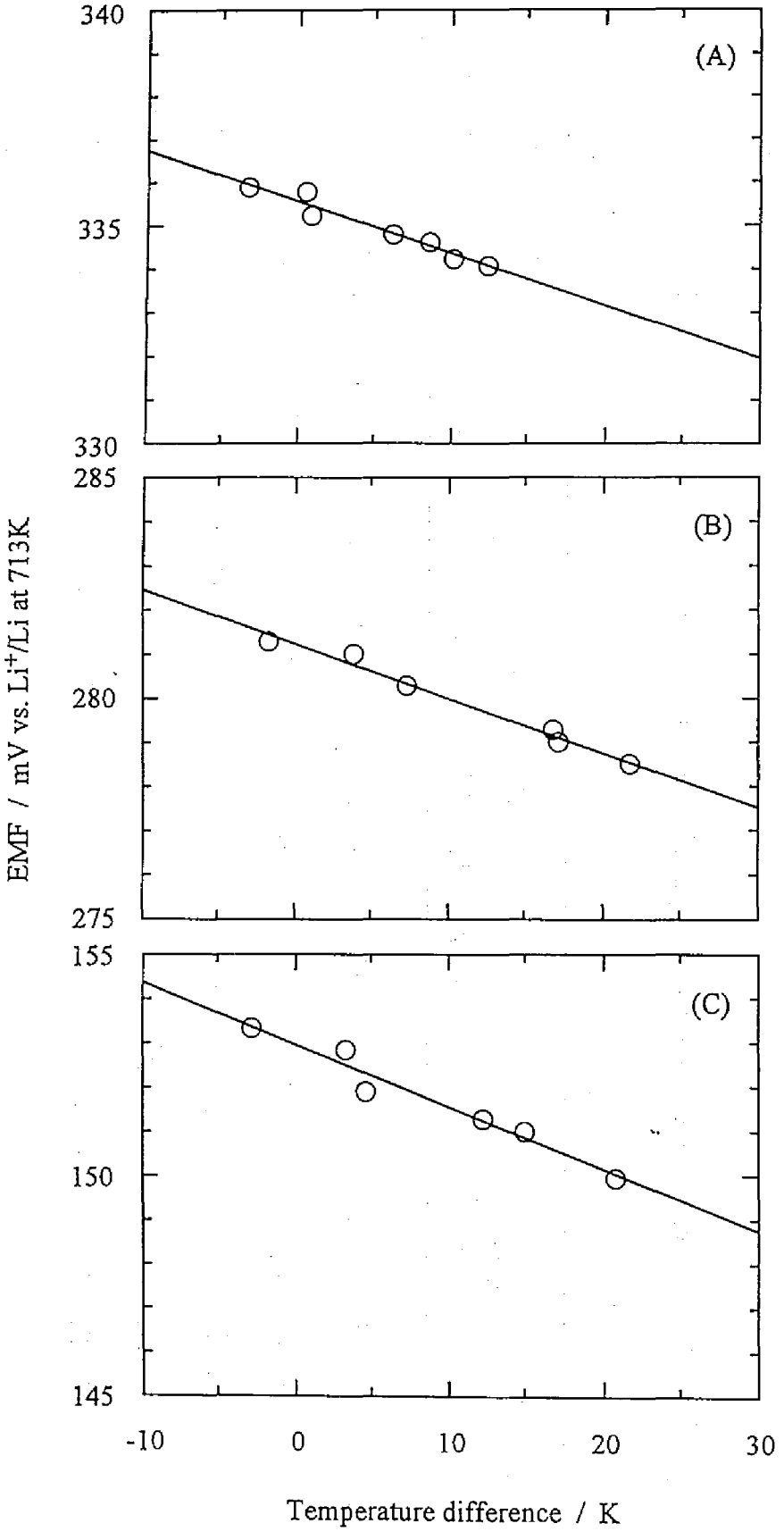
340
335
330
(A)
285
280
275
(B)
155
150
145
(C)
EMF / mV vs. Li+/Li at 713K
-10
0
10
20
30
Temperature difference / K

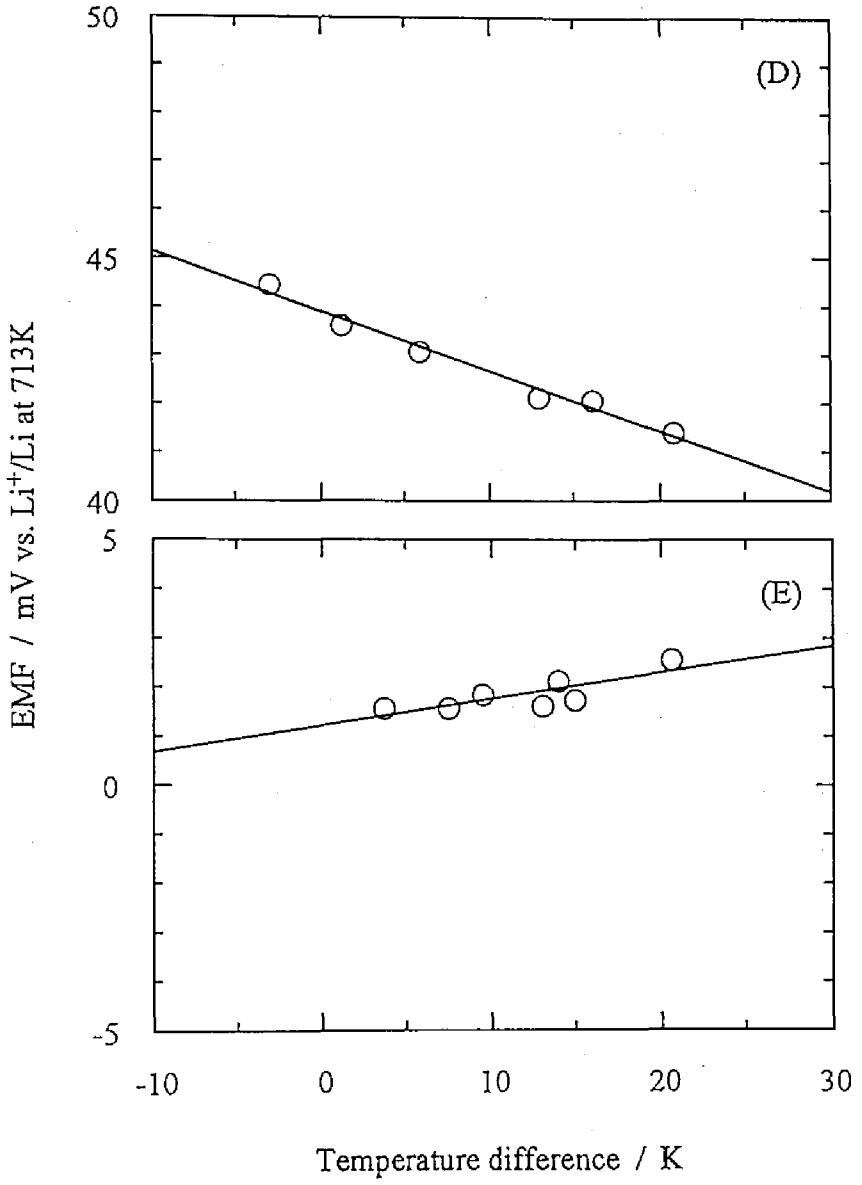

Fig.I-22. *Emf* as a function of temperature in the nonisothermal cell (I-f) with a Li-Si alloy electrode in the coexisting phase state: (A) $Si+Li_{12}Si_7$, (B) $Li_{12}Si_7+Li_7Si_3$, (C) $Li_7Si_3+Li_{13}Si_4$, (D) $Li_{13}Si_4+Li_{22}Si_4$, and (E) $Li_{22}Si_5$+liq..

for the coexisting phase states in Li-Si alloys are given in Table I-7. The estimated thermoelectric power values of Li-Si alloy electrodes in various coexisting phase states are presented in Table I-8. The estimated values agree well with those obtained by experiments within the experimental error given.

Let us consider the relation between thermoelectric power and lithium activity. The relative partial molar entropy of lithium can be expressed by using lithium activity as follows;

$$\Delta\bar{S}_{Li} = -R\ln a_{Li} - RT\frac{\partial(\ln a_{Li})}{\partial T} \tag{I-68}$$

Combining eqs. (I-34) and (I-68), eq. (I-69) is obtained;

$$\varepsilon_{Li\text{-}alloy} + \frac{RT}{F}\frac{\partial(\ln a_{Li})}{\partial T} = \varepsilon_{Li} - \frac{R}{F}\ln a_{Li} \tag{I-69}$$

Figure I-23 provides the values of $\left\{\varepsilon_{Li\text{-}alloy} + RT/F \times \partial(\ln a_{Li})/\partial T\right\}$ for various two-phase regions in Li-Si alloy plotted against logarithm of lithium activity. A good linear relationship is observed. The slope of the line accords well with the theoretical slope

Table I-8. Measured and estimated thermoelectric power of Li-Si alloy electrodes in coexisting phase states in LiCl-KCl eutectic melt.

Phase state	Thermoelectric power / $mV \cdot K^{-1}$	
	Measured value	Estimated value
$Si + Li_{12}Si_7$	-0.121 (±0.009)	-0.116 (±0.020)
$Li_{12}Si_7 + Li_7Si_3$	-0.121 (±0.006)	-0.116 (±0.026)
$Li_7Si_3 + Li_{13}Si_4$	-0.150 (±0.011)	-0.144 (±0.022)
$Li_{13}Si_4 + Li_{22}Si_5$	-0.126 (±0.008)	-0.135 (±0.027)
$Li_{22}Si_5$ + liq.	+0.051 (±0.015)	+0.048 (±0.021)

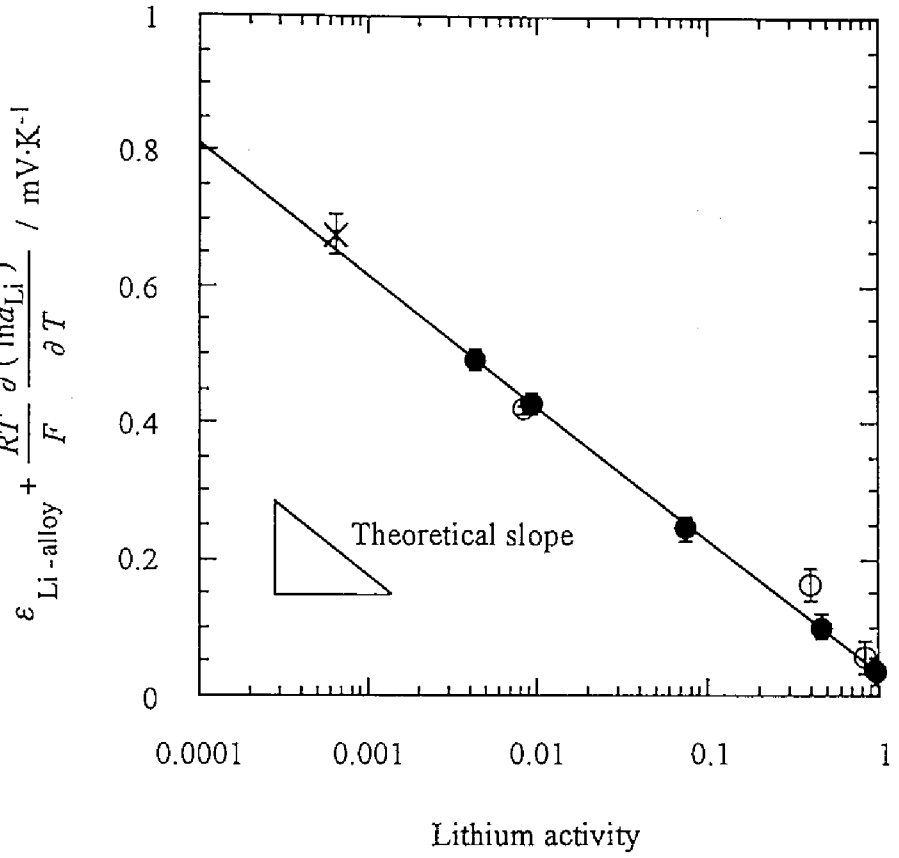

Fig.I-23. Lithium activity dependence of $\{\varepsilon_{Li\text{-}alloy} + RT/F \times \partial(\ln a_{Li})/\partial T\}$ for the coexisting phase states in Li-Si (●), Li-Al (○), and Li-Sn (×) [6] alloys.

expected from eq. (I-69). Equation (I-69) also holds for other Li-alloy electrode systems. The values for Li-Al and Li-Sn [6, 7] alloy electrode systems are also shown in Fig. I-23. The values in these alloy electrode systems fit well with the line obtained in Li-Si alloy electrode systems. According to eq. (I-69), the thermoelectric power of a Li^+/Li electrode can be estimated from the vertical value, when the line in Fig. I-23 is extrapolated to the point a_{Li} =1. It is evaluated to be +0.033(±0.013) mV·K^{-1}, which is in good agreement with the experimental value by Kamata et al., +0.030(±0.013) mV·K^{-1} [6].

4.3.4. Thermoelectric power of an alloy electrode in a solid-liquid coexisting phase

According to eqs. (I-34) and (I-47), the thermoelectric power of a Li-Si alloy electrode in the two-phase ($Li_{22}Si_5$+liq.) region can be estimated from thermodynamic properties of the single liquid phase, the phase diagram data and the thermoelectric power of a Li^+/Li electrode. For the single liquid phase in Li-Si alloy, the subregular solution model can be used to describe thermodynamic properties [2]. Then the relative partial molar entropy of lithium can be expressed as eq. (I-58). The values of the lattice stability parameter and the interaction parameters for the single liquid phase in Li-Si alloy were given by Okamoto [2], and are $F_{Li}^{liq.}$=0, $A_{Li}^{liq.}$=-53790 and $B_{Li}^{liq.}$=-40180. The lithium concentration at the solubility limit of the single liquid phase in Li-Si alloy was measured as a function of temperature by Fedorov et al. [9]. The dashed and the dash-dotted lines in Fig. I-24(A) show the estimated thermoelectric power of the two-phase ($Li_{22}Si_5$+liq.) alloy electrode by assuming the subregular solution and that by assuming the ideal solution, respectively. In Fig. I-24(A), the experimental values is also given by the solid line for comparison. Both estimated results by assuming the subregular solution and those by assuming the ideal solution are in agreement with experimental results.

The estimated curves in Fig. I-24(A) suggest that the thermoelectric power of a Li-Si alloy electrode in the two-phase ($Li_{22}Si_5$+liq.) region increases slightly with increasing temperature, whereas a constant value, +0.051(±0.015) $mV \cdot K^{-1}$, was observed in experiments for the temperature range of 703~743 K. However, temperature dependence of the thermoelectric power of this alloy phase is predicted to be very small: +0.062~+0.080 $mV \cdot K^{-1}$ at 703~743 K in the case of assuming the subregular solution. The experimental error in this study may include such small temperature dependence.

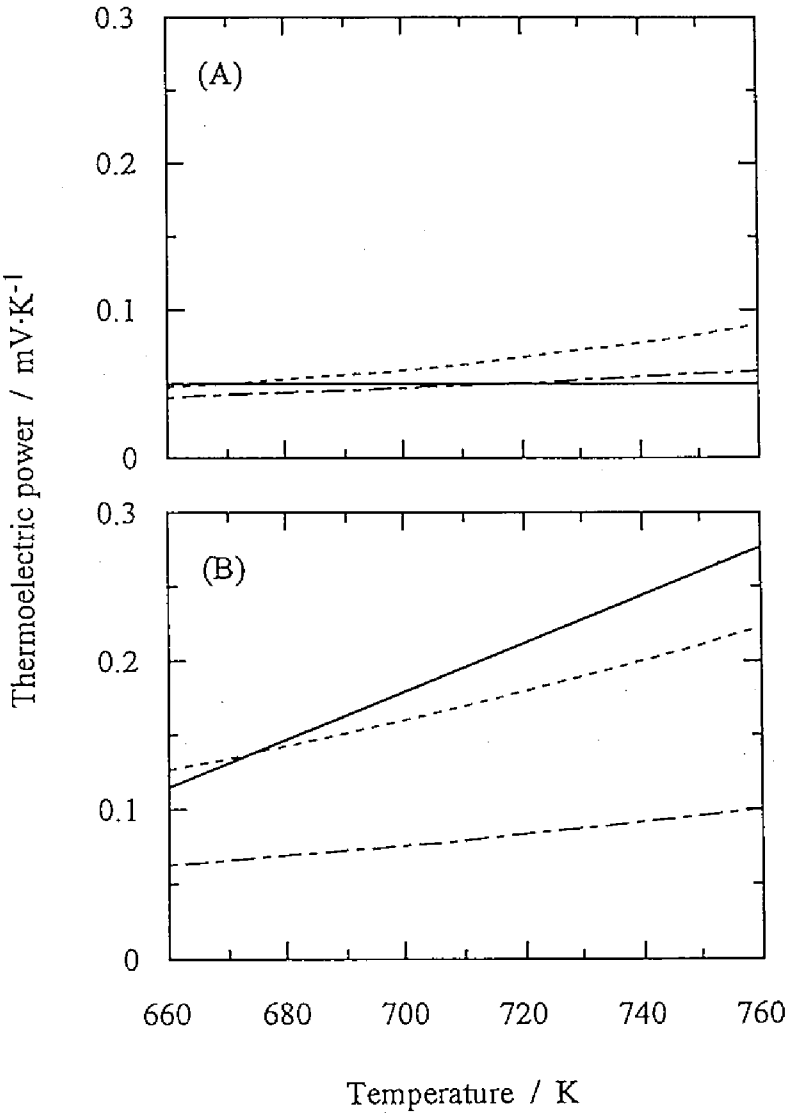

Fig.I-24. Thermoelectric power of a lithium alloy electrode in the solid-liquid coexisting phase state: (A) Li-Si alloy and (B) Li-Al alloy. The dotted line, the dash-dotted line, and the solid line show the values estimated by assuming the subregular solution, those by assuming the ideal solution and experimental data, respectively.

The thermoelectric power of a Li-Al alloy electrode in the two-phase (γLi_3Al_2+liq.) region increases significantly with increasing temperature, as already shown in chapter 2. The estimated thermoelectric power values of the two phase (γLi_3Al_2+liq.) alloy electrode by assuming the subregular solution and those by assuming the ideal solution are presented by the dashed and the dash-dotted lines in Fig. I-24(B), respectively. The values of the interaction parameters in the subregular solution model for the liquid Li-Al alloy are given in Table I-6 [9]. The calculated thermoelectric power by assuming the subregular solution exhibits similar temperature dependence as that observed in experiments. On the other hand, the calculated values by assuming the ideal solution differs from the experimental data. In lithium alloy systems, the approximation by assuming the ideal solution is available only for very high lithium concentration region [10, 11]. The lithium concentration at the solubility limit of the liquid phase in Li-Al alloy is far from unity: 0.85~0.78 at 683~783 K [9], while that in Li-Si alloy is close to unity: 0.98~0.95 at 683~783 K [2]. This would be the reason why the estimation by assuming the ideal solution is applicable to Li-Si alloy system but not to Li-Al alloy system.

4.3.5. Single electrode Peltier heat

The single electrode Peltier heat for the cathodic reaction of a Li-alloy electrode, i.e. for the electrochemical formation of Li-alloy, can be evaluated from its thermoelectric power according to eq. (I-35). Single electrode Peltier heats for electrochemical formation reactions of various phases in Li-Si alloy in LiCl-KCl eutectic melt are shown in Table I-9. It is found that the electrochemical formation of the $Li_{12}Si_7$, Li_7Si_3, $Li_{13}Si_4$, $Li_{22}Si_5$ phases, which are expressed by the reaction formulae (I-ix)~(I-ix), are accompanied by heat evolution. On the other hand, heat is absorbed for the electrochemical formation of liquid phase in Li-Si alloy, which is represented by the reaction formula (I-x). Similar tendencies were observed in Li-Al alloy electrode system.

Table I-9. Single electrode Peltier heats for the formation reactions of Li-Si alloys in LiCl-KCl eutectic melt.

Temperature / K	Single electrode Peltier heat / $J \cdot C^{-1}$				
	$Si \rightarrow Li_{12}Si_7$	$Li_{12}Si_7 \rightarrow Li_7Si_3$	$Li_7Si_3 \rightarrow Li_{13}Si_4$	$Li_{13}Si_4 \rightarrow Li_{22}Si_5$	$Li_{22}Si_5 \rightarrow$ liq.
650	-0.079	-0.079	-0.098	-0.082	+0.033
700	-0.085	-0.085	-0.105	-0.088	+0.036
750	-0.091	-0.091	-0.113	-0.095	+0.038

4.4. Conclusions

1. Single electrode Peltier heats for electrochemical formation reactions of various phases in Li-Si alloy were evaluated from measured thermoelectric power values. It was found out that the formation reactions of the $Li_{12}Si_7$, Li_7Si_3, $Li_{13}Si_4$, $Li_{22}Si_5$ phases are accompanied by heat evolution, while that of liquid Li-Si alloy phase is accompanied by heat absorption.

2. The estimation method of the thermoelectric power of a Li-alloy electrode, which was offered in the chapter 2, was validated by the experimental results for coexisting phase states in Li-Si alloy.

3. The thermoelectric power of the two-phase ($Li_{22}Si_5$+liq.) alloy electrode and that for the two-phase (γLi_3Al_2+liq.) alloy electrode were estimated by assuming the liquid phases as the subregular solution. The estimated results agrees well with the experimental results in the values as well as in the temperature dependence.

References

[1] C. J. Wen and R. A. Huggins, *J. Solid State Chem.*, **37**, 271 (1981).

[2] H. Okamoto, *Bull. Alloy Phase Diagrams*, **11**, 306 (1990).

[3] R. A. Sharma and R. N. Seefurth, *J. Electrochem. Soc.*, **123**, 1763 (1976).

[4] S. -C. Lai, *J. Electrochem. Soc.*, **123**, 1196 (1976).

[5] V. P. Nikolaiev, A. G. Morachevskii, A. I. Demidov and E. V. Bairachnyi, *Zh. Prikl. Khim.*, **53**, 1549 (1980).

[6] M. Kamata, Y. Ito, M. Inoue and J. Oishi, *J. Electrochem. Soc.*, **136**, 528 (1989).

[7] C. J. Wen and R. A. Huggins, *J. Electrochem. Soc.*, **128**, 1181 (1981).

[8] P. I. Fedorov and A. A. Ioffe, *Zh. V.U.Z. Tsvet. Met.*, **1**, 127 (1962).

[9] A. J. McAlister, *Bull. Alloy Phase Diagrams*, **3**, 177 (1982).

[10] A. G. Morachevskii and A. I. Demidov, *Zh. Fiz. Khim.*, **57**, 2113 (1983).

[11] M. -L. Saboungi, J. Marr and M. Blander, *J. Chem. Phys.*, **68**, 1375 (1978).

Chapter 5

Conclusions

The main results obtained in this work are summarized as follows;

1. The single electrode Peltier heats for the formation reactions of various phases in Li-Al alloy and Li-Si alloy in LiCl-KCl eutectic melt were determined from thermoelectric power measurements. In Li-Al alloy and Li-Si alloy systems, it was found that the formation reactions of the solid phases are accompanied by heat evolution, while those of the liquid phases are accompanied by heat absorption.

2. According to the theory of irreversible thermodynamics, it turned out that the thermoelectric power of a Li-alloy electrode can be expressed by the sum of the relative partial molar entropy of lithium in the alloy and the thermoelectric power of a Li^+/Li electrode. This relation was validated by experimental results of Li-Al alloy and Li-Si alloy electrodes in coexisting phase state. Similar estimation would be applicable also to the other alloy electrode systems.

3. The single electrode Peltier heat of a Li-Al alloy electrode was evaluated as a function of lithium concentration. It was found that the single electrode Peltier heat of the alloy electrode exhibits discontinuities at the phase boundary compositions.

4. The relation between relative partial molar thermodynamic properties in a coexisting phase state and those in its adjacent single phase state are theoretically discussed. According to this relation, the changes of the single electrode Peltier heat at the phase boundary compositions could be explained. Moreover, this relation was applied to estimate the thermoelectric power of a Li-Al alloy and a Li-Si alloy electrodes in a solid-liquid coexisting phase state from thermodynamic properties for the single liquid phase state and phase diagram data. The estimated results were in good agreement with the experimental results.

5. In the single βLiAl phase, the relative partial molar thermodynamic properties, thus the single electrode Peltier heat, considerably depends on lithium concentration. The lithium concentration dependence of the relative partial molar thermodynamic properties near the stoichiometric composition could be statistically interpreted in terms of its defect structure.

Part II

Proton and Native Conduction in 5mol% Sr-substituted $LaPO_4$ Studied by Thermoelectric Power Measurements

Proton and native conduction in 5 mol% Sr-substituted $LaPO_4$ studied by thermoelectric power measurements

1. Introduction

Significant proton conduction has been found in many solids containing structural hydrogen (protons), such as acid salts and hydroxides, but also in several classes of materials inherently without protons, such as oxides, sulphates, and phosphates (see, for instance, a recent review by Kreuer [1]). Materials of the latter group, in which protons dissolve as defects in the presence of hydrogen-containing gases, become proton conductors mainly at high temperatures. Such high temperature proton conductors (HTPCs) are candidate materials for the electrolyte in high temperature fuel cells [2, 3]. A main advantage of a fuel cell with a proton conductor is that fuel cleaning will not be necessary, because water is produced at the oxygen (air) electrode, in stead of at the hydrogen electrode. It is also interesting that other sources of hydrogen than H_2 gas can be used as fuel [2]. Other applications of HTPC's are hydrogen and water vapor sensors, and electrochemical hydrogen separation systems [2, 3].

However, HTPCs tend to exhibit mixed conduction due to conductivity contributions arising from native charge carriers, typically oxide ions and electrons or electron holes (see, for instance, ref. [4]). The relative contribution of the different charge carrier species to the total conductivity may vary considerably with temperature, hydrogen partial pressure, p_{H_2}, (or water vapor partial pressure, p_{H_2O}), and oxygen

partial pressure, p_{O_2}. From a fundamental point of view it is of interest to characterize the conduction properties of HTPCs under various conditions, and from an applied point of view one needs to determine the conditions for pure protonic conduction.

Different experimental techniques can be employed to reveal the conduction mechanisms in HTPCs. Conductivity measurements versus p_{H_2} (or p_{H_2O}) and p_{O_2} may give fundamental information on the defect structure, charge carrier types and conduction mechanisms. H/D isotope effects in the conductivity are particularly suitable for qualitative identification of protonic conduction [5]. *Emf* measurements on concentration cell [4, 6] and faradaic transport experiments [7, 8] can be used to determine protonic and other transport numbers. Thermoelectric power measurements have also been employed in studies of mixed protonic, oxide ion, and electronic conduction in oxides [9, 10], though the thermoelectric power of these materials have not been quantitatively interpreted yet.

$LaPO_4$, in which La is partially substituted with a divalent metal (acceptor) has been suggested as an interesting system for dissolution and transport of defect protons, thus a candidate for a HTPC. Based on this, the total ac conductivity of $LaPO_4$ substituted with 5 mol% Ca or Sr has been investigated under oxidizing conditions as a function of temperature and water vapor partial pressure by Norby and Christiansen [11]. They concluded that the conductivity is due to mainly protons at low temperature and high water vapor partial pressures, supported by the presence of a H/D isotope effect in this region. At higher temperature and/or drier conditions a native conduction became predominant. In wet atmospheres the protonic conductivity was predominant below 1073 K. The protonic conductivity increased with water vapor partial pressure and was higher in the Sr-substituted than in the Ca-substituted sample.

Although it was assumed as a working hypothesis that the protons charge compensates the acceptor dopants, there were details in the conductivity behavior that did not confer with this model: The proton conductivity did not reach a plateau as a

function of water vapor partial pressure, and the native (non-protonic) conductivity contributions did not appear to vary with water vapor partial pressure so much. In this respect, the present phosphate behaved differently from oxides.

In this work, a bar-shaped sample of 5 mol% Sr-substituted $LaPO_4$ fabricated in parallel with the one used in conductivity measurements in ref. 11 is used for studies of the thermoelectric power of this mixed, partially protonic conductor. By using the theory of irreversible thermodynamics by Førland et al. [12], theoretical expressions of the thermoelectric power for a pure conductor by protons, by oxide ions, by electronic defects, and for a mixed conductor by these three types of charge carrier species are derived. The purpose of this work is to test the application of derived theoretical expressions for thermoelectric power and to utilize the method for further characterization of this and other materials' conduction properties and defect structure.

2. Principles

2.1. Thermoelectric power

As a general case, the thermoelectric power of the cell (II-a) is discussed;

$$(T_1)\mathrm{Pt}\,|\,\mathrm{H_2O}(p_{H_2O}),\ \mathrm{O_2}(p_{O_2})\,|\,\text{Mixed conductor}\,|\,\mathrm{H_2O}(p_{H_2O}),\ \mathrm{O_2}(p_{O_2})\,|\,\mathrm{Pt}(T_2) \qquad \text{(II-a)}$$

A homogenous gas mixture of oxygen, inert gas, and water vapor (with partial pressures p_{O_2} and p_{H_2O}) is kept in the cell (II-a), while the two electrodes are at different temperature T_1 and T_2. In the following we derive the theoretical expressions for thermoelectric power using the theory of irreversible thermodynamics by Førland et al. [12]. In this derivation, only operationally defined variables are used, and single ion or

electrochemical potentials, which are not operationally defined, are avoided contrary to other derivation methods. We will first consider the thermoelectric power when the electrolyte conducts one type of charge carrier only. We choose to do this in the three cases of conduction by protons, by oxide ions, and by electronic defects. Thereafter, we address cases of mixed conduction.

2.1.1. Pure protonic conductor

When the electrolyte conducts only protons and the electrodes are reversible to protons, no chemical potential gradient of neutral components arises in the system. In such a system, the dissipation function of the system, $T\Theta$, is [12];

$$T\Theta = -J_q \nabla \ln T - j \nabla \phi^{obs} \qquad \text{(II-1)}$$

The fluxes are the measurable heat flux, J_q, and the electric current density, j. The forces are $-\nabla \ln T$ and the electric potential gradient of the cell (II-a), $-\nabla \phi^{obs}$. The flux equations of heat and charge are then accordingly;

$$J_q = -L_{11} \nabla \ln T - L_{12} \nabla \phi^{obs} \qquad \text{(II-2)}$$

$$j = -L_{21} \nabla \ln T - L_{22} \nabla \phi^{obs} \qquad \text{(II-3)}$$

where L_{ij}'s are phenomenological coefficients. When no net current is drawn (j=0), the following expression for the cell *emf* can be obtained using eqs. (II-2) and (II-3) together with the Onsagar reciprocal relation, $L_{ij}=L_{ji}$;

$$\left(\nabla \phi^{obs}\right)_{j=0} = -\left(\frac{L_{21}}{L_{22}}\right) \nabla \ln T = -\left(\frac{L_{12}}{L_{22}}\right) \nabla \ln T$$

$$= -\left(\frac{J_q}{j}\right)_{\Delta T = 0} \frac{\nabla T}{T} = -\left(\frac{\pi^{\dagger}}{T}\right) \nabla T \qquad \text{(II-4)}$$

The Peltier heat effect, $\left(\pi^{\dagger}/T\right)$, is obtained from the reversible heat balance at one electrode [12]. The reversible heat changes are given by entropy changes and the transported entropies. When the electrolyte is a pure protonic conductor, the half cell

reactions are;

$$\frac{1}{2}H_2O(T_1) = H^+(T_1) + \frac{1}{4}O_2(T_1) + e^-(T_1) \qquad \text{(II-i)}$$

$$H^+(T_2) + \frac{1}{4}O_2(T_2) + e^-(T_2) = \frac{1}{2}H_2O(T_2) \qquad \text{(II-ii)}$$

The reversible entropy changes in the system are summarized in Table II-1. From Table II-1, we have;

$$\frac{\pi^{\downarrow}}{T} = -\frac{1}{2}S_{H_2O} + \frac{1}{4}S_{O_2} + S^*_{H^+} + S^*_{Pt} \qquad \text{(II-5)}$$

where S_{H_2O} and S_{O_2} are the partial molar entropies of water vapor and oxygen, and $S^*_{H^+}$ and S^*_{Pt} are the transported entropies of protons in the electrolyte and of electrons in the electrode. Equations (II-4) and (II-5) give the expression for the cell *emf*,

Table II-1. Reversible entropy changes at the left hand electrode region of the nonisothermal cell (II-a) for the transfer of one faraday positive charges when the electrolyte is a pure protonic conductor.

	Entropy received
$\pi^{\downarrow}/T$	the interface receives entropy from the heat reservoir.
$1/2\ S_{H_2O}$	the disapearance of 1/2 mole of water vapor liberates entropy.
	Entropy consumed
$S^*_{H^+}$	entropy transported by protons through the electrolyte away from the interface.
S^*_{Pt}	entropy transported by electrons through the platinum electrode away from the interface.
$1/4\ S_{O_2}$	the formation of 1/4 mole of oxygen consumes entropy.

$$\left(\nabla\phi^{obs}\right)_{j=0} = \left(\frac{1}{2}S_{H_2O} - \frac{1}{4}S_{O_2} - S^*_{H^+} - S^*_{Pt}\right)\nabla T \qquad \text{(II-6)}$$

If we assume constant heat capacity for gases, c_p, over the considered temperature range, the temperature dependence of the partial molar entropies of water vapor and oxygen are;

$$S_{H_2O}(T) = S^0_{H_2O}(T_1) - R\ln\frac{p_{H_2O}}{p^0_{H_2O}} + c_{p,H_2O}\ln\frac{T}{T_1} \qquad \text{(II-7)}$$

$$S_{O_2}(T) = S^0_{O_2}(T_1) - R\ln\frac{p_{O_2}}{p^0_{O_2}} + c_{p,O_2}\ln\frac{T}{T_1} \qquad \text{(II-8)}$$

For the transported entropies we have;

$$S^*_i(T) = S^*_i(T_1) + \tau_i\ln\frac{T}{T_1} \qquad \text{(II-9)}$$

where τ_i is the Thomson coefficient. By introducing eqs. (II-7)~(II-9) into eq. (II-6), and integrating from T_1 to T_2, we obtain the practical expression of the thermoelectric power;

$$\left(\frac{\Delta E}{\Delta T}\right)_{j=0} = \frac{1}{F}\left(\frac{\Delta\phi^{obs}}{\Delta T}\right)_{j=0}$$

$$= \frac{1}{F}\left\{\frac{1}{2}S^0_{H_2O}(T_1) - \frac{R}{2}\ln\frac{p_{H_2O}}{p^0_{H_2O}} - \frac{1}{4}S^0_{O_2}(T_1) + \frac{R}{4}\ln\frac{p_{O_2}}{p^0_{O_2}} - S^*_{H^+}(T_1) - S^*_{Pt}(T_1)\right\}$$

$$-\frac{1}{F}\left(\frac{1}{2}c_{p,H_2O} - \frac{1}{4}c_{p,O_2} - \tau_{H^+} - \tau_{Pt}\right)\left(1 - \frac{T_2}{\Delta T}\ln\frac{T_2}{T_1}\right) \qquad \text{(II-10)}$$

In the limit of small temperature differences we have $\lim_{\Delta T\to 0}\left(\frac{T_2}{\Delta T}\ln\frac{T_2}{T_1}\right) = 1$, and then we obtain;

$$\left(\frac{dE}{dT}\right)_T = \lim_{\Delta T\to 0}\left(\frac{\Delta E}{\Delta T}\right)_{j=0}$$

$$= \frac{1}{F}\left\{\frac{1}{2}S^0_{H_2O}(T_1) - \frac{R}{2}\ln\frac{p_{H_2O}}{p^0_{H_2O}} - \frac{1}{4}S^0_{O_2}(T_1) + \frac{R}{4}\ln\frac{p_{O_2}}{p^0_{O_2}} - S^*_{H^+}(T_1) - S^*_{Pt}(T_1)\right\} \qquad \text{(II-11)}$$

2.1.2. Pure oxide ion conductor

When the electrolyte is a pure oxide ion conductor, the half cell reactions are;

$$\frac{1}{2}O^{2-}(T_1) = \frac{1}{4}O_2(T_1) + e^-(T_1) \qquad \text{(II-iii)}$$

$$\frac{1}{4}O_2(T_2) + e^-(T_2) = \frac{1}{2}O^{2-}(T_2) \qquad \text{(II-iv)}$$

The thermoelectric power can be obtained in a similar way as for a pure protonic conductor as follows;

$$\left(\frac{dE}{dT}\right)_T = \frac{1}{F}\left\{-\frac{1}{4}S^0_{O_2}(T_1) + \frac{R}{4}\ln\frac{P_{O_2}}{P^0_{O_2}} + \frac{1}{2}S^*_{O^{2-}}(T_1) - S^*_{Pt}(T_1)\right\} \qquad \text{(II-12)}$$

where $S^*_{O^{2-}}$ represents the transported entropy of oxide ions in the electrolyte.

2.1.3. Pure electronic conductor

In a cell with a pure electron or electron hole conductor, no electrochemical reactions take place with the gases. The thermoelectric power is then expressed only by transported entropy terms. The equation for a pure electron conductor is;

$$\left(\frac{dE}{dT}\right)_T = \frac{1}{F}\left\{S^*_e(T_1) - S^*_{Pt}(T_1)\right\} \qquad \text{(II-13)}$$

, and that for a pure electron hole conductor is;

$$\left(\frac{dE}{dT}\right)_T = \frac{1}{F}\left\{-S^*_h(T_1) - S^*_{Pt}(T_1)\right\} \qquad \text{(II-14)}$$

where S^*_e and S^*_h express the transported entropies of electrons and of electron holes in the electrolyte, respectively.

2.1.4. Mixed conductor

For a conductor having conduction by protons, oxide ions, and electronic defects, the assumption of no net current still can be applied and thus equation (II-4) is still valid, if the electrodes are reversible and there is no condensation or dilution of protons, oxide ions, and electronic defects in the electrolyte. The reversible entropy changes in the system are summarized in Table II-2, and then the Peltier effect can be

Table II-2. Reversible entropy changes at the left hand electrode region of the nonisothermal cell (II-a) for the transfer of one faraday positive charges when the electrolyte is a mixed protonic, oxide ion and electronic conductor.

	Entropy received
π^I/T	the interface receives entropy from the heat reservoir.
$1/2\ t_{H^+} S_{H_2O}$	the disapearance of 1/2 t_{H^+} mole of water vapor liberates entropy.
$t_{H^+} S^*_{H^+}$	entropy transported by t_{H^+} mole of proton through the electrolyte away from the interface.
$t_h\ S^*_h$	entropy transported by t_h mole of electron hole through the electrolyte away from the interface.
	Entropy consumed
$1/4\ t_{O^{2-}} S_{O_2}$	the formation of 1/4 $t_{O^{2-}}$ mole of oxygen consumes entropy.
$1/2\ t_{O^{2-}} S^*_{O^{2-}}$	entropy transported by 1/2 $t_{O^{2-}}$ mole of oxide ion through the electrolyte away from the interface.
$t_e\ S^*_e$	entropy transported by t_e mole of electron through the the electrolyte away from the interface.
S^*_{Pt}	entropy transported by electrons through the platinum electrode away from the interface.

expressed as follows;

$$\frac{\pi^{\downarrow}}{T} = -\frac{t_{H^+}}{2}S_{H_2O} + \frac{1}{4}S_{O_2} + t_{H^+}S^*_{H^+} - t_{O^{2-}}S^*_{O^{2-}} + t_hS^*_h - t_eS^*_e + S^*_{Pt} \qquad \text{(II-15)}$$

where t_i is the transport number of charge carrier species i. In a similar way as for the derivation of eq. (II-11), the expression of the thermoelectric power for a conductor having conduction by protons, oxide ions, and electronic defects can be derived as follows, when the temperature difference between electrodes is small;

$$\left(\frac{dE}{dT}\right)_{\Delta T=0,j=0} = \frac{1}{F}\left\{\frac{t_{H^+}}{2}S^0_{H_2O}(T_1) - \frac{t_{H^+}R}{2}\ln\frac{p_{H_2O}}{p^0_{H_2O}} - \frac{1}{4}S^0_{O_2}(T_1) + \frac{R}{4}\ln\frac{p_{O_2}}{p^0_{O_2}}\right.$$
$$\left. - t_{H^+}S^*_{H^+}(T_1) + t_{O^{2-}}S^*_{O^{2-}}(T_1) - t_hS^*_h(T_1) + t_eS^*_e(T_1) - S^*_{Pt}(T_1)\right\} \qquad \text{(II-16)}$$

Considering $t_{H^+} + t_{O^{2-}} + t_h + t_e = 1$, equation (II-16) can be rewritten as follows;

$$\left(\frac{dE}{dT}\right)_T = \frac{t_{H^+}}{F}\left\{\frac{1}{2}S^0_{H_2O}(T_1) - \frac{R}{2}\ln\frac{p_{H_2O}}{p^0_{H_2O}} - \frac{1}{4}S^0_{O_2}(T_1) + \frac{R}{4}\ln\frac{p_{O_2}}{p^0_{O_2}} - S^*_{H^+}(T_1) - S^*_{Pt}(T_1)\right\}$$
$$+ \frac{t_{O^{2-}}}{F}\left\{-\frac{1}{4}S^0_{O_2}(T_1) + \frac{R}{4}\ln\frac{p_{O_2}}{p^0_{O_2}} + S^*_{O^{2-}}(T_1) - S^*_{Pt}(T_1)\right\}$$
$$+ \frac{t_h}{F}\left\{-S^*_h(T_1) - S^*_{Pt}(T_1)\right\} + \frac{t_e}{F}\left\{S^*_e(T_1) - S^*_{Pt}(T_1)\right\} \qquad \text{(II-17)}$$

In the right hand side of eq. (II-17), the terms in the four braces are identical with the thermoelectric power for a pure conductor by protons, oxide ions, electron holes, and electrons in order. It is thus found that the thermoelectric power for a mixed conductor can be written as a sum of the thermoelectric power of each charge carrier weighted with their respective transport number. This corresponds to the so-called Chambers' relation found for mixed electron and electron hole conductors [13]. One should here note that the transport numbers in eq. (II-17) are functions of p_{O_2} and p_{H_2O} as well as temperature, although it is common to assume constant, average transport numbers over the small temperature gradient used in thermoelectric measurements.

2.2. Defect structures in Sr-substituted $LaPO_4$

The strontium ions are assumed to dissolve substitutionally for lanthanum in $LaPO_4$, forming acceptor defects which in Kröger-Vink notation are termed Sr'_{La} [11]. The effective negative charge of the acceptor substituents is compensated by effectively positive defects. In oxides these would comprise oxygen vacancies, electron holes, and protons (hydroxide ions). If Sr^{2+} can be incorporated, while the orthophosphate lattice grows and remains fully occupied, these defects may also be expected in phosphates. In phosphates we may have to consider oxygen deficiency in terms of defects of di- (pyro-) or poly- (meta-) phosphate groups in the orthophosphate lattice. Like in many oxides, electron holes may be regarded as O^- ions. Protons may be regarded as part of hydroxide ions, OH^-, or biphosphate ions, HPO_4^{2-}, but in the following we will refer to them as interstitial protons, denoted as $H_i^{\bullet}$. For further simplification we will use oxygen vacancies as a symbol of some kind of oxygen deficit (true vacancy, diphosphate, metaphosphate), i.e. some positive native point defects. We will disregard native cation defects as well as defect electrons.

If the substitution of Sr^{2+} for La^{3+} is done by reacting the substituent La and Sr orthophosphates there will be a permanent PO_4^{3-} deficit such that the main positive compensating defects are phosphate vacancies. These can not be annihilated through interaction with the atmosphere, but they can possibly be filled with O^{2-} and/or OH^- ions in various constellations.

If we express the defects in the phosphate in terms of simplified species like oxygen vacancies, interstitial protons, and holes, these defects are in equilibrium according to the following defect equilibria;

$$\frac{1}{4}O_2(g)+\frac{1}{2}V_O^{\bullet\bullet} \leftrightarrow \frac{1}{2}O_O^{\times}+h^{\bullet} \qquad \text{(II-v)}$$

$$K_1=\left[h^{\bullet}\right]\left[V_O^{\bullet\bullet}\right]^{-\frac{1}{2}}p_{O_2}{}^{-\frac{1}{4}} \qquad \text{(II-18)}$$

and

$$\frac{1}{2}H_2O(g) + h^{\bullet} \leftrightarrow H_i^{\bullet} + \frac{1}{4}O_2(g) \qquad \text{(II-vi)}$$

$$K_2 = \left[H_i^{\bullet}\right]\left[h^{\bullet}\right]^{-1} p_{H_2O}{}^{-\frac{1}{2}} p_{O_2}{}^{\frac{1}{4}} \qquad \text{(II-19)}$$

where Kröger-Vink notation is used and *K's* are the equilibrium constants, assuming ideal conditions (low concentrations and partial pressures). If we assume that electronic defects are present in minor concentrations and disregard the possibility of phosphate group vacancies, the electroneutrality condition can be approximated by;

$$2\left[V_O^{\bullet\bullet}\right] + \left[H_i^{\bullet}\right] = \left[Sr_{La}^{'}\right] \qquad \text{(II-20)}$$

which then resembles the situation found in many acceptor-doped oxides. The concentration of each defect can be obtained from eqs. (II-18)~(II-20) with knowledge of the doping level and the values of the equilibrium constants. When the native positive point defects, denoted as $V_O^{\bullet\bullet}$ here, are dominant defects, the concentration of majority and minority point defects can be expressed as eq. (II-21)~(II-23);

$$\left[V_O^{\bullet\bullet}\right] = \frac{1}{2}\left[Sr_{La}^{'}\right] \qquad \text{(II-21)}$$

$$\left[H_i^{\bullet}\right] = K_2\left(\frac{\left[Sr_{La}^{'}\right]}{2}\right)^{1/2}\left(p_{H_2O}\right)^{1/2} \qquad \text{(II-22)}$$

$$\left[h^{\bullet}\right] = K_1\left(\frac{\left[Sr_{La}^{'}\right]}{2}\right)^{1/2}\left(p_{O_2}\right)^{1/4} \qquad \text{(II-23)}$$

When protons are dominant defects, the concentrations of defects can be described as follows;

$$\left[H_i^{\bullet}\right] = \left[Sr_{La}^{'}\right] \qquad \text{(II-24)}$$

$$\left[V_O^{\bullet\bullet}\right] = \left(\frac{\left[Sr_{La}^{'}\right]}{K_2}\right)^{2}\left(p_{H_2O}\right)^{-1} \qquad \text{(II-25)}$$

$$\left[h^{\bullet}\right] = \left(\frac{K_1\left[Sr_{La}^{'}\right]}{K_2}\right)\left(p_{H_2O}\right)^{-1/2}\left(p_{O_2}\right)^{1/4} \qquad \text{(II-26)}$$

Figures II-1(A) and (B) show the defect concentrations versus p_{H_2O} under constant p_{O_2} and versus p_{O_2} under constant p_{H_2O} for the two limiting electroneutrality conditions.

2.3. p_{H_2O} and p_{O_2} dependencies of thermoelectric power

Kjelstrup Ratkje and Tomii [14] found that the transported entropy of oxide ions in yttria-stabilized zirconia (YSZ) does not depend on charge carrier concentration,

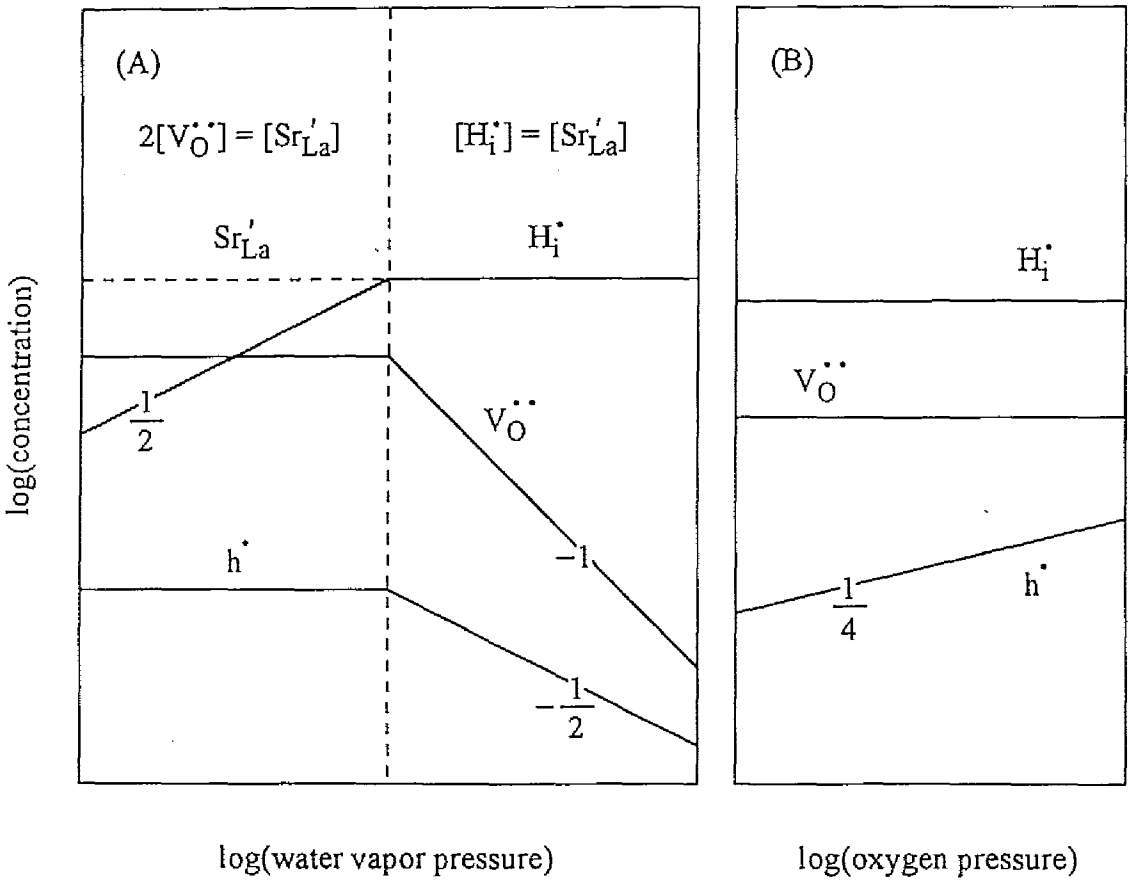

Fig.II-1. Schematic illustration of a possible defect situation in Sr-substituted $LaPO_4$ as a function of (A) water vapor partial pressure and (B) oxygen partial pressure. The concentration ratios are arbitrarily chosen for illustrative purposes.

while others have found certain variations [15]. If we assume that the transported entropy of protons is independent of p_{H_2O} and p_{O_2}, eq. (II-11) predicts that a pure protonic conductor will have a thermoelectric power with a slope of $-R/2F$ when plotted versus $\ln p_{H_2O}$ under constant p_{O_2} and a slope of $R/4F$ when plotted versus $\ln p_{O_2}$ under constant p_{H_2O}. Such distinctive pressure dependencies of the thermoelectric power can be a guide to detect the condition for pure protonic conduction. Similarly, eq. (II-12) predicts that a pure oxide ion conductor will have a thermoelectric power with a slope of $R/4F$ when plotted versus $\ln p_{O_2}$, while it will have a thermoelectric power independent of p_{H_2O}, if we assume the transported entropy of oxide ions is independent of p_{H_2O} and p_{O_2}.

The thermoelectric power of mixed conductors depends on the transport numbers, as shown in eq. (II-17). When the electrolyte conducts only protons and oxide ions, i.e. when the conduction by electronic defects is negligible, the expression for the thermoelectric power can be simplified by introducing the relation $t_{H^+} + t_{O^{2-}} = 1$, we obtain;

$$\left(\frac{dE}{dT}\right)_T = \frac{1}{F}\left\{-\frac{1}{4}S^0_{O_2}(T_1) + \frac{R}{4}\ln\frac{p_{O_2}}{p^0_{O_2}} - \frac{1}{2}S^*_{O^{2-}}(T_1) - S^*_{P_i}(T_1)\right\}$$

$$+\frac{t_{H^+}}{F}\left\{\frac{1}{2}S^0_{H_2O}(T_1) - \frac{R}{2}\ln\frac{p_{H_2O}}{p^0_{H_2O}} - \frac{1}{2}S^*_{O^{2-}}(T_1) - S^*_{H^+}(T_1)\right\} \quad \text{(II-27)}$$

In such a conductor, the concentration of protons and oxygen vacancies may be regarded independent of p_{O_2} as shown in Fig. II-1(B), i.e. the proton transport number may be regarded independent of p_{O_2}. As a consequence, the thermoelectric power for a mixed protonic and oxide ion conductor is then proportional to $\ln p_{O_2}$ with a slope of $R/4F$ at constant p_{H_2O} under the assumptions made. For mixed ionic electronic conductors, transport numbers depend on both p_{H_2O} and p_{O_2}, and complicate the p_{H_2O} and p_{O_2} dependencies of the thermoelectric power. According to these consideration,

thermoelectric power measurements versus p_{O_2} can be used to evaluate the contribution of the conduction by electronic defects to the total conductivity in a mixed conductor.

3. Experimental

The material examined in this work is 5 mol% Sr-substituted $LaPO_4$. The preparation of this material is as follows. 0.2 M solutions of $La(NO_3)_3$ and $Sr(NO_3)_2$ were mixed in the appropriate proportions, and then a 0.2 M solution of $(NH_4)_2HPO_4$ was added dropwise. The precipitation was calcined at 1073 K for 5 hours and was grounded into a powder. The Sample were cold pressed in a steel tool with 1.5 $t \cdot cm^{-2}$, and was sintered at 1573 K for 5 hours to bar with approximate dimensions 2 x 6 x 35 mm. The samples used for thermoelectric power measurements was fabricated in parallel with the one used in conductivity measurements in ref. 11. This makes it possible to compare the results obtained in this work directly with the results in conductivity measurements. It is not well known what content of phosphate relative to the cations this preparation method leads to. However, the atomic ratio in the sample after thermoelectric power measurements was estimated to be La:Sr:P = 0.965:0.036:1.000 by the inductively coupled plasma (ICP) spectrometry. That is, the sum of cation contents is approximately equal to P content in the material used. This may suggest that phosphate vacancies are not present in considerable amount in this material.

The thermoelectric power was determined from *emf* measurements of the following nonisothermal cell (II-b) at the investigated temperatures;

$$(T_1)\mathrm{Pt} \mid \mathrm{H_2O}(p_{H_2O}),\ \mathrm{O_2}(p_{O_2}) \mid \text{Sr - substituted } \mathrm{LaPO_4} \mid \mathrm{H_2O}(p_{H_2O}),\ \mathrm{O_2}(p_{O_2}) \mid \mathrm{Pt}(T_2) \qquad \text{(II-b)}$$

The experimental apparatus is illustrated in Fig. II-2. The cell was shielded by using an

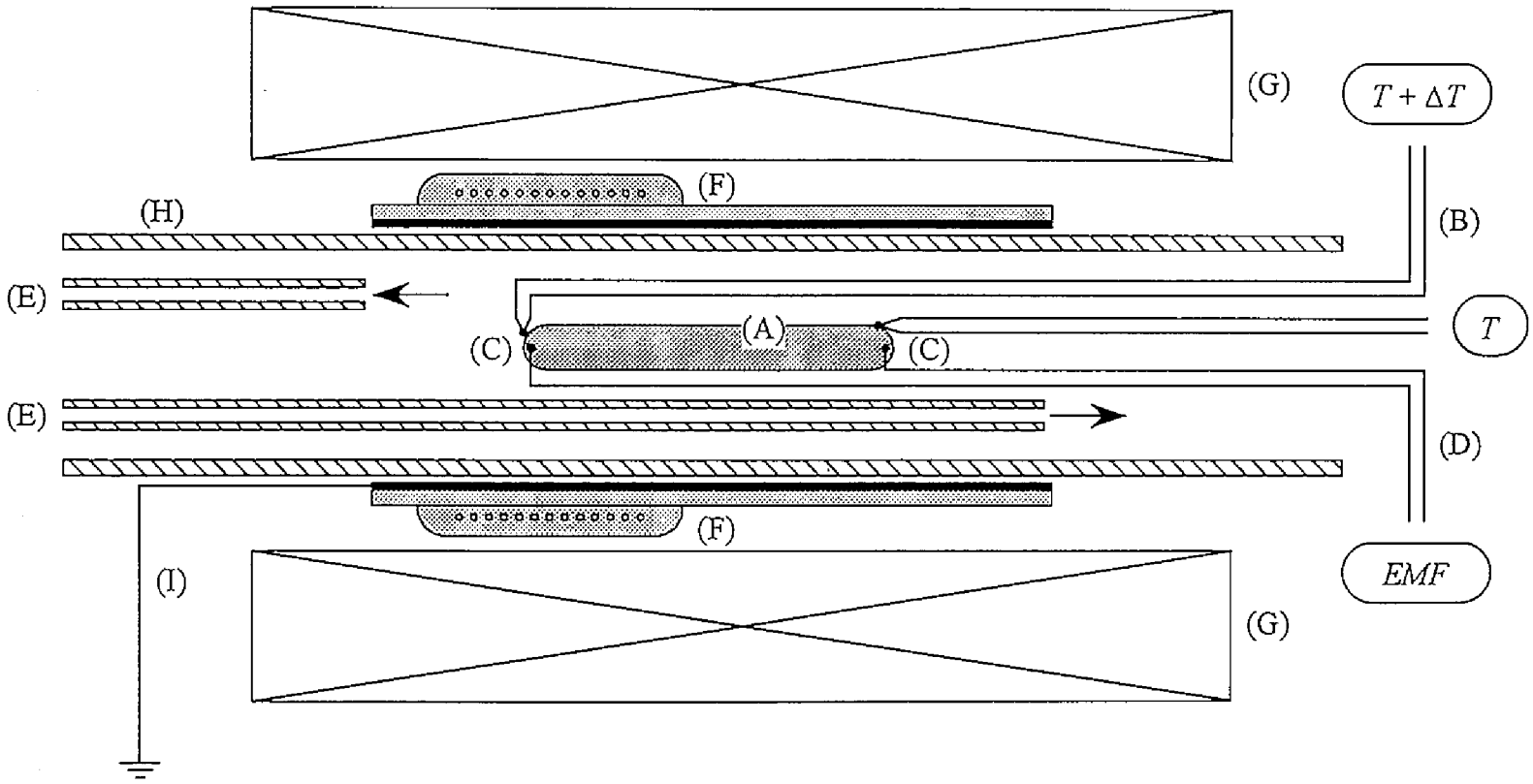

Fig.II-2. Schematic illustration of the cell used for thermoelectric power measurements; (A) sample (5 mol% Sr-sbstututed $LaPO_4$), (B) thermocouple (Pt-10%PtRh), (C) porous platinum electrode, (D) electrical lead (platinum wire), (E) alumina tubes for gas inlet and outlet, (F) inner heating element, (G) furnace, (H) silica tube, and (I) electrical shield.

earthed platinum foil to avoid electric noise from furnace. An extra heating element was used to produce temperature differences over the electrolyte. The temperatures were measured with two Pt/Pt10%Rh thermocouples placed on the electrodes. The furnace and the inner heating element were controlled individually. The temperature of one electrode was kept constant (reference temperature), while the temperature of the other electrode was set at seven higher temperatures to obtain temperature difference in the range of 0 K < ΔT < +30 K. The thermoelectric power was calculated from the linear regression slope of the *emf* plotted versus ΔT.

The partial pressures, p_{H_2O} and p_{O_2}, were the same at both electrodes, maintained by flowing the gas mixture through the cell. The p_{O_2} was varied from 0.4 to 100 kPa by using Ar-O_2 mixtures, air, and pure O_2. The p_{H_2O} was varied from 0.2 to 6 kPa by bubbling the gas through saturated aqueous solutions of KBr, NaBr, $MgCl_2$, LiCl or LiBr, or distilled water at 298~308 K. The gas line to the cell was heated to avoid water condensation. The values of p_{H_2O} and p_{O_2} were confirmed by humidity and YSZ oxygen sensors.

4. Results and discussion

4.1. Thermoelectric power

Typical experimental observations for the *emf* of the cell (II-b) as a function of the temperature difference are shown in Fig. II-3. The linear relation between the *emf* and the temperature difference was observed with a regression uncertainty of less than ± 0.006 mV·K^{-1} for all measurements. The slope of the line corresponds to the thermoelectric power of the cell (II-b) under given condition. The points on the lines were obtained by first increasing and next reducing the temperature of the right hand

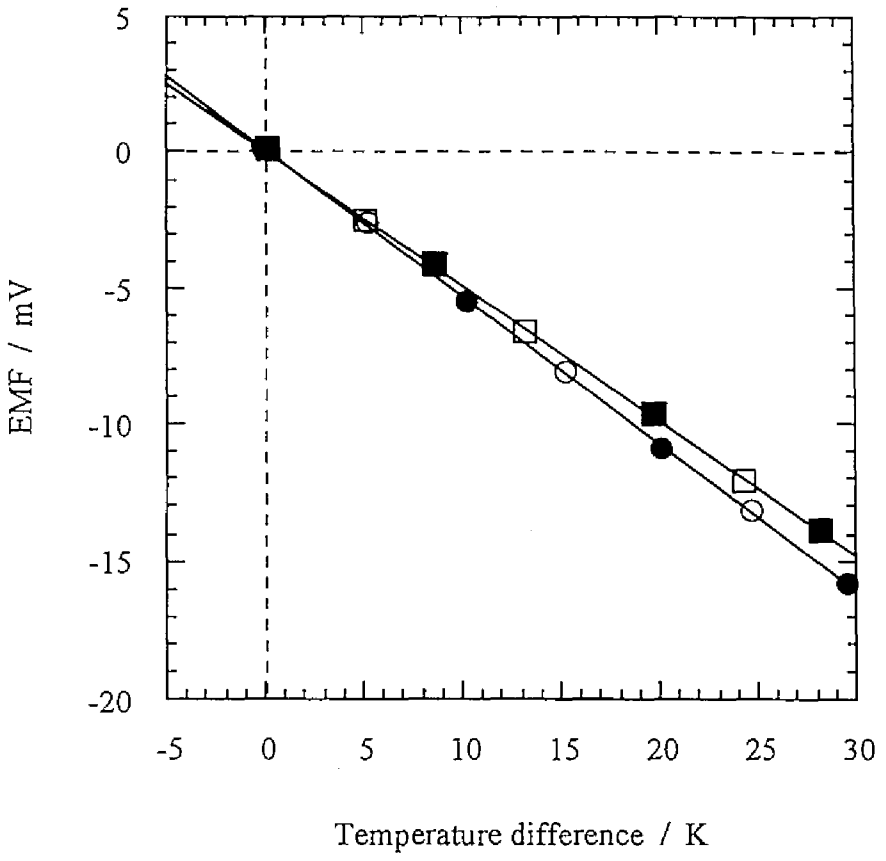

Fig.II-3. Typical observation of the emf of the cell (II-b) as a function of temperature difference in wet air at 873 K; p_{H_2O} = 5.3 kPa; solid circles; increasing ΔT; open circles; decreasing ΔT: p_{H_2O} = 1.5 kPa; solid squares; increasing ΔT; open squares; decreasing ΔT.

side electrode. The fact that slopes stayed constant demonstrates the reversibility of the phenomenon (no diffusion or thermal diffusion), and also no deterioration of the material.

4.2. Identification of charge carrier species

The thermoelectric power of the cell (II-b) in wet air as a function of p_{H_2O} at 873~1173 K are shown in Figs. II-4(A)~(D). A linear relation is observed for 1 kPa <

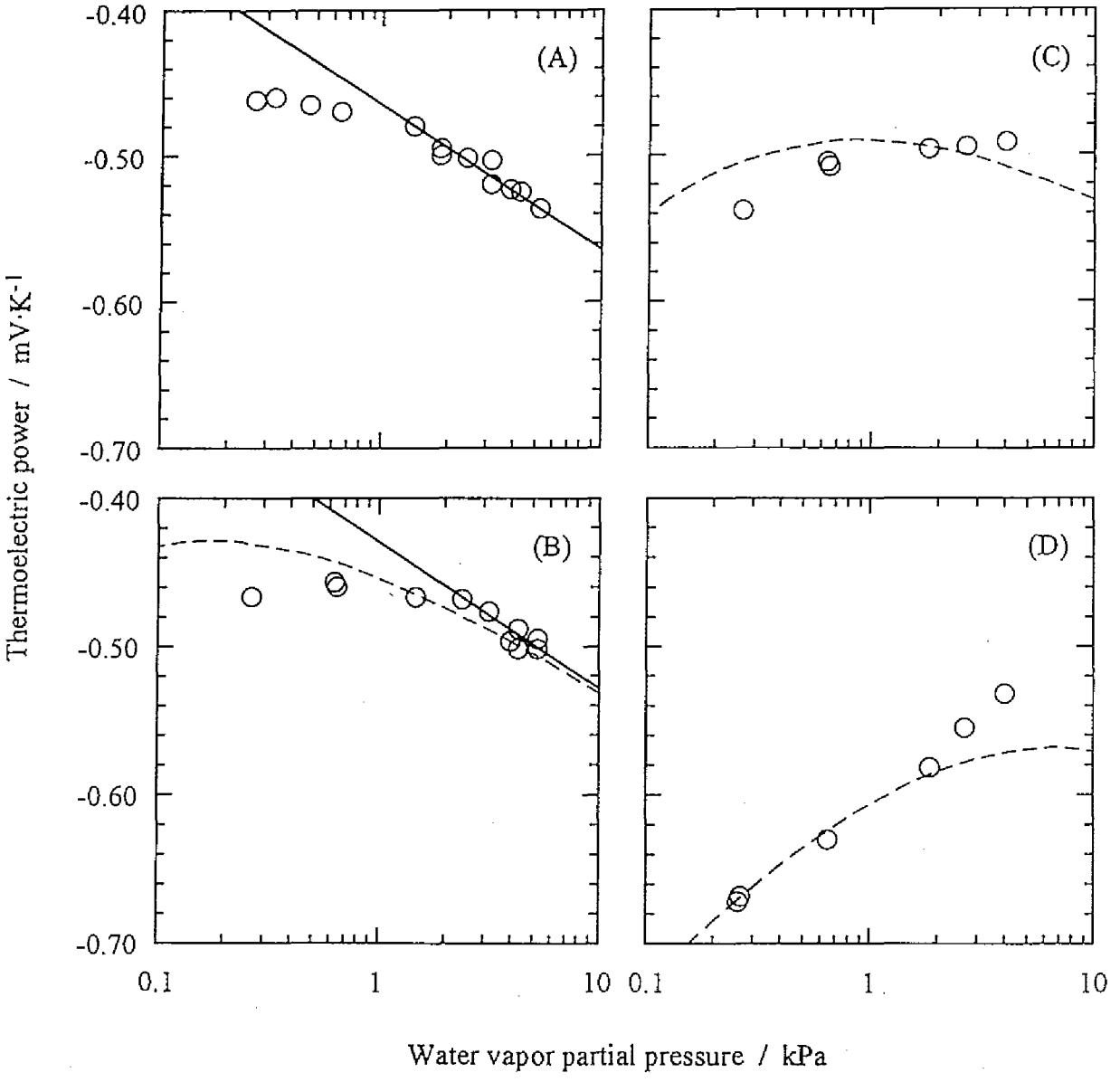

Fig.II-4. Thermoelectric power of the cell (II-b) as a function of water vapor partial pressure in wet air at (A) 873 K, (B) 973 K, (C) 1073 K and (D) 1173 K. The solid lines show the theoretical slope given by eq. (II-11). The doshed lines represent the calculated values by using eqs. (II-28) and (II-31).

p_{H_2O} < 6 kPa at 873 K and for 3 kPa < p_{H_2O} < 6 kPa at 973 K. The slopes of the lines are in good agreement with the theoretical slope -*R*/2*F* given by eq. (II-11) for a pure protonic conductor. It is thus concluded that the proton transport number in the electrolyte in wet air is unity above these water vapor partial pressures at 873 and 973 K. Deviations from the theoretical slope are observed for p_{H_2O} < 1 kPa at 873 K and p_{H_2O} < 3 kPa at 973 K. This suggests that the conduction by other charge carrier species becomes significant below these water vapor partial pressures. At 1073 and 1173 K, the thermoelectric power does not show the theoretical p_{H_2O} dependency in the range of p_{H_2O} investigated. The thermoelectric power decreases with decreasing p_{H_2O} and this tendency becomes stronger at 1173 K than at 1073 K. This indicates that the material exhibits mixed protonic conduction and that the conduction by other charge carrier species than protons becomes more significant as temperature increases.

The p_{O_2} dependence of the thermoelectric power for p_{H_2O} = 4.3 kPa at 873 K, p_{H_2O} = 4.3 kPa and 1.5 kPa at 973 K, p_{H_2O} = 4.3 kPa at 1073 K, and p_{H_2O} = 0.26 kPa at 1173 K are shown in Figs. II-5(A)~(D). At p_{H_2O} = 4.3 kPa and 873 K, and at p_{H_2O} = 4.3 kPa and 973 K, the thermoelectric power varies linearly with ln p_{O_2} in the range of p_{O_2} used. The slope of the lines is *R*/4*F*, which is in agreement with the theoretical slope predicted by eq. (II-11). These result support the conclusion obtained from p_{H_2O} dependence of the thermoelectric power that the proton transport number in Sr-substituted $LaPO_4$ is unity above a p_{H_2O} of 1 kPa at 873 K and above a p_{H_2O} of 3 kPa at 973 K. At p_{H_2O} = 1.5 kPa and 973 K, and at p_{H_2O} = 4.3 kPa and 973 and 1073 K, when the theoretical p_{H_2O} dependency was not observed in Figs. II-4(B) and (C), we also see deviations from the theoretical p_{O_2} dependency in Figs. II-5(B) and (C). In Figs. II-5(B) and (C), the theoretical relation (slope of *R*/4*F*) is observed below a p_{O_2} of approximately 10 kPa, while at higher oxygen partial pressure the results deviate slightly from the theoretical dependency. As mentioned in the theoretical section, such

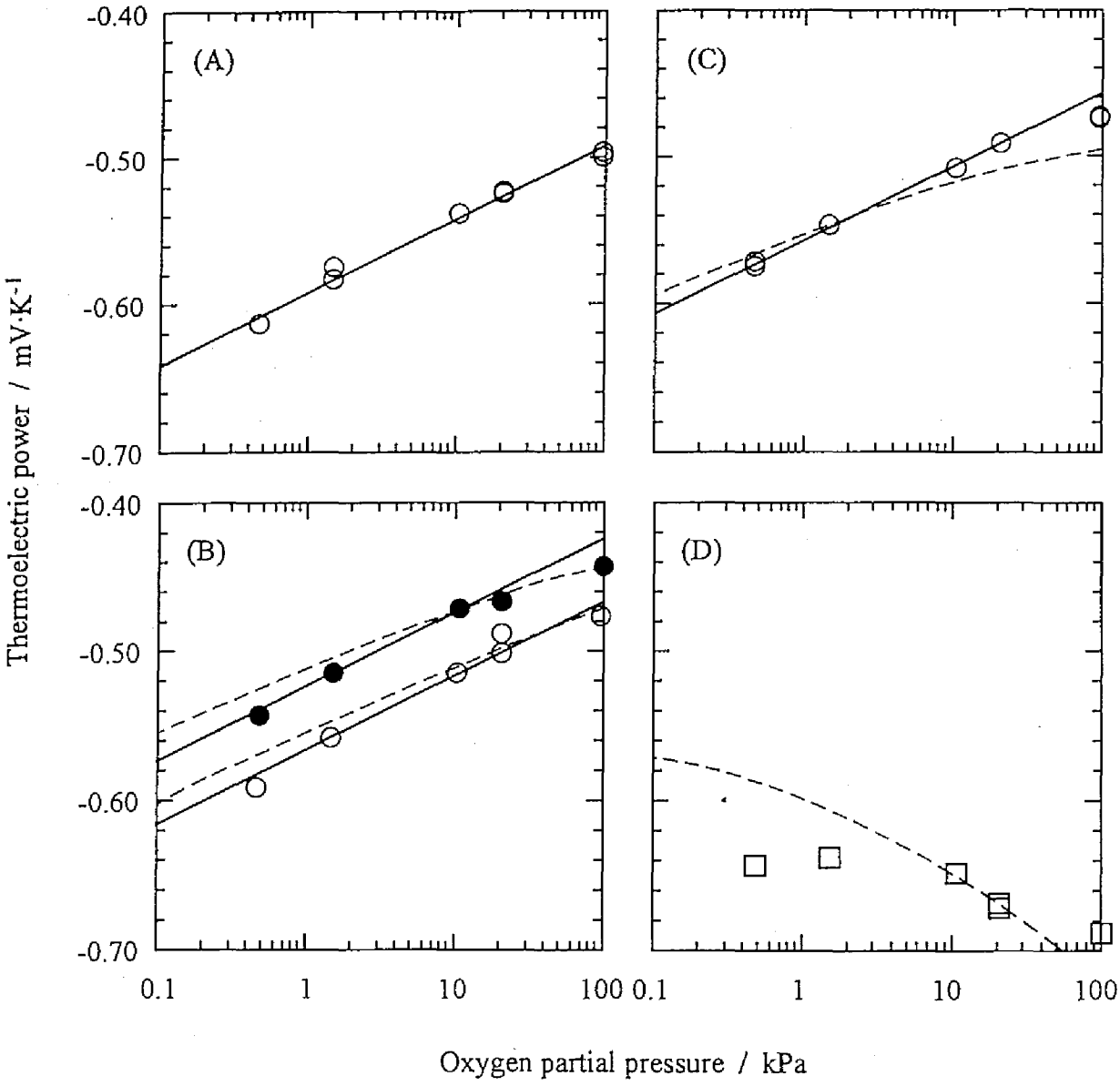

Fig.II-5. Thermoelectric power of the cell (II-b) as a function of oxygen partial pressure for (A) p_{H_2O} = 4.3 kPa at 873 K (○), (B) p_{H_2O} = 4.3 kPa (○) and p_{H_2O} = 1.5 kPa (●) at 973 K, (C) p_{H_2O} = 4.3 kPa at 1073 K and (D) p_{H_2O} = 0.26 kPa at 1173 K (□). The solid lines show the theoretical slope predicted by eq. (II-11). The dashed lines present the calculated values by using eq. (II-28) and (II-31).

deviation from the theoretical p_{O_2} dependency is expected only when the contribution of the conduction by electronic defects to total conductivity becomes significant. The deviations from the theoretical slopes become larger as p_{H_2O} decreases in wet air, and as p_{O_2} increases. These results indicate that a contribution by electron hole conduction becomes more significant, as this would increase the more p_{H_2O} decreases and p_{O_2} increases according to the defect model proposed. For p_{H_2O} = 0.26 kPa at 1173 K, the theoretical p_{O_2} dependency for a pure protonic conductor is not observed at all in the p_{O_2} range investigated, and the thermoelectric power decreases with increasing p_{O_2} (Fig. II-5(D)).

The proton transport number in Sr-substituted $LaPO_4$ can be approximately estimated to be unity at 873 K, 0.96 at 973 K, 0.90 at 1073 K, and 0.73 at 1173 K for p_{O_2} = 21 kPa and p_{H_2O} = 2.5 kPa from conductivity data by Norby and Christiansen [11], where the authors also suggested a contribution from electronic hole conduction by comparing the conductivities under different p_{O_2} conditions. The obtained information on partial conductivities in Sr-substituted $LaPO_4$ from this work agrees well with the conclusions obtained in ref. 11.

4.3. Transported entropies

The thermoelectric power assigned to protons at high p_{H_2O}, low p_{O_2}, and low temperature can be introduced into eq. (II-11). By eliminating the known constants, the transported entropy of protons, $S^*_{H^+}$, can be obtained. The value for the entropy of water vapor and oxygen gas was taken from JANAF [16], and the value for the transported entropy of electrons in platinum electrode was obtained from the results by Moore and Graves [17]. Figure II-6 gives the transported entropy of protons as a function of temperature. The transported entropy of protons is calculated to be 113±1

$J \cdot mol^{-1} \cdot K^{-1}$ at 873 K, 112±2 $J \cdot mol^{-1} \cdot K^{-1}$ at 973 K, and 112±2 $J \cdot mol^{-1} \cdot K^{-1}$ at 1073 K. The magnitude of the transported entropy of protons is surprisingly large. It compares well with thermodynamic entropies of large molecules. A similar value was obtained, however, for a very different material, a proton conducting ion exchange membrane [18].

If we assume that the electrolyte conducts only protons and electron holes, the thermoelectric power can be expressed as eq. (II-28) by introducing $t_{H^\cdot} + t_h = 1$ into eq. (II-17);

$$\left(\frac{dE}{dT}\right)_T = \frac{t_{H^\cdot}}{F}\left\{\frac{1}{2}S^0_{H_2O}(T_1) - \frac{R}{2}\ln\frac{p_{H_2O}}{p^0_{H_2O}} - \frac{1}{4}S^0_{O_2}(T_1) + \frac{R}{4}\ln\frac{p_{O_2}}{p^0_{O_2}} - S^*_{H^\cdot}(T_1) + S^*_h(T_1)\right\} + \frac{1}{F}\left\{S^*_h(T_1) + S^*_{H^\cdot}(T_1)\right\} \quad \text{(II-28)}$$

As discussed in the previous section, the main charge carrier species in 5 mol% Sr-substituted $LaPO_4$ at low p_{H_2O}, high p_{O_2}, and high temperature are believed to be protons and electron holes. Assuming that 5 mol% Sr-substituted $LaPO_4$ conducts only protons and electron holes in mixed conduction conditions, the transported entropy of electron holes can then be estimated from eq. (II-28) and the thermoelectric power data for mixed conduction conditions, if the proton transport number and the transported entropy of protons are known. When the transport number estimated from conductivity measurements is employed, the transported entropy of electron holes is calculated to be approximately 90 $J \cdot mol^{-1} \cdot K^{-1}$ at 973 and 1073 K.

Howard and Lidiard [19] have proposed that the transported entropy of ions can be expressed as a sum of the partial molar entropy, $\bar{S}_{H^\cdot}$, and the heat of transport of ions, $q^*_{H^\cdot}$;

$$S^*_{H^\cdot} = \bar{S}_{H^\cdot} + \frac{q^*_{H^\cdot}}{T} \quad \text{(II-29)}$$

The heat of transport is a term related to thermal diffusion [12]. Although there exists a question whether such an expression of the transported entropy as eq. (II-29) is really possible (see appendix A for details), eq. (II-29) is conventionally used to interpret the

transported entropy. Ahlgren has applied this equation to interpret thermoelectric power of high temperature protonic conductors [9, 10] as well as that of oxide ion conductors [15]. From this point forward in this section, we discuss what conclusions we can obtain, if the conventional interpretaion of the transported entropy expressed by eq. (II-29) is applied to our system. The partial molar entropy of protons in the electrolyte may include configurational and vibrational parts similarly as partial molar entropies of neutral component. The configurational part may be expressed by $\bar{S}_{H^{\cdot}(\mathrm{conf.})} = -R\ln c_{H^{\cdot}}$, where $c_{H^{\cdot}}$ is the site occupancy of protons in the electrolyte [15, 20, 21]. If we assume that the vibrational part is negligibly small and $c_{H^{\cdot}}$ is constant at moderate temperatures and under wet conditions, a plot of $S^{\bullet}_{H^{\cdot}}$ vs. $1/T$ yields $q^{\bullet}_{H^{\cdot}}$ as well as $c_{H^{\cdot}}$. Our experimental results gives $q^{\bullet}_{H^{\cdot}} = 7\ \mathrm{kJ\cdot mol^{-1}}$ and $c_{H^{\cdot}} = 3 \times 10^{-6}$ in the temperature range of 873~1073 K. In $LaPO_4$, protons can have three almost equivalent sites on each oxygen pointing towards nearest neighbors within the PO_4^{3-} octahedron. Thus a sample with nominally 5 mol% of Sr will have a site occupancy of protons of ~0.004, if it has 5 mol% of protons. The value for $c_{H^{\cdot}}$ estimated from the thermoelectric power is considerably small and is only 1/1000 of this.

Similarly, in order to interpret the transported entropy of electronic defects in small polaron hopping conductor, the equation proposed by Heikes has been frequently used [22];

$$S^{\bullet}_{h} = R\ln\frac{\beta(1-c_h)}{c_h} + s \qquad \text{(II-30)}$$

where β is a factor due to spin and orbital degeneracy, c_h is the fraction of hopping sites occupied by charge carriers that are free to take part in the conduction, and s is interpreted as the vibrational entropy associated with the ions surrounding a polaron [23]. Normally, the term β is treated to be one and the term s is negligibly small [24, 25]. Then the value for c_h could be estimated from the transported entropy of holes, and is estimated to be 2×10^{-5} for 5 mol% Sr-substituted $LaPO_4$ at 973~1073 K.

The estimated values for c_h and $q^*_{H^+}$ can not be verified experimentally. The c_{H^+} can be found by using other experimental methods, but is yet known. One should also note that eqs. (II-29) and (II-30) themselves can not be verified by experiments (see appendix A). Further theoretical as well as experimental investigations will be needed to clarify the relation between transported entropy and defect structures.

4.4. p_{H_2O} and p_{O_2} dependencies of the thermoelectric power under mixed conduction conditions

As a simple case of mixed conductors, let us here consider the thermoelectric power for an acceptor doped material which conducts only protons and electron holes. that the 5 mol% Sr-substituted $LaPO_4$ conducts only protons and electron holes. From eqs. (II-22) and (II-23) or eqs. (II-24) and (II-26), the transport number of protons in such a conductor can be expressed;

$$t_{H^+} = \frac{1}{1 + A\left(p_{H_2O}\right)^{-1/2}\left(p_{O_2}\right)^{1/4}} \tag{II-31}$$

where

$$A = \left(\frac{K_1}{K_2}\right)\left(\frac{u_h}{u_{H^+}}\right) \tag{II-32}$$

In eq. (II-32) u_{H^+} and u_h are the mobilities for protons and electron holes. At a constant temperature, the equilibrium constants and the mobilities, thus the term A, can be regarded to be constant. By combining eq. (II-31) with (II-28), the p_{H_2O} and p_{O_2} dependencies of the thermoelectric power can be computed, if the values for $S^*_{H^+}$, S^*_h, and A are known.

The dashed lines in Figs. 4 (B)~(D) and 5 (B)~(D) represent the computed thermoelectric power at 973~1173 K, when we assume $S^*_{H^+} = 112$ J·mol^{-1}·K^{-1}, $S^*_h = 90$ J·mol^{-1}·K^{-1}. The value of the term A at each temperature was estimated from

conductivity data [11]. The transported entropies of protons and electron holes may depend on their concentration, thus on p_{H_2O} and p_{O_2}, as expected from the theories of the transported entropy proposed by Howard and Lidiard for ionic conductors and by Heikes for electronic conductors [15, 19, 22]. However, constant values for the transported entropies were assumed for the calculation, because the validity of these theories has not been confirmed yet and because such p_{H_2O} and p_{O_2} dependencies of the transported entropies anyhow give only small differences in the calculated results in the narrow partial pressure ranges investigated. All computed curves qualitatively reproduce the shape of the p_{H_2O} and p_{O_2} dependencies as well as the values of the thermoelectric power. These results suggest the conclusions regarding the charge carrier species and the proposed defect structure in Sr-substituted $LaPO_4$ are reasonable.

5. Conclusions

1. The theoretical expressions of the thermoelectric power for materials conducting protons, oxide ions, and electronic defects were derived. It was found that thermoelectric power of HTPCs exhibits distinctive p_{H_2O} and p_{O_2} dependencies according to conduction conditions.

2. Based on above theoretical consideration, thermoelectric power measurements were applied to investigate conduction in Sr-substituted $LaPO_4$. It was found that the proton transport number in Sr-substituted $LaPO_4$ can be regarded as unity when $p_{H_2O} > 1$ kPa at 873 K and $p_{H_2O} > 3$ kPa at 973 K in wet air. This is in agreement with earlier findings by conductivity measurements: the material is a protonic conductor at moderate temperature.

3. Deviations in p_{O_2} and p_{H_2O} dependencies of the thermoelectric power at high temperature, high p_{O_2}, and low p_{H_2O} indicate that electron holes becomes significant

charge carriers in these conditions. The contribution of the electron hole conduction to the total conductivity becomes significant with temperature increases, p_{O_2} increases, and p_{H_2O} decreases.

4. p_{O_2} and p_{H_2O} dependencies of the thermoelectric power in the mixed conduction conditions were computed based on the proposed defect model and the conclusion regarding charge carrier species obtained above. The computed results were in good agreement with the experimental results. This implies that the conclusion regarding the charge carrier species and the proposed defect structure in Sr-substituted $LaPO_4$ are reasonable.

5. The transported entropy of protons in Sr-substituted $LaPO_4$ was almost independent of temperature, and was calculated to be 112±2 $J \cdot mol^{-1} \cdot K^{-1}$ at 873~1073 K. The transported entropy of electron holes was 90 $J \cdot mol^{-1} \cdot K^{-1}$.

References

[1] K. -D. Kreuer, *Chem. Mater.*, **8**, 610 (1996).

[2] H. Iwahara, *Solid State Ionics*, 77, 289 (1995).

[3] K. -D. Kreuer, *Solid State Ionics*, **97**, 1 (1997).

[4] T. Norby, O. Dyrlie, and P. Kofstad, *Solid State Ionics*, **53-56**, 446 (1992).

[5] A. S. Nowick and A. V. Vaysleyb, *Solid State Ionics*, **97**, 17 (1997).

[6] D. P. Sutija, T. Norby, and P. Byörnbom, *Solid State Ionics*, 77, 167 (1995).

[7] H. Iwahara, T. Yajima, T. Hibino, K. Ozaki, and H. Suzuki, *Solid State Ionics*, **61**, 65 (1993).

[8] H. Iwahara, T. Yajima, and H. Uchida, *Solid State Ionics*, **70/71**, 264 (1994).

[9] E. O. Ahlgren, *Solid State Ionics*, **97**, 489 (1997).

[10] E. O. Ahlgren, *J. Phys. Chem. Solid*, **58**, 1475 (1997).

[11] T. Norby and N. Christiansen, Solid State Ionics, 77, 240 (1995).

[12] K. S. Førland, T. Førland, and S. K. Ratkje, *Irreversible Thermodynamics; Theory and Applications*, 2nd repr., Wiley, Chichester (1994).

[13] R. G. Chambers, *Proc. Phys. Soc.*, **65**, 903 (1952).

[14] S. K. Ratkje and Y. Tomii, *J. Electrochem. Soc.*, **140**, 59 (1993).

[15] E. O. Ahlgren and F. W. Poulsen, *Solid State Ionics*, **70/71**, 528 (1995).

[16] *JANAF Thermochemical Tables*, 3rd ed., *American Chemical Society*, New York (1965).

[17] J. P. Moore and R. S. Graves, *J. Appl. Phys.*, **44**, 1174 (1973).

[18] S. K. Ratkje, M. Ottøy, R. Halseid, and M. Strømgård, *J. Membr. Sci.*, **107**, 219 (1995).

[19] R. E. Howard and A. B. Lidiard, *Disc. Faraday Soc.*, **23**, 113 (1957).

[20] V. N. Chebotin, S . L. Fridman, and S. F. Pal'guev, *Elektrokhimiya*, **5**, 325 (1969).

[21] V. N. Chebotin, S . L. Fridman, and S. F. Pal'guev, *Elektrokhimiya*, **6**, 1300 (1970).

[22] R. R. Heikes, *Thermoelectricity: Science and Engineering*, edited by R. R. Heikes and R. W. Ure, Interscience Publishers (1961).

[23] H. L. Tuller and A. S. Nowick, *J. Phys. Chem. Solids*, **38**, 859 (1977).

[24] I. G. Austin and N. F. Mott, Materials Adv. Phys., **18**, 41 (1969).

[25] J. B. Goodenough, *Prog. Solid State Chem.*, 5, 145 (1971).

General conclusions

In this thesis, single electrode Peltier heat of an alloy electrode and conduction properties in a mixed conductor were investigated by thermoelectric power measurements. The results were mainly discussed by means of irreversible thermodynamics.

In chapter 2 of part I, the single electrode Peltier heats for formation reactions of various phases in Li-Al alloy in LiCl-KCl eutectic melt were determined. The formation reactions of the βLiAl and the γLi_3Al_2 phases were found to be exothermic, while the formation reactions of the liquid phase from the βLiAl phase and that from the γLi_3Al_2 phase were found to be endothermic. The relation between thermoelectric power and thermodynamic properties of the alloy was theoretically established. It was found that the thermoelectric power of a Li-alloy electrode can be expressed as a sum of the relative partial molar entropy of lithium in the alloy and the thermoelectric power of a Li^+/Li alloy electrode. Experimental results of the thermoelectric power and the thermodynamic properties of Li-Al alloy system validated this relation.

In chapter 3 of part I, the effect of the phase change on the single electrode Peltier heat of an alloy electrode was discussed. The single electrode Peltier heat of a Li-Al alloy electrode was estimated as a function of the lithium concentration. The single electrode Peltier heat of a Li-Al alloy in single phase states considerably depends on the alloy composition, while that in coexisting phase states is independent of the alloy composition. It turned out that the single electrode Peltier heat of a Li-Al alloy electrode

exhibits discontinuities on the coexisting-single phase boundary compositions. The change of the single electrode Peltier heat on the phase boundary composition was discussed thermodynamically, and could be related to thermodynamic properties in the single phase and phase diagram data. According to this relation, the changes of the single electrode Peltier heat on the phase boundaries in Li-Al alloy system were estimated. The estimated results were in good agreement with experimental values.

In chapter 4 of part I, the single electrode Peltier heats for formation reactions of various phases in Li-Si alloy in LiCl-KCl eutectic melt were elucidated. The formation reactions of the $Li_{12}Si_7$, Li_7Si_3, $Li_{13}Si_4$ and $Li_{22}Si_5$ phases were found to be exothermic, while the formation reaction of the liquid phase was found to be endothermic. The thermodynamic relations derived in chapters 2 and 3 were confirmed by using experimental results of thermoelectric power and thermodynamic properties of Li-Si alloy system.

Li-Al and Li-Si alloys are considered to be used as a negative electrode in lithium-based batteries. The single electrode Peltier heat obtained in this work can directly contribute to the heat analysis in such batteries. Furthermore, the knowledge on thermoelectric power obtained in this work would be available to not only lithium alloys but also other alloys.

In part II of this thesis, thermoelectric power measurements were applied to investigate conduction conditions in Sr-substituted $LaPO_4$, which is a mixed, partially protonic conductor. The theoretical expressions of the thermoelectric power for materials conducting protons, oxide ions and electronic defects were derived. The derived expressions predict that the thermoelectric power of a high temperature protonic conductor exhibits distinctive p_{H_2O} and p_{O_2} dependencies according to conduction conditions. The experimental results for Sr-substituted $LaPO_4$ were interpreted in terms of protonic and electron hole conduction. The conditions where the proton transport number is regarded as unity were determined. Finally, p_{H_2O} and p_{O_2} dependencies of the

thermoelectric power in mixed conduction conditions were computed based on the proposed defect structures. The computed results fairly reproduced the experimental results, which suggested that the obtained conclusion on conduction conditions and defect structures are reasonable. It was shown that thermoelectric power measurements can be one of useful experimental techniques for investigating electrochemical properties of mixed conductors.

The main results obtained in this investigation have been or will be published in scientific journals as follows;

1. K. Amezawa, M. Osugi, Y. Tomii, and Y. Ito, "The Effect of Phase Change of Li-Al Alloy Electrode on Thermoelectric Power in LiCl-KCl Eutectic System.", *Denki Kagaku*, **61**, 736 (1993).
(chapter 2 in part I)

2. K. Amezawa, Y. Tomii, and Y. Ito, "The Single Electrode Peltier Heats of Li-Al Alloy Electrodes in LiCl-KCl Eutectic System." , *J. Electrochem. Soc.*, **141**, 3096 (1994).
(chapter 2 in part I)

3. K. Amezawa, N. Yamamoto, Y. Tomii, and Y. Ito, "Thermodynamic Properties and Single Electrode Peltier Heats of Li-Al Alloy in LiCl-KCl Eutectic Melt.", *J. Electrochem. Soc.*, to be published.
(chapters 2 and 3 in part I)

4. K. Amezawa, N. Yamamoto, Y. Tomii, and Y. Ito, "Single Electrode Peltier Heats of Li-Si Alloy Electrodes in LiCl-KCl Eutectic Melt.", *J. Electrochem. Soc.*, **145**, 1986 (1998).

(chapter 4 in part I)

5. K. Amezawa and S. K. Ratkje, "Thermoelectric Power Measurements of Proton Conducting Sr-doped $LaPO_4$.", *Denki Kagaku*, **64**, 688 (1996).
(part II)

6. K. Amezawa, S. Kjelstrup, T. Norby and Y. Ito, "Protonic and Native Conduction in Sr-substituted $LaPO_4$ Studied by Thermoelectric Power Measurements.", *J. Electrochem. Soc.*, in press.
(part II)

Appendix A

Transported entropy and thermodynamic entropy

As already described in chapter 2 of part I, a transported entropy is a transport property and is not a thermodynamic property. However, this does not mean that the transported entropy is independent of thermodynamic entropies of components. In this section, the relations between transported entropies and thermodynamic entropies are presented. The relation between transported entropies and thermodynamic entropies is first derived based on the theory of irreversible thermodynamics by Førland et al. [1~3], in which only neutral chemical species are considered as thermodynamic components. We will see that quantities used in this derivation method are defined on the operational level. Thereafter, the derived relation is compared with the relations obtained by conventional derivation methods [4~7], and thermodynamic importance of the quantities used in conventional derivation methods are discussed.

The system discussed in this section is the nonisothermal cell (I-a). The flux equations are expressed as eqs. (I-7)~(I-9). When there exists no pressure gradient in the system, eq. (I-11) is still valid. The flux equations are then rewritten as follows;

$$J_q = -L_{11}\nabla \ln T - L_{12}\frac{\nabla \mu_{AX,T}}{x_{BX}} - L_{13}\nabla \phi^{obs} \qquad \text{(A-1)}$$

$$J_{AX} = -L_{21}\nabla \ln T - L_{22}\frac{\nabla \mu_{AX,T}}{x_{BX}} - L_{23}\nabla \phi^{obs} \tag{A-2}$$

$$j = -L_{31}\nabla \ln T - L_{32}\frac{\nabla \mu_{AX,T}}{x_{BX}} - L_{33}\nabla \phi^{obs} \tag{A-3}$$

From eqs. (A-1)~(A-3) together with the Onsager reciprocal relation (see eq. (I-10)), the transference coefficient of the component AX and the Peltier heat are related to phenomenological coefficients as follows;

$$t_{AX} = t_{B^+} = \left(\frac{J_{AX}}{j}\right)_{\nabla\mu=0,\nabla T=0} = \frac{L_{23}}{L_{33}} = \frac{L_{32}}{L_{33}} \tag{A-4}$$

$$\pi^{\downarrow} = \left(\frac{J_q}{j}\right)_{\nabla\mu=0,\nabla T=0} = \frac{L_{13}}{L_{33}} = \frac{L_{31}}{L_{33}} \tag{A-5}$$

From eq. (A-3), we have for j=0;

$$\nabla \phi^{obs} = -\frac{L_{31}}{L_{33}}\nabla \ln T - \frac{L_{32}}{L_{33}}\frac{\nabla \mu_{AX,T}}{x_{BX}} \tag{A-6}$$

By introducing eq. (A-6) into eqs. (A-1) and (A-2), we have for j=0;

$$J_q = -l_{11}\nabla \ln T - l_{12}\frac{\nabla \mu_{AX,T}}{x_{BX}} \tag{A-7}$$

$$J_{AX} = -l_{21}\nabla \ln T - l_{22}\frac{\nabla \mu_{AX,T}}{x_{BX}} \tag{A-8}$$

where the coefficient l_{ij} is called an electrode independent phenomenological coefficient, and is related to phenomenological coefficients as follows;

$$l_{ij} = L_{ij} - \frac{L_{i3}L_{3j}}{L_{33}} \tag{A-9}$$

Considering the Onsager reciprocal relation (see eq. (I-10)), we have the following relation between electrode independent phenomenological coefficients;

$$l_{ij} = l_{ji} \tag{A-10}$$

In a system consisting a mixture of two or more electrolyte components with a temperature gradient, there may be a mass flux leading to a partial separation of the electrolyte. When there is no mixing by convection, the separation process continues

until the thermal force is balanced by the chemical force, i.e. stationary state. The stationary state is the situation where there is no mass transfer, i.e. $J_{AX}=0$. From eqs. (A-7), (A-8) and (A-10), we have the following relation between the gradients in chemical potential and temperature at the stationary state;

$$\left(\frac{\nabla\mu_{AX,T}}{x_{BX}}\right)_{j=0,J_{AX}=0}=-\left(\frac{l_{21}}{l_{22}}\right)\nabla\ln T=-\left(\frac{l_{12}}{l_{22}}\right)\nabla\ln T=-\left(\frac{J_q}{J_{AX}}\right)_{j=0,\nabla T=0}\nabla\ln T \tag{A-11}$$

In eq. (A-11), the term $\left(J_q/J_{AX}\right)_{j=0,\nabla T=0}$ is the heat transported by diffusion at constant temperature, and corresponds the heat of transport, q^*. Equation (A-11) then provides;

$$\left(\frac{\nabla\mu_{AX,T}}{x_{BX}}\right)_{j=0,J_{AX}=0}=-q^*\nabla\ln T \tag{A-12}$$

By introducing eqs. (A-4), (A-5) and (A-12) into eq. (A-6), we obtain;

$$\left(\nabla\phi^{obs}\right)_{j=0,J_{AX}=0}=\left(-\pi^{\downarrow}+t_B.q^*\right)\nabla\ln T=\left(-\frac{\pi^{\downarrow}}{T}+t_B.\frac{q^*}{T}\right)\nabla T \tag{A-13}$$

Since the phenomenological coefficients in eqs. (A-1)~(A-3) are independent of the forces, the Peltier heat at the stationary state is also given by eq. (I-22). Equation (A-13) is then rewritten as follows;

$$\left(\nabla\phi^{obs}\right)_{j=0,J_{AX}=0}=\left(\bar{S}_A-t_B.\bar{S}_{AX}+t_B.\bar{S}_{BX}-t_A.S_A^*-t_B.S_B^*+t_B.\frac{q^*}{T}\right)\nabla T \tag{A-14}$$

Equation (A-14) shows that the heat of transport contributes to the *emf* of the nonisothermal cell (I-a) at the stationary state. The *emf* at the stationary state is thus different from that at the initial state.

At stationary state, the mass flux is equal to zero, $J_{AX}=0$. That is, the migration of A^+ away from the left hand side electrode must be balanced by the diffusion of A^+. A similar balance must be achieved for B^+. The entropy changes at the electrode-electrolyte interface are then the same as those caused by the transport of one mole of A^+ away from the interface in the nonisothermal cell;

$$t_{B^*}\bar{S}_{AX} - t_B.\bar{S}_{BX} + t_{A^*}.S^*_{A^*} + t_B.S^*_{B^*} - t_{B^*}.\frac{q^*}{T} = S^*_{A^*} \tag{A-15}$$

Rearranging eq. (A-15) and remembering that $t_{A^*} + t_{B^*} = 1$, we obtain;

$$S^*_{A^*} - S^*_{B^*} = \bar{S}_{AX} - \bar{S}_{BX} + \frac{q^*}{T} \tag{A-16}$$

All terms in eq. (A-16) are independent of the forces, eq. (A-16) is valid whether we have stationary state or not. Equation (A-16) means that the difference between the transported entropies is different from the difference between the thermodynamic entropies of components and that the transported entropies are related to the interchange of positions of the charge carriers.

From eq. (A-14), the expression of the thermoelectric power for the nonisothermal cell (I-a) at the stationary state, $\varepsilon^{st}_{A_xM_{1-x}}$, can be obtained;

$$\varepsilon^{st}_{A_xM_{1-x}} = \frac{1}{F}\left(\bar{S}_A - t_B.\bar{S}_{AX} + t_B.\bar{S}_{BX} - t_A.S^*_{A^*} - t_B.S^*_{B^*} + t_{B^*}.\frac{q^*}{T}\right) \tag{A-17}$$

Introducing eq. (A-16) into eq. (A-17), the expression of the thermoelectric power at the stationary state, $\varepsilon^{st}_{A_xM_{1-x}}$, can be simplified;

$$\varepsilon^{st}_{A_xM_{1-x}} = \frac{1}{F}\left(\bar{S}_A - S^*_{A^*}\right) \tag{A-18}$$

Similarly, from eqs. (A-16) and (I-23), the thermoelectric power at the initial state, $\varepsilon_{A_xM_{1-x}}$, can be expressed;

$$\varepsilon_{A_xM_{1-x}} = \frac{1}{F}\left(\bar{S}_A - S^*_{A^*} + t_{B^*}.\frac{q^*}{T}\right) \tag{A-19}$$

Equations (A-16), (A-18) and (A-19) tells us that the transported entropies of ions and the heat of transport can be determined independently by experiments.

In the literature, the transported entropy of ions is conventionally expressed as the sum of the partial molar entropy of ions and the heat of transport of ions [4~7];

$$S^{*}_{A^+} = \overline{S}_{A^+} + \frac{q^{*}_{A^+}}{T} \tag{A-20}$$

$$S^{*}_{B^+} = \overline{S}_{B^+} + \frac{q^{*}_{B^+}}{T} \tag{A-21}$$

$$S^{*}_{X^-} = \overline{S}_{X^-} + \frac{q^{*}_{X^-}}{T} \tag{A-22}$$

The partial molar entropies of ions may be related to the thermodynamic entropy of neutral component as follows;

$$\overline{S}_{A^+} + \overline{S}_{X^-} = \overline{S}_{AX} \tag{A-23}$$

$$\overline{S}_{B^+} + \overline{S}_{B^-} = \overline{S}_{BX} \tag{A-24}$$

Considering the relation between the fluxes of AX and BX, i.e. eq. (I-3), the heat of transport in the electrolyte may be split into its ionic contributions, i.e. the heats of transport of ions, $q^{*}_{A^+}$ and $q^{*}_{B^+}$;

$$q^{*} = q^{*}_{A^+} - q^{*}_{B^+} \tag{A-25}$$

If we use the relations shown by eqs. (A-23)~(A-25), eqs. (A-20)~(A-22) yield eq. (A-16). That is, equations (A-20)~(A-22) give a similar interpretation on the transported entropy as eq. (A-16) does: the transported entropy of ions is related to not only thermodynamic entropy change in the electrolyte but also the heat of transport.

However, the expressions of the transported entropy of ions given by eqs. (A-20)~(A-22) fundamentally have a question whether such expressions using the partial molar entropy of ions and the heat of transport of ions have any physical realities or not. The partial molar entropy is defined as follows;

$$\overline{S}_i = \left(\frac{\partial S}{\partial n_i} \right)_{n_{j(j \neq i)}} \tag{A-26}$$

But when i and j are ions, this operation can not be done in reality because of the electroneutrality principle. That is, the entropy of ions is an undefined and unmeasurable quantity in terms of physical realities. They therefore do not have any physical significance and are rather considered as mathematical devices. For the heat of

transport in a system containing two electrolyte components, it is not possible to experimentally distinguish between the heats of transport of ions, q_A^*. and q_B^*., and there is only one measurable heat of transport, q^*, because the fluxes of AX and BX depend on each other. From these consideration, we can conclude that the expression of the transported entropy such as eqs. (A-20)~(A-22) does not have any physical realities.

In the first half of this section, we have seen that the thermoelectric phenomena can be well described without introducing individual ionic thermodynamic properties. Thermoelectric power of the nonisothermal cell (I-a) at the initial and the stationary states can be expressed by eqs. (I-23) and (A-17) or eqs. (A-19) and (A-18), respectively. The relation between the transported entropies and thermodynamic entropies is given by eq. (A-16). These expressions can give similar understandings of the system as those obtained in conventional methods do, while using only quantities which are well defined and measurable.

References

[1] K. S. Førland, T. Førland, and S. K. Ratkje, *Irreversible Thermodynamics; Theory and Application*, 2nd repr., Wiley, Chichester (1994).

[2] S. K. Ratkje and Y. Tomii, *J. Electrochem. Soc.*, **140**, 59 (1993).

[3] A. Grimstvedt, S. K. Ratkje, and T. Førland, *J. Electrochem. Soc.*, **141**, 1236 (1994).

[4] R. E. Howard and A. B. Lidiard, *Disc. Faraday Soc.*, **23**, 113 (1957).

[5] J. N. Agar, *Advances in Electrochemistry and Electrochemical Engineering*, **3**, ed. by P. Delahay, Interscience Publ., New York (1963).

[6] R. Haase, *Thermodynamics of Irreversible Processes*, Addison-Wesley (1969).

[7] E. O. Ahlgren and F. W. Poulsen, *Solid State Ionics*, **70/71**, 528 (1995).

Nomenclature

A_A^i	Interaction parameter of component A in *i* phase ($J \cdot mol^{-1}$)
a_A	Activity of component A (—)
B_A^i	Interaction parameter of component A in *i* phase ($J \cdot mol^{-1}$)
$c_{p,i}$	Heat capacity of gas *i* ($J \cdot mol^{-1} \cdot K^{-1}$)
c_i	Site occupancy (—)
E	Electric force (V)
F	Faraday constant (96487 $C \cdot mol^{-1}$)
F_A^i	Lattice stability parameter of component A in *i* phase ($J \cdot mol^{-1}$)
$\Delta\overline{G_i}$	Relative partial molar free energy of component A ($J \cdot mol^{-1}$)
$\Delta\overline{H_i}$	Relative partial molar enthalpy ($J \cdot mol^{-1}$)
I	Current density ($A \cdot m^{-2}$)
J_i	Mass flux of component *i* ($J \cdot m^{-2} \cdot s^{-1}$)
J_q	Heat flux ($J \cdot m^{-2} \cdot s^{-1}$)
j	Current density ($mol \cdot m^{-2} \cdot s^{-1}$)
K	Equilibrium constant
L_{ij}	Phenomenological coefficient
l_{ij}	Electrode independent phenomenological coefficient
ℓ	half distance between electrodes (m)
p_i	Partial pressure of gas *i* (Pa)
Q^i	Single electrode heat ($J \cdot C^{-1}$)
q^*	Heat of transport for electrolyte ($J \cdot mol^{-1}$)
q_i^*	Heat of transport of charge carrier *i* ($J \cdot mol^{-1}$)
R	Universal gas constant (8.314 $J \cdot mol^{-1} \cdot K^{-1}$)
S_i	Molar entropy of *i* ($J \cdot mol^{-1} \cdot K^{-1}$)

$\overline{S}_i$	Partial molar entropy of component i ($J \cdot mol^{-1} \cdot K^{-1}$)
S_i^*	Transported entropy of charge carrier i ($J \cdot mol^{-1} \cdot K^{-1}$)
$\Delta\overline{S}_i$	Relative partial molar entropy of component i ($J \cdot mol^{-1} \cdot K^{-1}$)
s	Vibrational entropy associated with the ions surrounding a polaron ($J \cdot mol^{-1} \cdot K^{-1}$)
T	Temperature (K)
t_i	Transference coefficient of component i (—)
t_{i^+} or t_{i^-}	Transport number of charge carrier i (—)
x_i	Molar fraction of component i (—)
z	Vacancy concentration (—)

Greek symbols

α	Intrinsic disorder parameter (—)
β	Degeneracy factor (—)
ε	Thermoelectric power ($V \cdot K^{-1}$)
ϕ	Electric potential ($J \cdot mol^{-1}$)
ϕ^{obs}	Observed electric potential ($J \cdot mol^{-1}$)
η	Overpotential (V)
$\mu_{i,T}$	Chemical potential of component i at constant temperature ($J \cdot mol^{-1}$)
π^1	Single electrode Peltier heat ($J \cdot C^{-1}$)
ρ	Electrical resistivity ($S^{-1} \cdot m$)
Θ	Entropy production per unit volume and unit time ($J \cdot m^{-3} \cdot s^{-1} \cdot K^{-1}$)
τ_i	Thomson coefficient of charge carrier i ($J \cdot mol^{-1} \cdot K^{-1}$)
χ	Concentration deviation from stoichiometry (—)

Acknowledgments

First of all, the author wishes to give his sincere gratitude to Professor Yasuhiko Ito (Graduate School of Energy Science, Kyoto University) for his supervision, stimulating discussion, and kind encouragement throughout the thesis work. Grateful acknowledgment is due to Professor Signe Kjelstrup (Department of Physical Chemistry, Norwegian University of Science and Technology, Norway) for her guidance, indispensable discussion, and continual encouragement during and even after the stay in her laboratory. The author is grateful to Professor Naoichi Yamamoto (Graduate School of Human and Environmental Studies, Kyoto University) for valuable discussion. The author's special thanks go to Associate Professor Yoichi Tomii (Graduate School of Energy Science, Kyoto University) for his support in the experimental works and for always inspiring the author to work harder. The author is extremely indebted to Professor Truls Norby (Center for Materials Science, University of Oslo) for his material supports and valuable discussion on defect chemistry in phosphate electrolyte.

The discussions with Associate Professor Masahiro Kamata (Department of Science Education, Tokyo Gakugei University) and Professor Toshio Oishi (Department of Materials Science and Engineering, Kansai University) were quite helpful for progressing with this work. Dr. Niels Christiansen (Haldor Topsøe A/S, Denmark) is acknowledged for his material supports of the phosphate electrolyte. The author appreciates valuable helps by Professor Osamu Tamada (Graduate School of Human and Environmental Studies, Kyoto University), Professor Hirotake Moriyama (Kyoto University Research Reactor Institute), Associate Professor Rika Hagiwara (Graduate School of Energy Science, Kyoto University), Mr. Masayuki Tada and Ms. Keiko Ema (Graduate School of Energy Science, Kyoto University). Ms. Mitsuko

Osugi is acknowledged for her collaboration. Deepest thanks also to all the colleagues in Prof. Ito's, Prof. Kjelstrup's and Prof. Yamamoto's laboratories for their companies both at work and in all other activities.

The Norwegian Research Council of Science and Technologies is acknowledged for the financial support that made the author's stay in Norway possible. The Japan Society of Powder and Powder Metallurgy is acknowledged for the financial support for the work on high temperature protonic conductors.

The author want to thank his parents, Akio and Mine Amezawa, for their kind and continual support. Finally, but certainly not least, the author will express his deepest respect and love to his wife, Izumi, and dear daughter, two years old Hikari. The two of them fill the author's life with happiness.

Kyoto, May 1998

Koji Amezawa